2021

Glucocorticoid receptor dysregulation underlies 5-HT2A receptor-dependent synaptic and behavioral deficits in a mouse neurodevelopmental disorder model

Justin M. Saunders
Virginia Commonwealth University

“Glucocorticoid receptor dysregulation underlies 5-HT_{2A} receptor-dependent synaptic and behavioral deficits in a mouse neurodevelopmental disorder model”

A dissertation submitted in partial fulfillment of the requirements for the degree of Doctor of Philosophy at Virginia Commonwealth University

by

Justin Saunders, BS
Villanova University
2012

Director: Dr. Javier González-Maeso, PhD
Professor, Department of Physiology and Biophysics

Virginia Commonwealth University
Richmond, VA
August, 2021

Acknowledgments

The author wishes to thank his parents, siblings, cousins, and grandparents for being a wonderful, nurturing family and a constant source of support.

I would also like to thank members of the Maeso lab for sharing their knowledge, expertise, and good nature with me over the past five years.

I would like to thank the VCU MD/PhD and Neuroscience programs for being scientific homes throughout this process.

I would also like to thank Dr. Janice Knepper for being my first PI and introducing me to the concept of an MD/PhD program.

I would like to thank Dr. Javier González-Maeso for his guidance and for being a supportive mentor throughout this process.

Table of Contents

List of Publications

Saunders JM, Muguruza C, Sierra S, Beardsley PM, Meana JJ, González-Maeso J. Glucocorticoid receptor dysregulation underlies 5-HT_{2A} receptor-dependent synaptic and behavioral deficits in a mouse neurodevelopmental disorder model (*Experiments complete*).

Saunders JM, Moreno JL, Ibi D, Sikaroodi M, Kang DJ, Muñoz-Moreno R, Dalmet SS, García-Sastre AG, Gillevet PM, Dozmorov MG, Bajaj JS, González-Maeso J. Gut microbiota manipulation during the prepubertal period shapes behavioral abnormalities in a mouse neurodevelopmental disorder model. ***Scientific Reports*** (2020). PMID: 32170216.

Ibi D, de la Fuente Revenga M, Kezunovic N, Muguruza C, **Saunders JM**, Gaitonde SA, Moreno JL, Ijaz M, Santosh V, Kozlenkov A, Holloway T, Seto J, García-Bea A, Kurita M, Mosley GE, Jiang Y, Christoffel DJ, Callado LF, Russo SJ, Dracheva S, López-Giménez JF, Ge Y, Escalante CR, Meana JJ, Akbarian S, Huntley GW, González-Maeso, J. Antipsychotic-induced *Hdac2* transcription via NF-κB leads to synaptic and cognitive side effects. ***Nature Neuroscience*** (2017). PMID: 28783139.

Fomsgaard L, Moreno JL, de la Fuente Revenga M, Brudek T, Adamsen D, Rio-Alamos C, **Saunders J**, Bue Klein A, Oliveras I, Cañete T, Blazquez G, Tobeña A, Fernandez-Teruel A, González-Maeso J, Aznar S. Differences in 5-HT2A and mGlu2 Receptor Expression Levels and Repressive Epigenetic Modifications at the 5-HT2A Promoter Region in the Roman Low-(RLA-I) and High-(RHA-I) Avoidance Rat Strains. ***Molecular Neurobiology*** (2017). PMID: 28265857.

López-Giménez JF, de la Fuente Revenga M, Ruso-Julve F, **Saunders JM**, Moreno JL, Crespo-Faccoro B, González-Maeso J. Validation of schizophrenia gene expression profile in a preclinical model of maternal infection during pregnancy. **Schizophrenia Research** (2017). PMID: 28202291.

de la Fuente Revenga M, Ibi D, **Saunders JM**, Cuddy T, Ijaz MK, Toneatti R, Kurita M, Holloway T, Shen L, Seto J, Dozmorov MG, González-Maeso J. HDAC2-dependent Antipsychotic-like Effects of Chronic Treatment with the HDAC Inhibitor SAHA in Mice. ***Neuroscience*** (2018). PMID: 30025863.

Hideshima KS; Hojati A; **Saunders JM**; On DM; de la Fuente Revenga M; Sánchez-González A; Dunn CM; Pais AB; Pais AC; Miles MF; Wolstenholme JT; Shin JM; González-Maeso J. Role of mGlu2 in the 5-HT2A receptor-dependent antipsychotic activity of clozapine in mice. ***Psychopharmacology*** (2018). PMID: 30209534.

Editorial: **Saunders JM**, González-Maeso J, Bajaj, JS. The *Toll* of Hyperammonemia on the Brain. ***Cellular and Molecular Gastroenterology and Hepatology*** (2019). PMID: 31536718.

Toneatti R, Shin JM, Shah UH, Mayer CR, **Saunders JM**, Fribourg M, Arsenovic PT, Janssen WG, Sealfon SC, López-Giménez JF, Benson DL, Conway DE, González-Maeso J. Interclass GPCR heteromerization affects localization and trafficking. ***Science Signaling*** (2020). PMID: 33082287.

Sánchez-Gonzalez A, Thougaard E, Tapias-Espinosa C, Cañete T, Sampedro-Viana D, **Saunders JM**, Toneatti R, Tobeña A, González-Maeso J, Aznar S, Fernández-Teruel A. Increased thin-spine density in frontal cortex pyramidal neurons in a genetic rat model of schizophrenia-relevant features. **Eur Neuropsychopharmacol** (2021). PMID: 33485732.

Vohra HZ, **Saunders JM^**, Jaster AM^, de la Fuente Revenga M, Jimenez J, Fernández-Teruel A, Wolstenholme JT, Beardsley PM, and González-Maeso J. Sex-specific effects of psychedelics on prepulse inhibition of startle in 129S6/SvEv mice Psychopharmacology (2021). PMID: 34345931. ^These authors contributed equally to the work.

de la Fuente Revenga M, Zhu B, Guevara CA, Naler LB, **Saunders JM**, Zirui Z, , Toneatti R, Sierra S, Wolstenholme JT, Beardsley PM, Huntley GH, Lu C, González-Maeso J. Prolonged epigenetic and synaptic plasticity alterations following single exposure to a psychedelic in mice (*Preprint, Revision submitted to Cell Reports*).

Naler LB, Zhu B, **Saunders JM**, González-Maeso J, Lu C. Frontal cortex cell type-specific epigenomic reprograming in a mouse neurodevelopmental disorder model (*Experiments in progress*).

List of Tables

List of Figures

List of Abbreviations

Abbreviation	*Definition*
AAV	adeno-associated virus
AP	antipsychotic
BAG1	Bcl2-associated athanogene 1
BDNF	brain-derived neurotrophic factor
BSA	bovine serum albumin
CaMKIIα	Ca^{2+}/calmodulin-dependent protein kinase II alpha
cDNA	complementary DNA
ChIP	chromatin immunoprecipitation
CMV	cytomegalovirus
Con	control
Cort	corticosterone
COX-2	cyclooxygenase 2
CRISPR/dCas9	clustered regulatory interspaced short palindromic repeat/nuclease dead Cas9
CRL	Charles River
ddH_2O	double distilled water
diH_2O	deionized water
DEPC	diethylpyrocarbonate
DPBS	Dulbecco's phosphate-buffered saline
DMSO	dimethylsulfoxide
DOI	2,5-dimethoxy-4-iodoamphetamine
DSM	Diagnostic and Statistical Manual of Mental Disorders
DUSP1	dual-specificity phosphatase 1
D_2	dopamine D_2 receptor
ECL	enzymatic chemiluminescence
Egr-1	early growth response 1
Egr-2	early growth response 2
ELISA	enzyme-linked immunosorbent assay
E9.5, E12.5	embryonic day 9.5, embryonic day 12.5
eYFP	enhanced yellow fluorescent protein
FBS	fetal bovine serum
FISH	fluorescence *in situ* hybridization
FKBP4	FK506 binding protein 4
FKBP5	FK506 binding protein 5
GFP	green fluorescent protein
GILZ	glucocorticoid-induced leucine zipper
GR	glucocorticoid receptor
GRE	glucocorticoid response element
gRNA	guide RNA
HRP	horseradish peroxidase
IF	immunofluorescence
IgG	immunoglobulin G

IL-1β	interleukin 1 beta
IL-6	interleukin 6
IL-17a	interleukin 17a
i.p.	intraperitoneal
JAX	Jackson Laboratories
kDa	kilodaltons
KO	knockout
LB	lysogeny broth
LPS	lipopolysaccharide
LSD	lysergic acid diethylamide
mGluR2	metabotropic glutamate receptor 2
MIA	maternal immune activation
N2a cell	Neuro-2a cell
PBS	phosphate-buffered saline
PCR	polymerase chain reaction
PER1	period circadian regulator 1
PFA	paraformaldehyde
PLCβ1	phosopholipase C beta 1
PMD	postmortem delay
Poly-(I:C)	polyinosinic:polycytidylic acid
PPI	prepulse inhibition of the startle response
PTGES3	prostaglandin E synthase E
P42	postnatal day 42
qPCR	quantitative polymerase chain reaction
RT	reverse transcription
SATB2	special AT-rich sequence binding protein 2
s.c.	subcutaneous
Scz	schizophrenia
SDS-PAGE	sodium dodecyl sulfate polyacrylamide gel electrophoresis
SFB	segmented filamentous bacteria
siRNA	small interfering RNA
TAC	Taconic
TBST	tris-buffered saline with tween
TCF3	transcription factor 3
TCF4	transcription factor 4
T_h17 cell	helper T 17 cell
TLR3	toll-like receptor 3
TLR4	toll-like receptor 4
TMB	3,3’,5,5’-tetramethylbenzidine
TNF-α	tumor necrosis factor alpha
TrkB	tropomyosin receptor kinase B
TSS	transcriptional start site
VMax	maximum voltage transduced by the Startle Response system
WT	wild type
5-HT_{2A}R	serotonin 5-HT_{2A} receptor
5-HT_{2B}R	serotonin 5-HT_{2B} receptor
5-HT_{2C}R	serotonin 5-HT_{2C} receptor
16S rRNA	16S ribosomal RNA

Statement of Contributions

Justin Saunders, unless otherwise noted, conducted experiments and wrote the dissertation.

Dr. Salvador Sierra designed and generated the *5-$HT_{2A}R$* antisense RNA probe and negative control sense probe for FISH. He also optimized the FISH hybridization protocol.

Dr. Carolina Muguruza Millan, in the laboratory of Dr. J. Javier Meana, performed and analyzed subcellular fractionation and western blotting experiments in postmortem human brain samples. She also wrote the methods subsection describing the postmortem brain samples, provided a draft for the methods subsection describing subcellular fractionation and western blotting in postmortem samples, and generated Tables M2 and M3.

Dr. Javier González-Maeso oversaw the project and experiments and edited the dissertation.

Abstract

Schizophrenia is a severe neuropsychiatric disorder that presents with diverse symptoms, some of which remain resistant to treatment. Increased risk of neurodevelopmental disorders such as schizophrenia has been observed following gestational infection in humans, leading to development of maternal immune activation (MIA) animal models. Increased density of the serotonin 5-HT_{2A}R receptor (5-HT_{2A}R), the primary target of hallucinogenic drugs and a key target of atypical antipsychotics, has been observed in postmortem antipsychotic-free prefrontal cortex samples from schizophrenia subjects, a change reflected in frontal cortex of adult MIA offspring. To model MIA, we administered 20 mg/kg i.p. of the viral mimetic poly-(I:C) on E12.5 of murine pregnancy and observed increased *5-HT_{2A}R* mRNA in adult MIA offspring frontal cortex. Prepulse inhibition of startle deficits, a phenotype seen within disorders such as schizophrenia, were also seen in MIA offspring. Dendritic spines are essential for appropriate synaptic communication and synaptic plasticity. MIA decreases mature mushroom spine density in mouse frontal cortex in a 5-HT_{2A}R-dependent manner, implicating the receptor in MIA-induced synaptic deficits. Due to evidence that glucocorticoid receptor (GR) signaling and stress affect 5-HT_{2A}R expression in other experimental systems, we investigated GR dysregulation as a potential underlying factor for increased 5-HT_{2A}R expression following MIA. We observed decreased GR immunoreactivity in the nuclear, but not cytoplasmic, compartment of MIA offspring frontal cortex as well as decreased GR enrichment at a binding site on the *5-HT_{2A}R* promoter. Postmortem human samples demonstrate dysregulation of GR immunoreactivity in prefrontal cortex of schizophrenia subjects relative to controls as well. Directly manipulating GR signaling by administering the endogenous agonist corticosterone increased *5-HT_{2A}R* mRNA expression in mouse frontal cortex without affecting *5-HT_{2C}R* or dopamine *D_2* expression. This increase in expression is associated with decreased enrichment of the GR at the *5-HT_{2A}R* promoter binding site. Stereotaxic administration of an AAV vector to overexpress a constitutively translocating GR construct, ΔGR, decreased *5-HT_{2A}R*, but not *5-HT_{2C}R* or *D_2*, expression in mouse frontal cortex. Additionally, ΔGR expression in frontal cortex improved PPI in a 5-HT_{2A}R-dependent manner. These findings support a negative regulatory relationship between GR signaling and *5-HT_{2A}R* expression in mouse frontal cortex and may carry implications for the pathophysiology underlying *5-HT_{2A}R* dysregulation in neuropsychiatric disorders such as schizophrenia.

Introduction

IA. Maternal immune activation models reflect important elements of schizophrenia pathophysiology.

IA.1. Schizophrenia is a complex neuropsychiatric disorder produced by both genetic and environmental factors.

Schizophrenia continues to be one of the most severe neuropsychiatric disorders, generally presenting after adolescence and lasting for the remainder of life.[1] For formal diagnosis, a patient must exhibit evidence of the disorder for at least 6 months, distinguishing it from more transient psychotic illnesses.[1] Schizophrenia is relatively common for its degree of severity, affecting 0.3-1% of the population,[1, 2] and is characterized by the wide variety of ways in which it can present. Conventionally, schizophrenia symptoms have been categorized into clusters: positive, elements that are not present in healthy individuals; negative, elements that are present in healthy individuals and absent in schizophrenia patients; and cognitive, decreases in elements such as working memory and executive function, based on how they affect the patient.[3]

Current diagnostic criteria for schizophrenia include the presence of features such as hallucinations, sensory perceptions in the absence of concurrent stimuli; negative symptoms such as avolition, a decrease in will to perform actions; abnormal behaviors such as catatonia, a state of diminished responsiveness; delusions, beliefs that are strongly held despite inconsistence with available information; and significant alterations in patterns of speech.[1] Schizophrenia therefore affects a wide variety of domains, many of which are important for functioning within society.[4] Given that there is currently no cure for the disorder,[1] improved understanding of the condition and more effective treatments are necessary to decrease the burden of this disorder.

The current understanding of schizophrenia pathophysiology involves a complex process in which genetically susceptible individuals are exposed to insult stressors at key periods during the lifespan.[5] In line with this, both genetic and environmental components to schizophrenia development have been identified.[6] On the genetic side, large genome-wide association studies have identified key loci that contribute to increased risk of schizophrenia development,[7] though no gene by itself is capable of producing schizophrenia.[2] However, some disorders, such as the 22q11.2 deletion, carry significant schizophrenia risk.[8] In addition, there is a high degree of concordance between monozygotic twins, further emphasizing the genetic nature of the disorder.[9]

Schizophrenia development also involves a significant environmental component. A variety of factors, such as exposure to war, living in an urban environment, and adolescent cannabis use[10] have been found to be associated with increased schizophrenia risk. Maternal infection during human pregnancy is a particularly salient insult that has been found to be associated with schizophrenia risk, with increased risk being reported during both the first and second trimesters.[10-12] Interestingly, this risk has been found with a variety of agents. Bacterial infections, such as gonococcal and upper respiratory infections have been found to increase risk during the first trimester.[12] Increased risk of schizophrenia spectrum disorders has also been reported with viral infections such as influenza, in which anti-influenza antibodies in maternal serum trended towards association with increased risk of schizophrenia spectrum disorders in adult offspring [11] and multiple studies have found increased schizophrenia incidence in people born following influenza epidemics.[10] Higher rates of schizophrenia spectrum disorders were observed in a cohort of subjects with gestational exposure to rubella as compared to the general population.[13] A trend has also been reported with the parasite toxoplasmosis in a study evaluating the relationship between anti-toxoplasmosis antibodies in maternal serum collected during pregnancy and development of schizophrenia spectrum disorders in a birth cohort.[14] Interestingly, maternal infection has also been found to be associated with increased risk of other neurodevelopmental conditions, such

as autism.[15] In a large Danish study of about 1.6 million children, maternal hospitalization with first trimester viral infection or second trimester bacterial infection during pregnancy was associated with increased risk of autism spectrum disorder.[16]

IA.2. Maternal immune activation models have been developed in animals.

Following findings of similar effects resulting from diverse infectious agents, it has been proposed that this increased risk is due to the convergence of the agents on the maternal immune system.[17] These infections are believed to elicit a maternal immune response, which results in cytokines that exert effects on the fetus.[17] This has led to the concept of maternal immune activation, in which a maternal immune response to infection produces long lasting neurodevelopmental effects on the offspring.[18] The effects of this immune response, interacting with additional stressors later in life, are thought to produce disorders such as schizophrenia in genetically susceptible hosts.[5, 18]

Following these associations in humans, maternal immune activation (MIA) animal models have been developed to explore this environmental aspect of neurodevelopmental disorder pathophysiology.[5] Similar to the variety of infections linked to increased risk of schizophrenia, a diverse set of agents have been used to induce MIA.[19-22] Among the approaches that have been used, one of the most intuitive is the direct use of infectious agents. A mouse-adapted influenza virus in pregnant mice, for example, was used in early MIA experiments to induce phenotypes in the offspring.[20, 23] A direct approach such as this contains both advantages and disadvantages. An important advantage is that induction of complete agents has the potential to elicit both innate and adaptive immune responses, which might allow for a more complex series of induced effects.[24] In terms of downsides, an infectious agent requires an incubation period, which can make it more difficult to determine the critical period for the maternal immune response-induced effects that are observed.[25] For example, a paper that uses both mouse-

adapted influenza as well as a viral mimetic agent administers influenza at embryonic day 9.5 (E9.5) of gestation while administering the agent at E12.5, citing previous studies showing that the peak immune response elicited by the two would occur on the same day.[23] Thus, using infectious agents for MIA produces a wider ranging, but less precise, response than other approaches.

In addition to these intact infectious agents, agents that mimic their presence have also been used for MIA.[5] They produce a more precise, controlled immune response that can be observed within hours[26, 27] and do not require the same biosafety containment associated with infectious agents.[24] These mimetic agents tend to bind a particular molecular target that recognizes specific elements of infectious agents, resulting in downstream signaling cascades as if the infectious agent had been present. Lipopolysaccharide (LPS), for example, a component of the outer membrane of gram negative bacteria, is recognized by toll-like receptor 4 (TLR4).[28] When administered to a pregnant rodent, it binds the TLR4 and elicits a downstream signaling cascade, resulting in sickness behaviors (such as lethargy, ptosis, and decreased feeding in the dam[29]) and producing MIA-induced phenotypes in the adult offspring.[30-32] Other approaches to MIA induction have involved viral mimetics[26] and, in some cases, variable stress without administration of any agent.[22]

IA.3. Poly-(I:C) is a well-validated approach for MIA induction.

The MIA-inducing agent used in these studies is polyinosinic:polycytidylic acid (poly-(I:C)), a double-stranded RNA analog which consists of a string of inosines and cytidines.[33] It exerts its effect primary through binding to TLR3, which acts to recognize the double-stranded RNA of viruses, resulting in a downstream immune cascade,[33] including production of proinflammatory cytokines such as interleukin 6 (IL-6), TNF-α, and IL-1β.[27] In one study, cytokine induction was observed to peak around 3 hours after administration.[27] Among acute sickness behaviors produced by poly-(I:C) are decreased activity,

diminished body weight, and increased body temperature.[27] Poly-(I:C) has been extensively used to produce MIA-induced phenotypes by a variety of laboratories, with variable dosage, timing, and administration schedules.[19, 22, 23, 34, 35] These approaches reveal the complex interplay of factors needed to properly execute a MIA model.

One of these factors is related to poly-(I:C) itself. There can be significant variability between poly-(I:C) lots, with an order of magnitude in plasma IL-6 induction being possible between batches.[36] In addition, factors such as the vendor and molecular weight of the poly-(I:C) can influence the degree of immune response seen in injected mice.[37] In addition to the variability in poly-(I:C), factors inherent to the animals used in the studies are also important for observing MIA effects in offspring. Mice from different vendors have been reported to exhibit varying degrees of susceptibility to MIA-induced phenotypes.[35] At least part of this has been reported to be due to gut microbiome components, with segmented filamentous bacteria (Candidatus *Savagella*) in the gut being necessary for development of maternal gut T_h17 helper T cells.[38] These cells have been shown to be essential for IL-17a production and MIA-induced phenotypes within a particular poly-(I:C)-induced model.[38] Downstream signaling mediators after TLR3 also include IL-6,[26, 33] which has been shown to be both necessary within the mother to elicit MIA phenotypes as well as sufficient, when administered to pregnant mice on E12.5, to induce MIA-like phenotypes in offspring.[39] MIA models therefore require the successful triggering of complex signaling cascades in mice possessing factors that make them susceptible to immune activating agents.

IA.4. MIA induces neurodevelopmental disorder-related phenotypes in offspring.

In line with the disorders it intends to model, MIA has proven to be a pleiotropic insult, producing phenotypes reminiscent of multiple neurodevelopmental disorders such as schizophrenia and autism.[5, 15, 19, 35] This variegated presentation remains a key limitation of the model. Offspring within MIA models

have disruptions in a variety of body systems, highlighting the impact of disrupting development during critical periods of gestation. Some of these changes are anatomic. Clear alterations of cortical layering, detected by decreased special AT-rich sequence binding protein 2 (SATB2) staining[35] and involving cortical patches centered around the dysgranular zone of primary somatosensory cortex,[40] have been reported in MIA offspring. Alterations in the integrity of the gut barrier, accompanied by alterations in gut expression of tight junction genes, gut microbiota changes, and increased gut permeability, have also been reported.[19]

In addition to these more overt alterations, MIA models also exhibit a diverse range of functional impairments. Similar to the difficulties that schizophrenia symptoms pose for patients attempting to function in society,[4] MIA offspring exhibit deficits in a variety of domains necessary for survival and reproduction. At the molecular level, key signaling molecules needed for appropriate neuronal function, such as brain-derived neurotropic factor;[34] phosphorylation of its receptor, TrkB;[34] and the extracellular signaling molecule reelin;[41] are dysregulated in frontal cortex of MIA offspring. At the behavioral level, MIA offspring have been shown to exhibit deficits in patterns of locomotor behavior.[20] Altered memory function[34, 42, 43] and social deficits[19, 35, 38, 40] have also been reported in MIA offspring. As pups, MIA offspring mice exhibit altered patterns of ultrasonic vocalizations in response to maternal separation.[35, 38, 40] Adult male MIA offspring mice have also been shown to produce fewer ultrasonic vocalizations in response to a novel female. Decreased social contacts, increased latency to contact, and decreased social interaction time have also been reported.[19, 20] Increased stereotyped behavior has been observed in the marble burying assay[19, 38] and increased anxiety-like behavior has been seen in the open field in MIA offspring.[19, 38, 40] In a more complex executive task, MIA offspring have decreased performance in the delayed spatial alternation task at 40 s, but not 10 s of delay.[22] MIA therefore produces a variety of behavioral effects in adult offspring, resulting in numerous possibilities for impaired survival.

MIA offspring have also been shown to exhibit deficits in sensorimotor gating,[5] a phenotype observed to be dysregulated in schizophrenia as well as other conditions such as obsessive-compulsive disorder, Tourette syndrome, and Huntington's disease.[44] Sensorimotor gating is an evolutionarily conserved phenomenon in which organisms are able to manage incoming sensory information, excluding information that is not needed for survival.[45] Sensorimotor gating is observed across a variety of modalities, with gating to acoustic and tactile stimuli being possibilities for evaluation in organisms.[44] The most common mechanism of evaluating sensorimotor gating is prepulse inhibition of startle (PPI), in which a stimulus of sufficient magnitude to elicit a startle response (pulse) is presented to an organism with or without a lower magnitude, but detectable, stimulus (prepulse). In an organism with a properly functioning nervous system, the presence of the prepulse will decrease the magnitude of the startle to the pulse. The prepulse thus, in essence, telegraphs the pulse, allowing an organism to reduce the resources devoted to responding to it.[44] Prepulse inhibition involves both cortical and subcortical structures, with both prepulse processing and top-down modulatory circuits being involved.[46] A variety of MIA approaches have revealed PPI deficits in adult offspring, supporting the validity of the model.[19, 20, 47] In addition, it has been shown that the antipsychotics clozapine and chlorpromazine, which have been used in schizophrenia treatment, promote improvement in PPI specifically in MIA offspring.[20]

In addition to the gross anatomic, molecular, and behavioral changes, MIA models have also been shown to exhibit synaptic dysfunction.[48] This, similar to other changes in MIA models, reflects alterations observed in neurodevelopmental disorders such as schizophrenia. Postmortem samples from schizophrenia subjects have shown a decrease in basal spine density in prefrontal cortex pyramidal neurons.[49] In the tufts of apical dendrites of cortical pyramidal neurons, a decrease in total dendritic spines is observed in juvenile mice, an alteration that lasts until adulthood.[48] Layer 5 neurons in the medial prefrontal cortex of rats, in contrast, exhibited a decrease in total basal spine density in adult, but not juvenile, MIA offspring.[50] Increased total and filopodia spines in basal dendrites of layer 5

intrinsically bursting neurons have also been reported following MIA.[51] Dendritic spine dysregulation, accompanying behavioral alterations, is therefore a well-established phenotype in MIA offspring.

IB. Multiple lines of evidence implicate the 5-HT_{2A}R in schizophrenia pathophysiology.

IB.1. 5-HT_{2A}R pharmacology is relevant for schizophrenia and associated phenotypes.

Alterations in neurotransmitter signaling systems have long been proposed to be a crucial component of schizophrenia pathophysiology.[2] Drugs targeting monoaminergic receptor systems have been a mainstay of schizophrenia treatment for decades, with both typical and atypical antipsychotics targeting them, particularly the dopamine D_2 receptor.[52] Among the monoaminergic receptors implicated in schizophrenia pathophysiology is the serotonin 5-HT_{2A} receptor (5-HT_{2A}R).[52, 53] The 5-HT_{2A}R is a G_q-coupled seven-transmembrane receptor within the serotonergic receptor system.[54] It, alongside the closely related 5-HT_{2B} and 5-HT_{2C} receptors, belongs to one of the seven serotonin receptor subfamilies, all of which, excluding 5-HT_3R, are G protein-coupled receptors.[55, 56] The 5-HT_{2A}R is found in brain regions such as the cortex, thalamus, and hippocampus,[57] as well as on vascular and immune cells.[58, 59] Within mouse cortex, 5-HT_{2A}R expression is observed primarily on layer 5 pyramidal cells, a subset of interneurons, and cells in layer 6b adjacent to the corpus callosum.[60]

5-HT_{2A}R pharmacology implicates the receptor in schizophrenia-related phenotypes. Hallucinogenic drugs, also called psychedelics, such as psilocybin, lysergic acid diethylamide (LSD), and 2,5-dimethoxy-4-iodoamphetamine (DOI), represent a substantial subset of 5-HT_{2A}R agonists.[61, 62] In humans, these drugs produce thought and perceptual alterations that are reminiscent of features observed in schizophrenia.[63] Other 5-HT_{2A}R agonists, such as lisuride, do not produce these perceptual alterations in humans.[64] Explorations into mechanisms to explain this difference are ongoing, but these pharmacologic effects are thought to in part involve elements such as differential receptor phosphorylation,[65] biased

agonism,[66] and divergent activation of downstream signaling genes.[62] In rodents, 5-HT_{2A}R agonists that produce hallucinations in humans elicit a specific behavior called the head twitch response. In 5-HT_{2A}R knockout mice, psychedelics fail to increase rates of head twitch response[62, 67] and 5-HT_{2A}R antagonists are similarly able to block the effect of psychedelics, both in rodents[68, 69] and in humans.[70] This evidence therefore converges on the fact that psychedelic drugs elicit their hallucinogenic effect in a 5-HT_{2A}R-dependent manner. 5-HT_{2A}R signaling is therefore able to prominently impact thought and perception, phenomena whose disruption are hallmarks of schizophrenia.

In addition to the psychedelic effect of some 5-HT_{2A}R agonists, many atypical antipsychotic drugs, such as clozapine and risperidone, possess a relatively high affinity for the 5-HT_{2A}R and serve as antagonists for the receptor.[52] Some of these drugs, clozapine in particular, have been found to be more effective in the context of treatment-resistant schizophrenia than first generation, or typical, antipsychotics, such as haloperidol.[4] Inhibition of 5-HT_{2A}R signaling is thought to play a role in the effectiveness of this class of antipsychotics.[52] In addition, the highly selective 5-HT_{2A}R inverse agonist pimavanserin is effective in Parkinson's disease psychosis, for which it has exhibited improvement relative to placebo.[52, 71, 72] Therefore, through drugs that promote and inhibit its signaling, the 5-HT_{2A}R is implicated in schizophrenia-relevant phenotypes.

IB.2. 5-HT_{2A}R dysregulation has been demonstrated in both schizophrenia and MIA models.

In addition to the pharmacologic evidence suggesting 5-HT_{2A}R relevance for schizophrenia, more direct evidence is available from postmortem samples. Within the prefrontal cortex (Brodmann area 9), postmortem samples from human schizophrenia subjects exhibit increased 5-HT_{2A}R density relative to age-matched controls.[53] Interestingly, this finding was only present in samples from subjects that were antipsychotic-free at death,[53] suggesting that a component of antipsychotic response may involve

decreasing 5-HT_{2A}R density. In another study in postmortem prefrontal cortex samples from schizophrenia subjects and controls, using a radiolabeled 5-HT_{2A}R agonist, neutral antagonist, and inverse agonists, it was found that increased density of the 5-HT_{2A}R was observed with the agonist, [^{3}H]LSD in samples from antipsychotic-free schizophrenia subjects, while decreased density was observed with the inverse agonist, [^{18}F]altanserin, suggesting that there is increased presence of a pool of 5-HT_{2A}R in a state able to be activated,[73] further supporting increased 5-HT_{2A}R signaling as a component of schizophrenia pathophysiology.

MIA models reflect the increase in 5-HT_{2A}R density observed in human samples. Increased 5-HT_{2A}R expression in mouse frontal cortex has been observed in MIA offspring at both the receptor density and mRNA level, with increases being observed in models induced with mouse-adapted influenza,[21, 43] poly-(I:C), and variable stress.[22, 74] Increased 5-HT_{2A}R immunoreactivity has also been shown in prefrontal cortex in male, but not female, MIA offspring rats following induction with LPS.[32] In addition to the dysregulation of the receptor itself, increased expression of key downstream signaling molecules, *PLCβ1* and *RGS4*, has been shown.[74] The pharmacologic effects of 5-HT_{2A}R agonists have also been shown to be altered in MIA offspring. Induction of mRNA for genes such as *c-fos*, *Egr-1*, *Egr-2*, *BDNF*, and *COX-2* by the hallucinogen DOI are potentiated in frontal cortex of MIA offspring mice.[21, 74] In MIA offspring rats, increased c-Fos protein is observed following DOI administration in the ventromedial prefrontal cortex in males while MIA offspring females exhibit decreased c-Fos induction in both dorsomedial and ventromedial prefrontal cortex.[32] At the behavioral level, increased rates of the head twitch response following DOI administration are observed in MIA mouse offspring.[21, 22, 74] Interestingly, both this increase in head twitch as well as the increase in 5-HT_{2A}R density itself are not observed in prepubertal mice.[21, 22] Thus, similar to schizophrenia being an adult onset disorder, 5-HT_{2A}R changes that occur in MIA models are an adult-onset phenomenon.

IB.3. The 5-HT_{2A}R and its signaling have been implicated in key MIA-related phenotypes.

In addition to the dysregulation of 5-HT_{2A}R and its signaling pathways in MIA models, there are specific MIA-associated phenotypes in which the 5-HT_{2A}R has been implicated, through both MIA models and independent paradigms. The degree to which MIA-induced alterations in these phenotypes are 5-HT_{2A}R-dependent, however, remains unknown. One of these paradigms is PPI. Multiple lines of evidence suggest that the 5-HT_{2A}R and its signaling are important modulators of PPI. In healthy humans, administration of the 5-HT_{2A}R agonist prodrug psilocybin produces PPI deficits at a short interstimulus interval while increasing it with longer interstimulus intervals.[75] In rats, psychedelics such as DOI and LSD have been shown to produce PPI deficits,[76] with the effect of LSD being blocked by the 5-HT_{2A}R antagonist MDL 11,939.[64] In addition, psychedelics such as DOI have in some studies been shown to induce PPI deficits in mice, though this effect appears to be less consistent than in other species.[77] In addition, homozygosity for the TT/AA allele of the T102C/A1438G allele of the *5-HT_{2A}R* promoter is associated with increased baseline PPI in healthy humans.[78] There is therefore a large body of evidence implicating 5-HT_{2A}R signaling in PPI, suggesting a need for further investigation into the significance of the receptor for this behavioral paradigm within the context of MIA.

Frontal cortex dendritic spine density also has evidence for potential 5-HT_{2A}R involvement. Dendritic spines are a receptive component of excitatory synapses that exhibit a variety of morphologies depending on synaptic strength and activity, rendering them an essential component of synaptic plasticity. Spine morphologies on mature neurons include stubby, thin, and mushroom, with mushroom spines being understood to represent the most robust synapses.[79] 5-HT_{2A}R knockout mice on a C57BL/6J background have been shown by our group to exhibit decreased frontal cortex total spine density as well as decreases in stubby and thin spines relative to wild types,[80] suggesting that the receptor plays a role in determining spine density in this brain region. The ability of 5-HT_{2A}R agonists to affect spine density and plasticity has been a recent topic of interest, particularly in the context of novel approaches

to depression treatment.[80-82] In rat cortical neuronal cultures, administration of the psychedelics LSD, DOI, and *N*,*N*-dimethyltryptamine increase dendritic spine density. Similar increases in spine density in rat cortex are observed with systemic *N*,*N*-dimethyltryptamine administration.[83] Chronic treatment with the atypical antipsychotic clozapine in mice results in a decrease in 5-HT_{2A}R density in mouse frontal cortex as well as a decrease in the density of mushroom spines in a manner dependent on a downstream 5-HT_{2A}R signaling target.[84] Additionally, the 5-HT_{2A}R agonist DOI has been shown by our group to produce increased stubby and thin spine density in a 5-HT_{2A}R-dependent manner in mouse frontal cortex.[80] Thus agents that promote or inhibit 5-HT_{2A}R signaling have impact on cortical dendritic spine density, prompting further inquiry into the degree to which 5-HT_{2A}R alterations underlie the dendritic spine alterations observed in MIA offspring.

IC. Glucocorticoid receptor alterations may underlie 5-HT_{2A}R dysregulation in MIA models.

IC.1. Stress and glucocorticoid receptor signaling have been implicated in 5-HT_{2A}R regulation.

Although there is strong evidence to demonstrate 5-HT_{2A}R dysregulation in MIA models, the underlying cause of this dysregulation remains unknown. In light of the numerous lines of evidence implicating the receptor in schizophrenia-related phenotypes, the underlying cause of altered 5-HT_{2A}R expression in the model is important to address. Among the potential causes of 5-HT_{2A}R dysregulation within the context of MIA, alterations in glucocorticoid receptor (GR) signaling are an appealing target for exploration. Schizophrenia is conceptualized as a disorder produced in part by stressors experienced by susceptible individuals[5, 18] and GR signaling, as a component of the hypothalamic-pituitary-adrenal axis, is an integral part of the mammalian stress response system.[85] Alterations in glucocorticoid signaling have been proposed to play a role in schizophrenia pathophysiology.[86] Some, but not all studies of cortisol secretion in schizophrenia patients relative to controls reveal alterations in the disorder.[87] Within an

Australian cohort, postmortem prefrontal cortex samples reveal dysregulation of key signaling molecules in the GR signaling system, with increased mRNA expressions of the negative regulator *FKBP5* and the chaperone *PTGES3* as well as decreased mRNA expression of the negative regulator *BAG1*.[88] Dysregulation of GR signaling has also been observed in MIA models, with increased plasma corticosterone being observed in female, but not male, MIA offspring rats under standard housing conditions.[31] *GR* mRNA was decreased in the amygdala of both male and female MIA offspring rats, with *FKBP5* mRNA also decreased in the female amygdala.[31] Although the finding was observed in juvenile (P42) rats, MIA offspring males, but not females, exhibit both increased corticosterone and decreased GR immunoreactivity in the hippocampus.[30]

The relationship of both receptors to stress serves as additional evidence that GR dysregulation may play a role in 5-HT_{2A}R dysregulation in MIA models. The 5-HT_{2A}R and its signaling have been found to be susceptible to a wide variety of stressors. Maternal separation of pups, an early life stressor, increases rates of head twitch in response to the 5-HT_{2A}R agonist DOI in rats.[89] LPS administration to adult mice has been shown to increase frontal cortex 5-HT_{2A}R immunoreactivity[90] while sleep deprivation in mice increases cortical expression of *5-HT_{2A}R* mRNA.[91] The pharmacologic stressor, acute methamphetamine binge, produces increased murine frontal cortex 5-HT_{2A}R immunoreactivity and rates of DOI-induced head twitch response as well.[92] Thus stress, a key component of the response to which is mediated by the hypothalamic-pituitary-adrenal axis, has been extensively found to regulate 5-HT_{2A}R.

Direct regulation of the 5-HT_{2A}R by the GR has also been observed. Use of transgenic mice containing a yeast artificial chromosome to increase GR expression results in increased 5-HT_{2A}R immunoreactivity in the hippocampus and increased 5-HT_{2A}R density in the frontal cortex, while GR heterozygote mice exhibit decreased 5-HT_{2A}R density in frontal cortex.[93] Exposure to corticosterone, the endogenous GR ligand in rodents, in organotypic hippocampal slice cultures from mice also increases 5-HT_{2A}R immunoreactivity.[93] In intact rats, a short course of high dose corticosterone is sufficient to increase

rates of the head shake behavior (essentially the same behavior as head twitch response in mice) following DOI administration, though this study did not investigate the molecular alterations that might be responsible for this phenotype.[94] Another study, using an intraventricular siRNA approach to knock down GR expression in the rat brain produces increased rates of DOI-induced head shakes as well as increased 5-HT_{2A}R density and mRNA expression in the frontal cortex.[95] There is therefore significant evidence establishing that GR signaling plays a role in modulating 5-HT_{2A}R expression. Apparent discrepancies between the various studies, however, prevent the directionality of the regulatory relationship from being clearly established.

IC.2. Potential mechanisms have been identified for GR regulation of 5-HT_{2A}R expression in MIA models.

To discuss potential mechanisms by which the GR might exert its regulatory effect on 5-HT_{2A}R expression, a discussion of basic GR signaling mechanisms is needed. The GR, alongside receptors such as those for progesterone and estrogen, is within the nuclear receptor family.[96] As a nuclear receptor, its endogenous ligand, cortisol in humans and corticosterone in rodents, is able to cross the cell membrane and bind the GR in the cytoplasm.[88, 96-98] Hormone binding induces conformational and protein interaction changes in the receptor, promoting nuclear translocation.[98] Once in the nucleus, the GR acts as a transcription factor, promoting or inhibiting gene expression depending on both the particular glucocorticoid response element (GRE) at a particular locus and the protein interaction partners of the GR within a particular context.[88, 98] The GR possesses a wide variety of protein binding partners, such as the immunophilin positive and negative regulators, FKBP4 and FKBP5, respectively, which modulate behavior of the receptor.[98] Given that the GR is at the center of a complex signaling pathway, potential

mechanisms by which it could regulate the 5-HT_{2A}R include both direct action as a transcription factor [96] as well as downstream signaling mechanisms within a more complex signaling cascade.[99]

In support of direct GR regulation of the 5-HT_{2A}R, a putative response element in the GR subfamily has been identified. This progesterone response element on the human *5-HT_{2A}R* promoter was demonstrated to be bound by the GR in vitro by electrophoretic mobility shift assay.[100] The site is conserved across species, with a similar sequence being found on the murine *5-HT_{2A}R* promoter.[100] Thus, a mechanism capable of linking GR signaling and 5-HT_{2A}R dysregulation within the context of MIA has been proposed.

In this dissertation, the contribution of GR signaling alterations to *5-HT_{2A}R* dysregulation in a poly-(I:C)-induced MIA mouse model is investigated. In MIA offspring and controls, GR immunoreactivity in the nuclear and cytoplasmic compartments of mouse frontal cortex are investigated; to determine potential MIA-induced alterations in GR occupancy of the putative binding site, enrichment of the GR at the *5-HT_{2A}R* promoter is also evaluated in these mice. 5-HT_{2A}R knockout mice were used to determine if key MIA-relevant phenotypes are 5-HT_{2A}R dependent. To evaluate the translational significance of these studies, GR immunoreactivity was investigated in postmortem prefrontal cortex samples from schizophrenia subjects and controls. To further explore the regulatory relationship between GR signaling and *5-HT_{2A}R* expression, additional models of corticosterone administration and intracortical viral vector gene delivery were also used. The data generated from these models support a negative regulatory relationship between GR signaling and 5-HT_{2A}R expression, with implications for the phenotypes observed in a MIA mouse model.

Methods

M1. Materials and Drugs

Poly-(I:C) potassium salt was obtained from Millipore Sigma (P9582). After weighing, poly-(I:C) was dissolved in normal saline to a concentration of 4 mg/ml poly-(I:C) (the total salt concentration was 40 mg/ml) in a 50 ml Falcon tube by rotating the tube and then spun down briefly at 800 × g. The resulting solution was then aliquoted and stored at -20°C until the day that mice were injected.

Corticosterone was obtained from Millipore Sigma (46148) and was diluted in DMSO to a concentration of 100 mg/ml. Aliquots were stored at -20°C until a working solution was needed. This solution was diluted 1:3 DMSO : ethanol to generate a final injection solution.

Diethylpyrocarbonate-treated water was generated by stirring 0.1% by volume DEPC (Sigma-Aldrich) into ddH_2O at room temperature overnight in a fume hood. The DEPC was then inactivated by autoclaving and the water was stored at room temperature until use.

M2. ΔGR Vector Generation

Neuro-2a Cell Culture

Neuro-2a cells (original stock obtained from ATCC, product CCL-131™) were maintained in a growth medium of DMEM with glucose, L-glutamine and sodium pyruvate (Corning) supplemented with 5% qualified FBS (Gibco) and 1% 10,000 U/ml penicillin/ 10,000 µg/ml streptomycin solution (Gibco). Cells were split as needed by removal of growth medium, washing with DPBS (Corning), incubation in 0.25%

trypsin-EDTA solution (Sigma Aldrich) to release the cells, and addition of growth medium to quench the trypsin. Cells were then transferred to new flasks with fresh growth medium.

Cloning, Restriction, and Ligation

The initial cDNA used to generate the ΔGR vector was obtained from a frontal cortex sample from an adult male 129S6/SvEv mouse (see Table M1 for primers). 100 ng of cDNA were amplified using 2.5 units of *PfuUltra* high fidelity DNA polymerase (Agilent) in a reaction buffer consisting of 1× *PfuUltra* HF reaction buffer supplemented to a final concentration of 3 mM Mg^{2+} with $MgSO_4$, 0.5 µM forward primer, 0.5 µM reverse primer, and 25 mM dNTPs (each). Primers were designed to amplify the coding sequence for residues 1-524 of the mouse glucocorticoid receptor as well as introduce a BamHI restriction site upstream and a AscI site downstream of the construct. Amplification was carried out in a thermal cycler according to the following program: 95**°**C for 2 min, 30× (95°C for 30 s, 60°C for 95°C, 72°C for 1 min), 72°C for 10 min.

The resulting PCR products were resolved on an 0.5% agarose gel containing 0.006% ethidium bromide in SB buffer (10 mM NaOH, 38 mM H_3BO_3 in diH_2O). The ΔGR amplification product band was visualized using a gel documentation system (Thermo Scientific) and excised. DNA from the band was then extracted using a PCR clean-up/gel extraction kit (Macherey-Nagel). The excised DNA in agarose was incubated in 200 µL Buffer NT1 at 50°C for 5-10 min with intermittent vortexing until the gel was dissolved. DNA was then bound to a NucleoSpin column and centrifuged at 11,000 × g for 30 s. The column was then washed twice by two rounds of adding 700 µL Buffer NT3 and centrifuging at 11,000 × g for 30 s. The column was then dried by an additional spin at 11,000 × g for 1 min. DNA was eluted in three rounds by addition of 20 µL of Buffer NE heated to 70°C, incubation at room temperature (5 min for the first round and 1 min for the subsequent two), and centrifugation at 11,000 × g for 1 min (final elution volume of 60 µL).

0.3 µL of the purified DNA was then amplified once again with the ΔGR primers, run on a 0.5% agarose gel, and purified a subsequent time as before, with the exception that the first incubation before elution was for 1 min. As a source for the destination vector for the ΔGR construct, we used an adeno-associated virus plasmid containing a *CaMKIIα*-BamHI-5-HT_{2A}R-AscI-P2A-eYFP construct (which was generated and is available within the Maeso lab). 1 µg of the vector plasmid and 0.5 µg of the ΔGR construct were cut with 10 units each of BamHI and AscI in CutSmart™ Buffer (New England Biolabs) for 1 hour at 37°C. For the vector reaction, 1 µL of calf intestine alkaline phosphatase (New England Biolabs) was added for the last 10 min. The vector reaction product was run on a 0.5% gel and the band of the appropriate size for the cut backbone vector was excised. Both this band and the ΔGR construct restriction product were purified using the same kit as before. These purified products were then ligated with T4 DNA ligase (New England Biolabs) with T4 DNA Ligase Buffer in ddH_2O and a 1:10 vector: insert ratio (25 ng vector, 62.5 ng insert).

Plasmid Purification and Vector Packaging

1 µL of this ligation product was added to 50 µL of XL1-Blue competent cells (Agilent) for transformation. The cells and ligation product were incubated on ice for 30 min, heat shocked at 42°C for 45 s, and then returned to ice for 2 min. 500 µL of room temperature S.O.C. medium (Invitrogen) were added and the cells were incubated at 37°C for 1 hour with shaking. Cells were then plated on ampicillin selective plates (0.05 mg ampicillin/ml LB agar) made with LB agar and incubated overnight at 3**7**°C. Colonies were picked the next day and further incubated in 5ml LB broth containing 0.05 mg/ml ampicillin. Plasmids from these colonies were then purified using a QIAPrep Miniprep kit (Qiagen). The colonies were pelleted by centrifugation at 5400 × g for 10 min at 4°C. The pellet was resuspended in 250 µL of Buffer P1 supplemented with RNase A and LyseBlue reagent. 250 µL of Buffer P2 were added and samples were mixed by inversion, then incubated at room temperature for 5 min. 350 µL of Buffer N3 were added and samples were mixed by inversion, then centrifuged at 17,900 × g for 10 min. 800 µL of

the supernatant was transferred to a QIAprep 2.0 Spin Column and centrifuged at 17,900 × g for 30 s. The column was washed with 500 µL Buffer PB and centrifuged at 17,900 × g for 30 s, then washed with 750 µL buffer PE. The column was then dried by centrifugation at 21,130 × g for 1 min. DNA was eluted in 50 µL Buffer EB by adding buffer to the column, incubating for 1 min, and centrifuging at 17,900 × g for 1 min. The resulting purified plasmids were sequenced (Eurofins) to confirm the correct insert.

A colony containing the correct insert confirmed by sequencing was grown in 250 ml LB with 0.05 mg/ml ampicillin overnight at 3**7**°C. Plasmids from the colonies were then purified using a Plasmid Maxi kit (Qiagen). The colonies were centrifuged at 6,000 × g for 15 min at 4°C and the pellet was resuspended in 10 ml of Buffer P1 supplemented with RNase A solution and LyseBlue reagent. 10 ml of Buffer P2 were added and samples were inverted and incubated at room temperature for 5 min. 10 ml of chilled Buffer P3 were added and mixed by inversion, then incubated on ice for 20 min. The samples were then centrifuged at 20,000 × g for 30 min at 4°C. A Qiagen 500 tip column was equilibrated with 10 ml of Buffer QBT and the supernatant from sample centrifugation was added to the column. The column was then washed twice with 30 ml of Buffer QC. DNA was eluted with 15 ml Buffer QF and DNA was precipitated with 10.5 ml of isopropanol. Samples were then centrifuged at 15,000 × g for 30 min at 4°C. The supernatant was removed and the DNA pellet was washed with 5 ml of 70% ethanol. Following centrifugation at 15,000 × g for 10 min, the supernatant was removed, the pellet was dried, and DNA was dissolved in 800 µL of DEPC-treated water (Quality Biological). Following validation of the construct in N2a cells (see below), the final *CaMKIIα*-ΔGR-P2A-eYFP plasmid was packaged into AAV8 viral particles by the UNC Vector Core.

Transfection of N2a Cells

To prepare a surface for adherence of N2a cells, #1 coverslips (Fisherbrand) were incubated in 10 M NaOH at room temperature overnight with gentle shaking, washed, and autoclaved. The coverslips were

coated in poly-D-lysine (Sigma-Aldrich) in borate buffer (50.1 mM BH_3O_3, 12.5 mM $Na_2B_4O_7{\cdot}10H_2O$) overnight. The next day, coverslips were washed three times in sterile water, then allowed to dry. For transfection experiments where immunofluorescence was the endpoint, N2a cells were then plated on these poly-D-lysine-coated coverslips and allowed to grow. N2a cells on coverslips in 6 well plates were transfected with 4 µg of plasmid DNA with 5 µL of polyethyleneimine made up to a final volume of 300 µL with Opti-MEM™ reduced serum medium (Gibco) that were added to growth medium. Prior to transfection, DNA, polyethyleneimine, and Opti-MEM™ were combined, shaken, and incubated for 10 min at room temperature. For mock transfection, only polyethyleneimine and Opti-MEM™ were added to cells. The medium was replaced with regular growth medium the day after transfection. Cells were processed for immunofluorescence 48 hours after transfection.

For western blotting, N2a cells in 10 cm plates were transfected with 6 µg of plasmid DNA with 10 µL of polyethyleneimine made up to a final volume of 300 µL with Opti-MEM™ as described above. To harvest, transfected N2a cells were washed with DPBS three times before being dislodged with a cell scraper in cold DPBS. Cells were then pooled and spun down for 5 min at 188 × g at room temperature. The supernatant was removed and pelleted cells were frozen at -80°C until they were subjected to subcellular fractionation as described below.

Immunofluorescence in N2a Cells

Transfected cells grown on coverslips were fixed by incubation in 4% PFA in PBS (137 mM NaCl, 2.68 mM KCl, 10.1 mM Na_2HPO_4, 1.76 mM KH_2PO_4, pH 7.4) at room temperature for 15 min with shaking. Cells were washed for 5 min in PBS three times with shaking before permeabilization in 0.2% Triton X-100 in PBS for 10 min. Cells were then washed again before incubation in blocking buffer (5% FBS, 1% BSA, 0.05% NaN_3 in PBS) for 30 min at room temperature with shaking. Coverslips containing the cells were then placed facedown in 50 µL of primary antibody (see below) in blocking buffer on a slide that had

been covered with Parafilm (Bemis) and incubated for 1.5 hours at room temperature. Cells were then washed in PBS and incubated in 50 µL of a fluorescent secondary antibody for 1 hour in the dark on a Parafilm-covered slide. After washing 6 times in PBS, nuclei were stained by incubation in a 1:1000 dilution of 20 mM Hoechst solution (final concentration 0.02 mM; Thermo Scientific) in DPBS for 5 min. Slides were washed twice in PBS, dried, and mounted in Prolong Diamond antifade mountant. After curing overnight, slides were sealed and stored at 4°C until use. The plasmids used were the *CaMKIIα*-ΔGR-P2A-eYFP plasmid described above as well as a plasmid to express the full-length human GR under the control of the CMV promoter (Addgene construct pCMV-GR11; plasmid #89105 deposited by the laboratory of Dr. Elizabeth Wilson). The primary antibody used was 1:50 mouse-anti-GR (Santa Cruz, sc-393232) and the secondary antibody used was 1:1000 Alexa Fluor 568-conjugated goat-anti-mouse (Invitrogen, A-11004).

Images were acquired using the 405, 488, and 561 nm laser lines of an LSM 710 confocal laser scanning microscope (Zeiss). A 63x objective was used, resulting in 1912 × 1912 pixel images with a 0.07 µm × 0.07 µm pixel size.

M3. Animal Techniques

Animals Used

Experiments were conducted in adult mice (10.5-22.5 weeks). Mice were obtained from either Charles River (C57BL6/N), Taconic (C57BL6/N and 129S6/SvEv), Jackson Laboratories (C57BL6/J) or, for wild type and 5-HT_{2A}R knockout mice, from the ongoing mouse colonies in the González-Maeso laboratory (on a background strain of Taconic 129S6/SvEv). The 5-HT_{2A}R KO mice used were complete knockouts that contain a stop cassette to interfere with transcription and translation (Weisstaub et al, 2006). Experiments requiring 5-HT_{2A}R KO mice and the corticosterone time course (see below) were conducted

in mice on a Taconic 129S6/SvEv background from the Maeso colony. All other experiments were conducted in C57BL6/N mice from Charles River. C57BL6/N mice from Taconic and C57BL6/J mice from Jackson Laboratories were used exclusively in the microbiome evaluation experiment (see below).

Male mice were used for experimental animals, except for dendritic spine experiments and for RT-qPCR validation of the ΔGR vector, where both sexes were used. Female mice were used for poly-(I:C) validation experiments, evaluation of cecal 16S rRNA gene presence, immunofluorescence validation of the ΔGR vector, and as mothers in maternal immune activation experiments. Older mice (39 weeks) were used for immunofluorescence validation of the ΔGR vector. Within experiments, mice were age matched between groups. All procedures involving animals were approved by VCU's Institutional Animal Care and Use Committee. Every effort was made to minimize animal use and distress.

Genotyping

Mouse ear samples were collected and proteinase K digested in GNT-K buffer (0.01% by weight gelatin, 0.45% by volume IGEPAL CA-630, 0.45% by volume Tween 20, 0.01% by weight proteinase K, 50 mM KCl, 1.5 mM $MgCl_2$, 10 mM Tris base, pH 8.5) for 2 hours at 55°C, followed by heat inactivation at 95°C for 15 min. 3 µL of the resulting DNA-containing solution were combined with 22 µL of working Taq polymerase and primer solution (12.5 µL 2× DreamTaq Green PCR Master Mix [Thermo Scientific], 0.455 µM WT forward primer, 0.909 µM 5-HT_{2A}R KO forward primer, 0.455 µM common reverse primer (see Table M1 for sequences), remainder of the volume made up with ddH_2O) and amplified according to the following program: 95°C for 1 min, 2× (95°C for 15 s, 64°C for 15 s, 72°C for 45 s), 6× (95°C for 15 s, 61°C for 15 s, 72°C for 45 s), 20× (95°C for 15 s, 58°C for 15 s, 72°C for 45 s), 20× (95°C for 15 s, 55°C for 15 s, 72°C for 45 s), 72°C for 10 min, hold at 4°C. Amplified samples were then resolved on a 0.5% agarose gel and visualized using a gel documentation system as described above. A 500 bp amplification product

indicated a WT allele and a 410 bp product indicated a *5-HT$_{2A}$R* KO allele. Earlier in the experiments, an approach using PuReTaq™ Ready-To-Go™ PCR beads (Cytiva) was used for genotyping.

Poly-(I:C) Validation

Adult female C57BL6/N WT or 129S6/SvEv 5-HT$_{2A}$R heterozygote mice were injected i.p. with 20 mg/kg poly-(I:C) and observed for sickness behavior, such as lethargy, ptosis, and hunched posture. After 2.5 hours, the mice were sacrificed by either decapitation and exsanguination for analysis of IL-6 in serum or by cervical dislocation for analysis of *IL-6* mRNA in frontal cortex. Following decapitation, trunk blood was collected and allowed to clot at room temperature for at least 30 minutes. The blood was then centrifuged at 1000 × g at 4°C for 10 minutes; the serum supernatant was collected and stored at -80°C until the day of the ELISA assay. For RT-qPCR, mice were sacrificed by cervical dislocation, the head was dissected, and the brain was removed and washed in normal saline at 4°C. Frontal cortex (+1.4 to +1.9 from bregma) was dissected and stored in an Eppendorf tube at -80°C until use.

Maternal Immune Activation

Female mice used as mothers for MIA experiments were WT C57BL6/N mice from Charles River that had been either ordered timed pregnant or ordered and bred with C57BL6/N males from Charles River. For experiments where WT and 5-HT$_{2A}$R KO offspring were needed, 129S6/SvEv female 5-HT$_{2A}$R heterozygote mice on a Taconic background were bred within the González-Maeso lab colony. For in-house bred mice, females were monitored for a mating plug and pregnancy was evaluated using both weight gain and visual appearance of the flanks. Mouse weights were tracked with a small laboratory scale (Ohaus). On day E12.5 of pregnancy, mice were weighed and injected i.p. with either 20 mg/kg poly-(I:C) or vehicle, then monitored for sickness behavior. MIA at E12.5 was chosen because the first and second trimesters have been shown to be a critical period for increased risk of schizophrenia development following infection in humans[2, 12] and induction at E12.5 has been demonstrated to

produce MIA-induced phenotypes in offspring.[26] To reduce litter loss, injected mice were pair housed with another female of the same strain and provided with enrichment Bio-Huts™ for mice (Bio-Serv) as shelter in the cage. Offspring were weaned between 3-4 weeks of age and were evaluated in molecular and behavioral experiments as adults.

Corticosterone Administration

Corticosterone was prepared as described in the Materials and Drugs section above. Adult mice were injected s.c. with 50 mg/kg corticosterone dissolved in a final solution of 1 DMSO: 3 ethanol. To minimize the amount of DMSO injected into animals, an injection volume of 2 µL/g was used. For the corticosterone time course, all mice (excluding the No Injection group, which received no injections during the time course) received a total of 16 injections over eight days, with the number of vehicle injections and corticosterone injections being determined by the treatment group. Injections were given twice a day, spaced roughly 12 hours apart. Mice were sacrificed 8.5-13 hours after the last injection for molecular analyses to allow washout from the acute effects of corticosterone.

For the short term, high dose corticosterone experiments, mice received 50 mg/kg corticosterone or vehicle s.c. twice a day for four days. Mice were then either sacrificed or tested for PPI 8.5-13.5 hours after the last injection.

Prepulse Inhibition of Startle

PPI experiments were conducted following a previously described paradigm.[101] Mice were placed in SR-Lab™ Startle Response system (San Diego Instruments) chambers and allowed to habituate to background noise for 5 minutes. Following habituation, mice were exposed to 5 startle only trials. They were then subjected to 65 pseudorandomized trials consisting of interspersed no stimulus trials; startle only trials; or 73 dB, 77 dB, or 85 dB prepulse trials. The session concluded with 5 additional startle only trials. %PPI was calculated based on the averages for each trial type during those 65 trials by the

equation: %PPI = (1 - $\frac{\text{VMax of prepulse trials}}{\text{VMax of stimulus only trials}}$) x 100%. Startle magnitude was calculated as the average of the VMax values for the 5 initial startle only trials. Background noise was maintained at 69 dB for the duration of the experiment. The startle-inducing stimulus was a 120 dB pulse lasting for 20 ms. For prepulse trials, a 20 ms prepulse of 73 dB, 77 dB, or 85 dB was administered prior to the startle stimulus. The interstimulus interval was 100 ms from the start of the prepulse to the start of the startle stimulus. The intertrial interval was an average of 15 s, with a range of 12-18 s. Each PPI session lasted a total of about 30 minutes.

M4. Molecular Techniques

ELISA

ELISAs were performed using the Mouse IL-6 ELISA MAX™ kit (BioLegend). The day before assay conduction, 100 µL of a 1:200 dilution of Capture Antibody (ELISA antibodies were included as part of the kit) in coating buffer (100 mM $NaHCO_3$, 33.6 mM Na_2CO_3 in ddH_2O, pH 9.5) was added to wells of a 96 well Nunc MaxiSorp™ plate (Invitrogen) and incubated at 4°C overnight. The next day, the wells were washed (solution added and then plate inverted and tapped on surface to remove liquid) in 300 µL Wash Buffer (137 mM NaCl, 2.68 mM KCl, 10.1 mM Na_2HPO_4, 1.76 mM KH_2PO_4, 0.05% Tween 20, pH 7.4) three times. The wells were then blocked in 200 µL Assay Diluent (137 mM NaCl, 2.68 mM KCl, 10.1 mM Na_2HPO_4, 1.76 mM KH_2PO_4, 1% BSA in ddH_2O, pH 7.4) by sealing and incubating at room temperature for 1 hour with shaking. The wells were then washed 4 times in Wash Buffer. 100 µL of 1:100 dilutions of serum samples in Assay Diluent were added to wells in triplicate, as were mouse IL-6 standards (7.8 – 500 pg/ml) diluted in Assay Diluent, before sealing and incubation with shaking at room temperature for 2 hours. The wells were then washed 4 times in Wash Buffer. 100 µL of a 1:200 dilution of Detection Antibody in Assay Diluent was added to each well and the plate was sealed and incubated at room

temperature for 1 hour with shaking. The wells were then washed 4 times in Wash Buffer before addition of 100 µL of a 1:1000 dilution of Avidin-HRP in Assay Diluent, sealing, and incubation at room temperature for 30 min with shaking. The plate was then washed 5 times in Wash Buffer, with soaking of wells for 30 sec to 1 min during each wash. 100 µL of TMB Substrate Solution (BioLegend, a 1:1 mixture of TMB Substrate A and TMB Substrate B) was added to each well and incubated in the dark for 5-10 min. The reaction was stopped by addition of 100 µL Stop Solution (BioLegend) and absorbance was read at 450 nm with subtraction of the absorbance at 570 nm using a VICTOR Nivo™ multimode plate reader (PerkinElmer). Sample concentrations were determined using the curve obtained using the IL-6 standards.

Total mRNA Extraction

Mouse frontal cortex samples that had been stored at -80°C (as described in Poly-(I:C) Validation above) were thawed on ice. Once thawed, samples were minced with a razor blade before transferring to an Eppendorf tube. The minced tissue was then homogenized in 1 ml of QIAzol lysis reagent (Qiagen) by passing it up and down using a 20G needle and syringe. The homogenized tissue was then transferred to a clean Eppendorf tube and 200 µL of chloroform were added before vortexing for 15 s. The samples were then incubated at room temperature for 3 minutes before centrifugation at 12,000 × g for 4 minutes at 4°C. The resulting aqueous phase was then transferred to a clean Eppendorf tube and mixed with an equivalent volume of 70% ethanol by vortexing. The remainder of the extraction process was completed using a Qiagen RNeasy kit. After vortexing with ethanol, samples were loaded onto RNeasy MinElute spin columns and centrifuged at 8000 × g at room temperature in rounds of 30 s until all of the sample had been loaded onto the columns (two rounds of loading and centrifugation). The columns were then washed with 350 µL of Buffer RW1 and centrifuged at 8000 × g at room temperature for 30 s. On-column DNase I digestion was performed by adding 80 µL of a 1:7 dilution of DNase I stock solution in Buffer RDD from an RNase-Free DNase Set (Qiagen) to the columns and incubating for 15 min at room

temperature. The columns were then washed with 350 µL of Buffer RW1 and centrifuged for 30 s at room temperature. The columns were washed in 500 µL of Buffer RPE and centrifuged for 30 s. For a final wash, 500 µL of Buffer RPE were added to the columns, which were then centrifuged at 21,130 × g for 3 min to remove all liquid. 50 µL of RNase-free water were then incubated on the columns for 2 min before elution of RNA by centrifugation at 8000 × g for 1 min. Sample concentrations were evaluated using a NanoDrop 2000 spectrophotometer measuring at wavelengths of 260 and 280 nm (Thermo Scientific) in anticipation of reverse transcription. Non-sterile tools used to manipulate frontal cortex samples during extraction were sprayed with RNaseZap™ solution (Invitrogen) and rinsed with diH_2O before use.

Reverse Transcription

1000 ng of RNA from each sample were brought to 10 µL volume with ddH_2O. 5 µL of Master Mix 1 (1 µL of 50 µM Oligo(dT), 1 µL 10 mM dNTP mix, 1 µL 100 mM dithiothreitol [all from Invitrogen], 2 µL ddH_2O per sample) were added to each sample before heating at 65°C for 5 minutes. 5 µL of Master Mix 2 (4 µL 5x First-Strand Buffer [250 mM Tris-HCl at pH 8.3, 375 mM KCl, 15 mM $MgCl_2$], 0.5 µL RNaseOUT™ Ribonuclease Inhibitor, 0.5 µL SuperScript™ III Reverse Transcriptase [all from Invitrogen]) were added to each sample, which was then incubated at 50°C for 1 hour followed by heat inactivation of Reverse Transcriptase at 70°C for 15 min. The resulting cDNA was then diluted 1:30 in ddH_2O and stored at -80°C until use.

qPCR

qPCR reactions were performed in quadruplicate for each combination of sample and primer. Each 5 µL reaction contained 2 µL of the 1:30 dilution of cDNA generated by reverse transcription (or 20 ng of DNA for the microbiome evaluation experiment, 2 µL of precipitated gDNA for ChIP experiments; see below) as well as 0.5 µL of 2 µM primer stock solution and 2.5 µL of PowerUp™ SYBR™ Green Master Mix.

Samples and primers were loaded onto MicroAmp™ optical 384 well plates (Applied Biosystems), which were sealed and briefly pulse centrifuged to collect samples at the bottom of the wells. qPCR was performed using a QuantStudio™ 6 Flex Real-Time PCR System (Applied Biosystems). Amplification was for 40 cycles (45 cycles were used for the GR ChIP-qPCR experiment in untreated mice). The median values from amplification quadruplicates were used for analysis. Primers used for qPCR are listed in Table M1.

Microbiome Evaluation

Adult female mice were sacrificed and the cecum and appendix was dissected out and cut based on previously described protocols.[102] Cecum and appendix contents were transferred to pre-weighed Eppendorf tubes using sterile inoculation loops (BD Difco). The tube filled with cecum contents was then weighed again to obtain wet weights and samples were frozen at –80°C until use. DNA was isolated using a PowerFecal DNA Isolation kit (MO BIO Laboratories). Samples were placed in a Dry Bead tube and vortexed with 750 µL of Bead Solution. 60 µL of Solution C1 were added and the tubes were vortexed, then heated at 65°C for 10 min. Cells in the sample were then lysed by vortexing at maximum speed for 10 min. Tubes were centrifuged at 13,000 × g for 1 min and the supernatant was transferred to a clean tube. 250 µL of Solution C2 were added to precipitate other compounds in the sample and tubes were vortexed before incubation at 4°C for 5 min. Tubes were again centrifuged at 13,000 × g for 1 min and the supernatant was transferred to a clean tube. 200 µL of Solution C3 were added and samples were vortexed, then incubated at 4°C for 5 min before an additional centrifugation at 13,000 × g for 1 min. The supernatant was transferred to a clean tube and 1,200 µL of Solution C4 were added and vortexed to facilitate binding of DNA to spin columns. Samples were transferred to a Spin Filter column and centrifuged at 13,000 × g for 1 min in three rounds to load samples onto columns. The columns were then washed with Solution C5 and centrifuged for 1 min at 13,000 × g. The column was then dried by an additional centrifugation at 13,000 × g. After placing the columns into a clean

Collection Tube, samples were eluted into 50 µL of Solution C6 by centrifugation at 13,000 × g for 1 min. The eluted DNA was then stored at -80°C until use. 20 ng of sample were loaded into each reaction for qPCR and values were reported based on copies of the 16S rRNA gene per wet weight of cecum contents.

Subcellular Fractionation

Neuro 2a cells or mouse frontal cortex samples were homogenized in 1 ml of Tris-HCl (50 mM, pH 7.4) supplemented with 0.25 M sucrose using a Teflon-glass homogenizer. The samples were then centrifuged at 1000 × g for 5 min at 4**°**C. The supernatant (S1 fraction) was transferred to a new tube. The pellet (P1 fraction) was resuspended in Tris-HCl and transferred to a new tube for use as the nuclear fraction, which was resuspended in Tris-HCl. The S1 fraction was centrifuged at 40,000 × g for 20 min at 4°C. The resulting supernatant (S2 fraction) was retained as the cytoplasmic fraction. The pellet (P2 fraction) was resuspended in 10 ml of Tris-HCl to wash the pellet. The P2 fraction was then resuspended in 1 ml of Tris-HCl. Protein was quantified using the Bradford protein assay (Bio-Rad Protein Assay Dye Reagent Concentrate) with 10-40 µg of BSA as the standard, measuring absorbance at 595 nm with a Genesys 20 spectrophotometer (Thermo Scientific). Following quantification, the nuclear fraction was centrifuged at 1000 × g for 5 min at 4°C and the supernatant was removed. The P2 fraction was centrifuged at 17,000 × g for 15 min at 4°C and the supernatant was removed. The nuclear, cytoplasmic, and P2 fractions were stored at -80°C until the day of western blotting.

Western Blotting

Samples for western blotting were prepared as follows: 20 µg of protein diluted in Tris-HCl were mixed with 5× Laemmli buffer (7.5% by volume β-mercaptoethanol, 313 mM tris, 10% SDS by weight, 67.5% glycerol by volume, scant volume of bromophenol blue to add color to buffer, in diH_2O). The samples were then heat denatured for 5-10 min at roughly 97**°**C. Samples were then kept on ice until loading.

Samples were loaded onto an SDS-PAGE gel (12%) and run at room temperature using an Mini-PROTEAN Tetra cell system (Invitrogen; running buffer: 192 mM glycine, 25.0 mM tris, 0.347 mM SDS). Samples were transferred onto a nitrocellulose membrane (Amersham™, 0.45 µm pore size) in a Mini Trans-Blot system overnight at 4°C (Invitrogen; transfer buffer: 192 mM glycine, 25 mM tris base, 10% methanol). Blots were then washed in TBST (65 mM tris base, 150 mM NaCl, 0.05% Tween 20, pH 7.6) and blocked for 1 hour at room temperature (blocking buffer: 2.5% by weight nonfat dry milk, 0.5% by weight BSA in TBST). Blots were then incubated in primary antibody (see below) in blocking buffer for 1 hour at room temperature or overnight at 4°C. The blots were washed in TBST, blocked for 30 min at room temperature, and incubated in a 1:5000 dilution of HRP-conjugated secondary antibody for 1-1.5 hours at room temperature. Following a final round of washing, the blots were incubated in a working solution of SuperSignal™ West Pico PLUS Chemiluminescent Substrate (Thermo Fisher, 1:1 mixture of Luminol/Enhancer and Stable Peroxide Solutions) for 5 min at room temperature. The blots were then dried and imaged using a ChemiDoc MP Imaging System (Bio-Rad). Blots were stripped between use of different antibodies by incubation in mild stripping buffer (200 mM glycine, 3.47 mM SDS, 1% Tween 20, pH 2.2) for 15 min at room temperature as necessary. Primary antibodies used were 1:100 mouse-anti-GR (Santa Cruz, sc-393232), 1:3000 mouse-anti-α-tubulin (Abcam, ab7291), and 1:3000 rabbit-anti-β-actin (Abcam, ab8227). Secondary antibodies used were 1:5000 ECL HRP-linked mouse IgG (Amersham, NA931) and 1:5000 ECL HRP-linked rabbit IgG (Amersham, NA934). Densitometry was evaluated using ImageJ (NIH).

Chromatin Immunoprecipitation

Crosslinked chromatin immunoprecipitation (as opposed to native chromatin immunoprecipitation for histones) was performed using a MAGnify™ Chromatin Immunoprecipitation System (Applied Biosystems). One hemisphere of mouse frontal cortex tissue was minced with a razor blade in 250 µL of cold DPBS (Corning), then transferred to an Eppendorf tube. The tissue was then homogenized by

passing it up and down through an 18G needle 10 times, then through a 21G needle 20 times. An additional 200 µL of room temperature DPBS were added, then formaldehyde was added to a final concentration of 1% for crosslinking. Chromatin was crosslinked for 10 min, with swirling of the tubes every 2 min. The reaction was then quenched with a final concentration of 125 mM glycine. The samples were then transferred to fresh tubes and centrifuged at 200 × g at 4**°**C for 10 min. The supernatant was discarded and, to wash the chromatin, 500 µL of cold DPBS were used to resuspend the pellet before centrifuging again at 200 × g at 4°C for 10 min. This process of washing was then repeated a second time.

150 µL of Lysis Buffer containing 1× Protease Inhibitors were added to each pellet and the samples were gently vortexed before incubation on ice for 5 min. Samples were then either snap frozen and stored at -80°C until further processing or taken directly for sonication. The chromatin was then sheared using a Covaris S2 ultrasonicator (done for 20 cycles at Intensity 2 with 200 bursts per cycle, a duty cycle of 5%, and a cycle time of 60 s at 4°C), then transferred to a fresh tube. Debris was pelleted by spinning at 17,000 × g for 5 min at 4°C. The chromatin supernatant was then transferred to a fresh tube.

10 µL Protein A/G Dynabeads (Invitrogen) were added to 100 µL cold Dilution Buffer in PCR tubes, then captured using a magnet. The buffer was removed, then 100 µL of cold Dilution Buffer were added to each tube. 2 µL of 1 mg/ml rabbit-anti-GR (Abcam ab3579) or 1 mg/ml rabbit negative control IgG (Millipore PP64B) were added to the tubes and antibodies were conjugated to beads for at least 1 hour at 4°C.

The sheared chromatin was diluted 1:9 in cold Dilution Buffer with 1× Protease Inhibitors. A 10 µL aliquot of this dilution was kept for the input control. The antibody-conjugated beads were collected on a magnet and the liquid was removed from the tubes. 100 µL of diluted chromatin were added to the beads and the tubes were rotated at 4°C overnight to immunoprecipitate the chromatin. The next day,

beads were captured on a magnet and the liquid was removed. 100 µL of cold IP Buffer 1 were added and used to resuspend the beads, the tubes were rotated at 4°C for 5 min, the beads were captured on a magnet, and the liquid was removed. This washing process was then repeated two more times. 100 µL of IP Buffer 2 were added to the beads, the beads were resuspended, the tubes were rotated at 4°C for 5 min, the beads were captured on a magnet, and the liquid was removed. This washing process was repeated one additional time.

The input samples were thawed and 43 µL of Reverse Crosslinking Buffer and 1 µL of Proteinase K were added. After the second wash with IP Buffer 2, 53 µL of Reverse Crosslinking Buffer and 1 µL of Proteinase K were added to the beads, which were then gently vortexed for resuspension. Crosslinking for the input and immunoprecipitation samples was then reversed by heating at 55°C for 15 min. The beads were then captured and the liquid, which contained the immunoprecipitated DNA, was transferred to a fresh tube. The tubes were incubated at 65°C for 15 min to inactivate Proteinase K, then cooled on ice for at least 5 min.

For each sample, 50 µL of DNA Purification Buffer were combined with 20 µL of DNA Purification Beads and added to the immunoprecipitated DNA and input samples. The samples were pipetted up and down to mix and incubated at room temperature for 5 min. The beads were captured on a magnet and the liquid was removed. 150 µL of DNA Wash Buffer was added to each sample and pipetted up and down to mix. The beads were captured on a magnet and the liquid was removed, then 150 µL of DNA Elution Buffer was added and samples were mixed by pipetting. Samples were incubated at 55°C for 20 min to elute the DNA and beads were captured on a magnet. The liquid, which contained the DNA, was transferred to a new tube and stored at -80°C until the day of analysis. Samples were evaluated by qPCR, with each anti-GR ChIP, IgG ChIP, and input sample being run in quadruplicate. Primers targeting sites on the 5-HT_{2A}R promoter and gene were used for amplification (see Table M1).

M5. Murine Surgeries and Imaging Techniques

Stereotaxic Surgeries

Adult mice were anesthetized with 2% isoflurane (Covetrus) and their heads were shaved around the surgical site using an electric razor. After securing the head in the bite and ear bars of a stereotaxis (Kopf Instruments), lubricant ophthalmic ointment (Major) was applied to protect the eyes and the head was cleaned and sterilized with povidone iodine swabsticks (Dynarex) interspersed with 70% ethanol. Anesthesia was maintained using 1-2% isoflurane via nose cone throughout the procedure. A midline incision was made on the dorsal surface of the head and the skin flaps were secured with bulldog clamps (Fine Science Tools). Subcutaneous tissue above the skull was removed using hydrogen peroxide. Bregma was identified and marked and the skull was established to be flat by adjusting the head until lambda and bregma were at the same dorsoventral coordinate. The injection coordinates were +1.6mm rostrocaudal, -2.4mm dorsoventral, +2.6mm mediolateral relative to bregma. Following calculation of final coordinate values, bilateral holes were drilled in the skull at the rostrocaudal and mediolateral coordinates using an Ideal brand Micro-Drill™. Bilateral Hamilton syringes were advanced through the drilled holes at a 10° angle and positioned at the injection coordinates in mouse brain. 0.5 µL (ΔGR experiments) or 1.5 µL (dendritic spine experiments) of adeno-associated viral vector solution were delivered at a rate of 0.1 µL/min. Following injection, the Hamilton syringes were left in mouse cortex for an additional 5 min before removal. The incision site was then closed using Vetbond™ tissue adhesive (3M) and the mouse was returned to a cage with a heat source for recovery. Mice were monitored for appropriate wound healing as well as signs of distress or hypothermia. Experiments were conducted in injected mice after 3 weeks, when transgene expression is maximal.[103] Vectors used for injection included AAV8-*CaMKIIα*-eYFP and AAV8-*CaMKIIα*-ΔGR-P2A-eYFP, both of which had been packaged by the UNC Vector Core.

Perfusion and Sectioning

Mice that had been injected with the AAV8-*CaMKIIα*-eYFP vector 3 weeks prior were anesthetized with 9 mg/ml ketamine (Henry Schein) / 5 mg/ml xylazine (AnaSed) i.p. in normal saline. Anesthetized mice were suspended using needles through their paws, the abdomen was opened, and the diaphragm was displaced by blunt dissection. The anterior portion of the rib cage was removed, exposing the heart. The left ventricle was pierced by a 22G needle (SURFLO winged infusion set, Terumo) and PBS was pumped into the circulatory system (Mini Pump Variable Flow, Thomas Scientific) to clear it of blood**.** The inferior vena cava was cut to allow for outflow. After about 10 ml of PBS had been pumped through the circulatory system, mice were perfused with 30 ml of 4% PFA in PBS. Following perfusion, the brain was dissected and stored in 30% sucrose in PBS at 4**°**C until sectioning. Perfused frontal cortex was cut into 50 µm sections on a VT1000S vibratome (Leica) using a speed of about 5 and a frequency of about 5 and sections were stored at 4**°**C in PBS until immunofluorescence.

Dendritic Spine Quantification

For immunofluorescence, sections were incubated in 4% PFA in PBS for 20 min. All washes during the IF protocol were conducted with shaking. Sections were washed in PBS for 10 min, then permeabilized in 0.1% Triton X-100 in PBS for 15 min. After an additional two washes in PBS, sections were blocked in blocking buffer (5% BSA in 0.1% Triton X-100 in PBS). Sections were then incubated in a 1:1000 dilution of rabbit-anti-GFP primary antibody (Invitrogen, A-11122) in blocking buffer overnight at 4**°C**. Sections were then washed in PBS and incubated in a 1:2000 dilution of Alexa Fluor 488-conjugated anti-rabbit secondary antibody (Invitrogen, A-11008) in blocking buffer at room temperature for 1 hour. The sections were then washed three times in PBS and mounted on #1.5 coverslips (Fisher) in ProLong Diamond antifade mountant (Invitrogen). After placement on slides, the sections were allowed to cure

overnight before sealing with nail polish top coat (Seche Vite). Slides were stored at 4°C in the dark until imaging.

Slides were imaged by confocal laser scanning microscopy using the 488 nm laser line of an LSM 710 microscope. Z-stacks were acquired for layer 5 dendrites in mouse frontal cortex using a 63× objective with 2.5× zoom, yielding stacks of 632 × 632 pixel images with a pixel size of 0.09 µm × 0.09 µm × 0.2 µm. Files were converted to TIFF files for analysis. Dendrite image stacks were then analyzed using NeuronStudio software[104] by a blinded experimenter. Dendritic lengths were determined by tracing the dendrite images within the software. With its Rayburst sampling algorithm, NeuronStudio was used to classify dendritic spines as stubby, thin, or mushroom in morphology.

Immunofluorescence in mouse cortex

Brains of mice that had been stereotaxically injected with AAV8-*CaMKIIα*-eYFP or AAV8-*CaMKIIα*-ΔGR-P2A-eYFP and perfused as described above were cut into 50 µm sections as described. The resulting slices were then subjected to the same immunofluorescence staining protocol as described in the Dendritic Spine Quantification section, with the following exceptions: The primary antibody used was a 1:50 mouse-anti-GR (Santa Cruz, sc-393232) and the secondary antibody was 1:2000 Alexa Fluor 568-conjugated goat-anti-mouse (Invitrogen, A-11004).

Images were acquired using the 488 and 561 nm laser lines of an LSM 710 confocal laser scanning microscope. A 63× objective was used, resulting in 1912 × 1912 pixel images with a 0.07 µm × 0.07 µm pixel size.

Fluorescein-labeled Probe Design

The National Center for Biotechnology Information Basic Local Alignment Search Tool and Primer-BLAST (NIH) were used to identify a unique 162 bp sequence in mouse *5-HT$_{2A}$R* cDNA spanning exons 1 and 2.

The primer sequences are included in Table M1. The target sequence was amplified from mouse cDNA by PCR with 4 units of Platinum™ *Taq* in 1× PCR Buffer containing 1.5 mM $MgCl_2$, 0.2 mM dNTPs (all from Invitrogen), 0.4 µM forward primer, and 0.4 µM reverse primer using the following program: 95°C for 1 min, 2× (95°C for 15 s, 64°C for 15 s, 72°C for 45 s), 6× (95°C for 15 s, 61°C for 15 s, 72°C for 45 s), 20× (95°C for 15 s, 58°C for 15 s, 72°C for 45 s), 20× (95°C for 15 s, 55°C for 15 s, 72°C for 45 s), 72°C for 10 min, hold at 4°C**.** The PCR product was then run on a 0.7% gel made with low-melting agarose (Gold Biotechnology) containing 0.006% ethidium bromide in SB buffer. The sample was excised and placed in an Eppendorf tube that had been pre-weighed to allow calculation of gel weight. The DNA was then purified using the same Macherey-Nagel PCR clean-up/gel extraction kit as described above, with the following exceptions: buffer NT1 was used at a volume of 200 µL/100 ng gel and the final elution was into 15 µL of Buffer NE.

The purified DNA was then introduced into a plasmid vector using a Zero Blunt™ TOPO™ PCR Cloning kit (Invitrogen). To accomplish this, 4 µL of purified DNA were combined with 1 µL of Salt Solution and 1 µL pCR™-Blunt II-TOPO™ vector (both Invitrogen) and incubated for 30 min at room temperature. 2 µL of the resulting plasmid solution were used to transform One Shot™ TOP10 Chemically Competent *E. coli* (Invitrogen). Cells were left on ice for 30 min, then heat shocked at 40**°**C for 30 s. 250 µL of S.O.C. medium were added and the cells were shaken in tubes at 37°C for 1 hour. 50 or 150 µL of this solution were spread on kanamycin selective plates made with LB agar and cultured at 37°C overnight. The next day, colonies were selected and grown in 5 ml of LB broth with 0.03 mg/ml kanamycin at 37°C overnight. The plasmid was then purified using a QIAprep Spin Miniprep kit (Qiagen) as described above, with the following exception: the initial spin was at 6,800 × g for 3 min at 15-25°C and DNA was eluted into 30 µL of Buffer EB. A NanoDrop 2000 spectrophotometer was used to evaluate plasmid concentration. 3 µg of plasmid were linearized using 60 units of high fidelity HindIII in CutSmart™ Buffer (New England Biolabs) for at least 1 hour at 37°C. The fluorescein-labeled RNA probe was then transcribed using 1 µg of

linearized probe with 40 units of SP6 or T7 polymerase (Thermo Scientific) and 1× Fluorescein RNA Labeling Mix (Roche) in 0.5× Transcription Buffer (Thermo Scientific) at 37°C for 2 hours. The kit enables labeling via incorporation of fluorescein-12-uridine triphosphate into RNA. DNA was removed from the probe by incubation with 2.73 Kunitz units (in 1 µL) of DNase I (Qiagen) at 37°C for 30 min; protein was subsequently removed by incubation with 0.3 milliAnson units (in 0.5 µL) of Proteinase K (Millipore) for 15 min at 55°C, followed by incubation at 90°C for 5 min in order to inactivate the enzyme. To this solution, RNA was precipitated by addition of 20 µL 1× TE buffer made with DEPC-treated water (DEPC-TE buffer; 10 mM tris, 1 mM EDTA, pH 8.0), 32 µL 5M ammonium acetate, and 200 µL ethanol, vortexing and incubating at -20°C for 1 hour. The sample was then centrifuged at 17,000 × g for 30 min at **4**°C and the supernatant was removed. The pellet was resuspended in 250 µL of 70% ethanol made with DEPC-H_2O. The tube was then agitated to remove the pellet from the wall of the tube and the probe was then stored at -80°C. The probe was then centrifuged at 17,000 × g for 30 min at **4**°C, the supernatant was removed, and the pellet was resuspended in 30 µL of RNase-free water (Invitrogen) for use. A sense strand probe for the same *5-HT_{2A}R* site was generated in the same manner and used as a negative control.

Fluorescence *in situ* Hybridization

Adult mice were perfused and brains sectioned as described above, with the following exceptions: RNaseZap™ solution was used to treat all non-sterile tools that contacted the brain and resulting sections. 10 ml DEPC-PBS was used to clear the circulation and perfusion was done with 10 ml of 4% PFA in DEPC-PBS made with electron microscopy grade PFA (Electron Microscopy Sciences). Following perfusion, brains were stored in cryoprotectant (2% by volume DMSO, 20% by volume glycerol in DEPC-PBS) until sectioning. Frontal cortices were cut into 20 µm sections in cryoprotectant and stored at 4°C until hybridization.

20 µm sections of mouse frontal cortex were washed for 5 min in DEPC-PBS twice with shaking. Sections were then mounted and dried on Superfrost™ Plus microscope slides (Fisherbrand). Slides were placed in Coplin jars and incubated for 10 min in SSC 5x buffer (748 mM NaCl, 74.8 mM $Na_3C_6H_5O_7 \cdot H_2O$ in DEPC-H_2O, pH 7) with shaking. A border was drawn around the sections with a Liquid Blocker hydrophobic pen (Daido Sangyo Co.) and slides were placed in a pre-heated, humidified StainTray™ Slide Staining System (Simport). The slides were covered with blocking solution (50% by volume formamide, 25% by volume SSC 20× buffer [2.99 M NaCl, 299 mM $Na_3C_6H_5O_7 \cdot H_2O$ in DEPC-H_2O, pH 7], 25% by volume DEPC-H_2O, 0.8% by volume salmon sperm DNA [Invitrogen]) and incubated at 37**°**C for 2 hours. The fluorescein-labeled RNA probe was diluted (1:40 for experimental; 1:20, 1:40, and 1:100 to evaluate probe dilution; 1:20 for sense strand negative control) in hybridization buffer (50% by volume formamide, 40% by volume 50% dextran sulfate solution [Millipore], 10% SSC 20×) and the resulting solution was heated at 77°C for 5 min. The blocking solution was removed from the sections and the probe in hybridization buffer was added; the slides were then covered with HybriSlip™ hybridization covers (Grace Bio-Labs), sealed with Fixogum rubber cement (Marabu), and incubated overnight at 37°C. The next day, the slide covers were removed and slides were washed at room temperature in SSC 2× buffer (299 mM NaCl, 29.9 mM $Na_3C_6H_5O_7 \cdot H_2O$ in ddH_2O, pH 7) for 5 min three times in Coplin jars with shaking. The slides were then washed for 30 min with shaking in SSC 2× buffer that had been heated to 43**°**C. The slides were washed for 30 min with shaking in SSC 0.1× buffer (15 mM NaCl, 1.5 mM $Na_3C_6H_5O_7 \cdot H_2O$ in ddH_2O, pH 7) that had been heated to 43°C. Autofluorescence was then reduced by incubating slides with shaking in Coplin jars containing 0.1% Sudan Black B that had been dissolved in 70% ethanol in the dark overnight and syringe filtered using a 0.45 µm filter (Corning). Slides were then washed three times in PBS with shaking. Sections were dried, mounted in Duolink *In Situ* Mounting Medium with DAPI (Sigma-Aldrich), covered with #1.5 coverslips, and sealed.

The 488 nm laser line of an LSM 710 confocal laser scanning microscope was used to acquire images from mouse frontal cortex (delineated by +1.4 to +1.9 mm relative to bregma). Images were acquired with a 63× objective, yielding 1912 × 1912 pixel images with a pixel size of 0.07 µm × 0.07 µm. Files were converted to TIFF format for analysis. Fluorescence intensity was evaluated by a blinded experimenter using ImageJ.

M6. Experiments Involving Postmortem Human Samples

Postmortem Human Brain Tissue Samples

The collection of postmortem tissue samples in the laboratory of Dr. J Javier Meana was described by Dr. Carolina Muguruza Millan: Human brains were obtained at autopsies performed in the Basque Institute of Legal Medicine, Bilbao, Spain. The study was developed in compliance with policies of research and ethical review boards for postmortem brain studies (Basque Institute of Legal Medicine, Spain). Retrospective searches were conducted for previous medical diagnosis and treatment using examiners' information and records of hospitals and mental health centers. After searching antemortem information, 32 subjects who had met criteria of schizophrenia according to the Diagnostic and Statistical Manual of Mental Disorders (DSM-IV[105] and DSM-IV TR[106]) were selected. Toxicological screening for antipsychotics, other drugs and ethanol was performed in blood, urine, liver and gastric contents samples. The toxicological assays were performed at the National Institute of Toxicology, Madrid, Spain, using a variety of standard procedures including radioimmunoassay, enzymatic immunoassay, high-performance liquid chromatography and gas chromatography–mass spectrometry. The schizophrenia subjects were divided into 16 antipsychotic-free (AP-free) and 16 antipsychotic-treated (AP-treated) subjects according with the presence or absence of antipsychotics in blood at the time of death.

Controls for the present study were chosen among the collected brains on the basis, whenever possible, of the following cumulative criteria: (i) negative medical information on the presence of neuropsychiatric disorders or drug abuse and (ii) appropriate sex, age, postmortem delay (time between death and autopsy, PMD) and freezing storage time to match each subject in the schizophrenia group. Causes of death among the schizophrenia patients included suicide (n=19), accidents (n=2) and natural deaths (n=11). Controls' causes of death included accidents (n=20) and natural deaths (n=12).

Specimens of prefrontal cortex (Brodmann's area 9) were dissected at autopsy (0.5–1.0 g tissue) on an ice-cooled surface and immediately stored at −80°C until use. Tissue pH values were within a relatively narrow range (control subjects: 6.48 ± 0.08; schizophrenia subjects: 6.28 ± 0.05). The definitive pairs of AP-free schizophrenia subjects and respective matched controls are shown in Table M2, and the definitive pairs of AP-treated schizophrenia subjects and respective matched controls are shown in Table M3. All the parameters taken into account for the pairs matching (age, PMD and storage time) were not statistically different between groups, as shown in Tables M2 and M3 ($p > 0.05$, two tailed *t*-test). Pairs of schizophrenia patients and matched controls were processed simultaneously and under the same experimental conditions.

Western Blotting in Postmortem Human Brain

300 mg of postmortem human prefrontal cortex samples were homogenized using a chilled Teflon-glass grinder containing 6 ml homogenization buffer (0.32 M sucrose in 5 mM Tris-HCl, pH 7.4). Samples were then centrifuged at 1,100 × g at 4°C for 15 min. The supernatant (S1 fraction) was transferred to a new tube and kept on ice. The pellet (P1 fraction) was resuspended in 6 ml homogenization buffer and centrifuged under the same conditions as before. The P1 fraction was retained as the nuclear fraction and resuspended in 700 µL incubation buffer (5 mM Tris-HCl, pH 7.4) to store at -80°C until use. The S1 fraction was centrifuged at 40,000 × g at 4°C for 10 min and the resulting supernatant (S2) was retained

as the cytoplasmic fraction. The cytoplasmic fraction was stored at -80°C. Protein concentration was determined using the Bradford protein assay with BSA as the standard.

Samples for western blotting were prepared by heating nuclear and cytoplasmic samples combined with denaturing and reducing agents (to final concentrations of 2.5% β-mercaptoethanol, 2% SDS, 8% glycerol, 0.01% bromophenol blue) at 95°C for 5 min. Appropriate amounts of sample to load on a blot were determined using a sample pool for each fraction. 25 µg of nuclear samples and 15 µg of cytoplasmic fraction were run on 12% SDS-PAGE gels and transferred onto nitrocellulose membranes (Amersham™, 0.45 µm pore size). Blots were then incubated for 1 hour in blocking buffer (2.5% by weight nonfat dry milk, 0.5% by weight BSA in 5 mM Tris-HCl, pH 7.4) and then incubated in primary antibodies overnight at 4°C in TBST incubation buffer (blocking buffer supplemented with 0.01% Tween 20). The next day, blots were washed and incubated in fluorescent secondary antibodies, then imaged using an Odyssey infrared imaging system (LI-COR Biosciences). Signal was quantified as integrated intensity using Image Studio™ Lite version 5.2 (LI-COR Biosciences). Primary antibodies used were 1:100 mouse-anti-GR (Santa Cruz, sc-393232) and 1:20,000 rabbit-anti-β-actin (Abcam, ab8227). Secondary antibodies used were 1:6000 Alexa Fluor 680-conjugated goat-anti-mouse (Invitrogen, A21057) and 1:10,000 DyLight™ 800-conjugated donkey-anti-rabbit (Rockland, 611-745-127).

M7. Statistical Analysis

For RT-qPCR experiments, amplification was normalized to a correction factor calculated from amplification of housekeeping genes. For each housekeeping gene, the difference between Ct values from individual samples and the overall median Ct value from all samples was calculated. For each sample, the median was then taken from all housekeeping genes for each sample to calculate the correction factor.

For western blotting in mouse samples, densitometry was analyzed with normalization to the housekeeping gene and by blot. For chromatin immunoprecipitation, data were analyzed by calculating anti-GR fold change over IgG. For dendritic spine analysis, densities for each spine types, as well as the total density, were calculated from spine number and dendritic segment length. Dendritic spine densities were then reported as spines per µm. For FISH, a region of interest was drawn around the border for each cell and mean fluorescence intensity in the region of interest was used for analysis. Cells were selected from among two fields for each animal. For western blotting in postmortem human samples, target protein immunoreactivity was corrected using both β-actin immunoreactivity and a standard pool sample that was loaded onto every gel. Each sample was analyzed on at least two gels, with at least four measurements taken per sample.

Statistical analysis was performed using GraphPad Prism software versions 8 and 9. For experiments with one factor with two levels, a two-tailed Student's *t*-test was used. For experiments with one factor with more than two levels, a one-way ANOVA was used with Bonferroni's post-hoc test as appropriate. Experiments with two factors were analyzed by two-way ANOVA with Bonferroni's post-hoc test as appropriate. For GR immunoreactivity in postmortem samples, a paired two-tailed Student's *t*-test was used and Grubb's test was used to identify outliers. For the corticosterone time course, a one-way ANOVA was used with Dunnett's post-hoc test to allow for direct comparison of every group with Vehicle. For corticosterone and ΔGR PPI experiments, a three-way ANOVA was also included. For analysis of the relationship between VMax and average %PPI, Pearson's correlation was used. Sample sizes were not formally calculated, but were determined based on previous experiments. Following analysis of results, power analysis was conducted using G*Power[107] to determine sample sizes necessary to determine if trends detected in experiments reflect genuine effects on relevant phenotypes. All figures depict the mean with SEM for error bars.

	Primer Set		Sequence	Source
Genotyping Primers				
	5-HT_{2A}R Genotyping	Wild Type Fwd	GTGTGATGGCTCTTGATTATGC	Ibi et al, 2017
		5-HT_{2A}R KO Fwd	TCTCTTGATTCCCACTTTGTGGTT	
		Common Rev	CTGTGGGATTTTCTTTCTGCTT	
Microbiome Primers				
	SFB	SFB736	GACGCTGAGGCATGAGAGCAT	Kim et al, 2017
		SFB884	GACGGCACGGATTGTTATTCA	
	Universal Bacteria	UniF340	ACTCCTACGGGAGGCAGCAGT	Kim et al, 2017
		UniR514	ATTACCGCGGCTGCTGGC	
qPCR Primers				
	IL-6	Fwd	TAGTCCTTCCTACCCCAATTTCC	Chow, Yan, and Wu, 2016
		Rev	TTGGTCCTTAGCCACTCCTTC	
	5-HT $_{2A}$R	Fwd	GCAGTCCATCAGCAATGAGC	Kurita et al, 2012
		Rev	GCAGTGGCTTTCTGTTCTCC	
	5-HT $_{2C}$R	Fwd	GTATTCCCTCCCTTCCTTGC	Kurita et al, 2012
		Rev	CGTGTGTGAATGAGCAGAGC	
	D $_2$	Fwd	CTCTACCCTCCAATCCACTC	Kurita et al, 2012
		Rev	CATCCACAGCCTCCTCTAAG	
	GR	Fwd	TTCGCAGGCCGCTCAGTGTT	Nguyen et al, 2016
		Rev	TTGGGAGGTGGTCCCGTTGCT	
	FKBP4	Fwd	GAGGAAATGCAAAAGGTCCA	Lebsack et al, 2010
		Rev	CTTCTCGTTGTTGCTGTCCA	
	FKBP5	Fwd	GTACAACAAAGCCGTGGAGTG	Zheng et al, 2016
		Rev	GCCCTGTTCTGAGGATTGACT	
	DUSP1	Fwd	CTGCCTTGATCAACGTCTCA	*
		Rev	GTCTGCCTTGTGGTTGTCCT	
	GILZ	Fwd	TGGTGGCCATAGACAACAAG	*
		Rev	CTTCAGGGCTCAGACAGGAC	
	PER1	Fwd	TACCAGCCATTCCGCCTAAC	*
		Rev	TCCGGGGAGCTTCATAACCA	
	Actin	Fwd	AGAGGGAAATCGTGCGTGAC	Chow, Yan, and Wu, 2016
		Rev	CAATAGTGATGACCTGGCCGT	
	GAPDH	Fwd	TGCGACTTCAACAGCAACTC	Kurita et al, 2012
		Rev	CTTGCTCAGTGTCCTTGCTG	
	MAPK5	Fwd	CATTGCCCAGTGTATCCTCC	Kurita et al, 2012
		Rev	ACCTGCTTTACCACCTCTGC	
	rpS3	Fwd	AGGTTGTGGTGTCTGGGAAG	Kurita et al, 2012
		Rev	GAGGCTTCTTGGGACCAATC	
ChIP Primers				
	-361 to -204	Fwd	CCATCCCTCCTGGACACATCA	
		Rev	GTCATATTTTTAGGCTGAGGGGTG	
	+92 to +201	Fwd	GATTCCTCTCTGTGCGCTCG	
		Rev	TTCCAGCACGGTTGAAGTCT	
	+698 to +886	Fwd	AGCAGCATATCCAACCCGAGAA	
		Rev	TGGCTCTTGATTATGCCTCGC	
	+1003 to +1137	Fwd	GACTCGCTAGTCTCTCCACA	
		Rev	GCCTCGAGTCGTCACCTAAT	
	+1170 to +1340	Fwd	TCCGAAGCCTCGAACTGGA	
		Rev	CCAGTATGTTTCCCGCAATGG	
	+1692 to +1880	Fwd	CCTGTATTCCAATACTCTGTGAGC	
		Rev	AGCACTAATGCTCTCTCTGCAA	
Cloning Primers				
	ΔGR Cloning	Fwd	TTTTGGATCCATGGACTCCAAAGAATCCTT	
		Rev	TTTTGGCGCGCCTGAGACTCCTGCAGTGGCTT	
FISH Probe Primers				
	5-HT $_{2A}$R Antisense Probe	Fwd	GCAGAATGCCACCAACTATTTC	
		Rev	TTTACCTGGATGTGCTCTTCTC	
	Negative Control Sense Probe	Fwd	GAGAAGAGCACATCCAGGTAAA	
		Rev	GAAATAGTTGGTGGCATTCTGC	

Table M1 | Primers used in these studies are listed. All primers were synthesized by Integrated DNA Technologies. For ChIP primers, numbering is relative to the transcriptional start site. Fwd: Forward, Rev: Reverse. Papers Listed in Table: Chow, Yan, and Wu, 2016;[26] Ibi et al, 2017;[84] Kim et al, 2017;[38] Kurita et al, 2012;[108] Nguyen et al, 2016;[109] Lebsack et al, 2010;[110] Zheng et al, 2016.[111] *Primer sequences for *DUSP1*, *GILZ*, and *PER1* were generously provided by Dr. Gretchen Neigh.

	Sex (F/M)	*Age at death (years)*	*Postmortem delay (h)*	*Storage time (months)*	*Antipsychotic treatment*	*Additional drugs*
Schizophrenia 1	M	30	51	203	(-)	(-)
Control 1	M	29	18	68		(-)
Schizophrenia 2	M	48	20	122	(-)	(-)
Control 2	M	47	18	142		BDZ
Schizophrenia 3	M	31	11	113	(-)	(-)
Control 3	M	31	13	99		ETH (0.96 g/l)
Schizophrenia 4	M	45	3	106	(-)	BDZ
Control 4	M	44	21	92		(-)
Schizophrenia 5	M	27	24	104	(-)	(-)
Control 5	M	28	30	178		(-)
Schizophrenia 6	M	46	22	69	(-)	(-)
Control 6	M	46	24	67		(-)
Schizophrenia 7	M	48	11	50	(-)	(-)
Control 7	M	49	8	43		(-)
Schizophrenia 8	M	45	18	59	(-)	(-)
Control 8	M	47	15	44		(-)
Schizophrenia 9	M	34	15	62	(-)	(-)
Control 9	M	36	48	117		(-)
Schizophrenia 10	M	52	7	66	(-)	BDZ
Control 10	M	51	13	46		(-)
Schizophrenia 11	M	49	12	33	(-)	BDZ
Control 11	M	46	6	28		ETH (1.91 g/l)
Schizophrenia 12	M	60	12	43	(-)	BDZ
Control 12	M	62	9	66		(-)
Schizophrenia 13	F	67	22	52	(-)	(-)
Control 13	F	66	16	24		(-)
Schizophrenia 14	M	34	23	116	(-)	(-)
Control 14	M	33	28	28		ETH (0.97 g/l)
Schizophrenia 15	M	32	52	121	(-)	BDZ
Control 15	M	32	4	44		ETH (2.98 g/l)
Schizophrenia 16	M	32	21	122	(-)	(-)
Control 16	M	32	16	33		(-)
Schizophrenia	1F/15 M	42.5±2.9	20.3 ±3.4	90.1±10.9		
Control	1F/15 M	42.4±2.9	17.9±2.7	69.9±11.2		

Table M2 | Demographic characteristics of antipsychotic-free schizophrenia subjects and their respective control subjects. Antipsychotics were not detected in blood samples of schizophrenia subjects. Abbreviations: benzodiazepines (BDZ), ethanol (ETH).

	Sex (F/M)	*Age at death (years)*	*Postmortem delay (h)*	*Storage time (months)*	*Antipsychotic treatment*	*Additional drugs*
Schizophrenia 17	M	30	18	130	OLZ	(-)
Control 17	M	29	36	185		ETH (1.71 g/l)
Schizophrenia 18	M	32	8	125	QTP	BDZ
Control 18	M	32	4	24		(-)
Schizophrenia 19	M	23	16	120	SUL	(-)
Control 19	M	23	17	93		(-)
Schizophrenia 20	M	35	3	120	QTP	BDZ
Control 20	M	36	23	63		(-)
Schizophrenia 21	M	33	23	107	CLZ	(-)
Control 21	M	33	4	99		(-)
Schizophrenia 22	M	35	11	70	CLZ	BDZ
Control 22	M	36	18	140		ETH (1.69 g/l)
Schizophrenia 23	F	42	38	129	CLZ, QTP, SUL	BDZ
Control 23	F	38	22	46		(-)
Schizophrenia 24	M	37	8	75	OLZ	BDZ, ETH (0.90 g/l)
Control 24	M	41	24	180		(-)
Schizophrenia 25	F	60	23	54	CLZ, SUL	BDZ
Control 25	F	60	48	60		BDZ
Schizophrenia 26	F	56	13	119	CLZ	(-)
Control 26	F	58	20	176		(-)
Schizophrenia 27	M	43	5	21	OLZ	BDZ
Control 27	M	44	29	24		(-)
Schizophrenia 28	M	58	6	21	CLP	(-)
Control 28	M	57	3	39		(-)
Schizophrenia 29	M	51	18	22	PAL	BDZ
Control 29	M	50	2	33		(-)
Schizophrenia 30	M	51	28	25	OLZ,CLP	BDZ
Control 30	M	50	24	20		(-)
Schizophrenia 31	M	34	21	28	HAL	BDZ
Control 31	M	33	17	33		(-)
Schizophrenia 32	M	58	16	33	APZ	(-)
Control 32	M	56	15	18		(-)
Schizophrenia	3F/13M	42.4±2.9	15.9 ±2.3	74.9±11.4		
Control	3F/13M	42.3±2.9	19.1±3.1	77.1±15.3		

Table M3 | Demographic characteristics of antipsychotic-treated schizophrenia subjects and their respective control subjects. Therapeutic levels of aripriprazole (APZ), clotiapine (CLP), clozapine (CLZ), haloperidol (HAL), olanzapine (OLZ), paliperidone (PAL), quetiapine (QTP) and sulpiride (SUL) were detected in blood samples of schizophrenia subjects. Abbreviations: benzodiazepines (BDZ), ethanol (ETH).

Results

RA. Poly-(I:C)-elicited immune responses and gut microbiota evaluation support use of 129S6/SvEv and C57BL6/N mice as mothers for maternal immune activation experiments

RA.1. Poly-(I:C) elicits an immune response in both 129S6/SvEv and C57BL6/N female mice

Maternal immune activation paradigms have been developed in rodents to model environmental risk factors for neurodevelopmental disorders such as schizophrenia and recapitulate alterations observed in those disorders.[5] Although poly-(I:C) has been extensively used to induce MIA models,[26] the immune response to poly-(I:C) has been demonstrated to be variable based on both source and lot.[36] To confirm effects of poly-(I:C) in adult mice within our experimental system, we administered 20 mg/kg poly-(I:C) i.p. to adult female mice of either the 129S6/SvEv or C57BL6/N strain and sacrificed the mice 2.5 hours later. Most, but not all, poly-(I:C)-treated mice exhibited sickness behavior (such as ruffled fur, hunched posture, decreased activity, and ptosis) following treatment (*data not shown*). Given that IL-6 is a key proinflammatory mediator elicited by poly-(I:C) administration,[39] we evaluated IL-6 induction in injected mice. Poly-(I:C) elicited immune responses in 129S6/SvEv mice, with both increased *IL-6* mRNA by RT-qPCR in mouse frontal cortex (**Fig. 1a**; $t_4 = 5.21$, $p < 0.01$) as well as increased serum IL-6 by ELISA (**Fig. 1c**; $t_4 = 10.65$, $p < 0.001$). Similarly, poly-(I:C) increased *IL-6* mRNA in mouse frontal cortex in C57BL6/N mice (**Fig. 1b**; $t_4 = 3.25$, $p < 0.05$), as well as serum IL-6 (**Fig. 1d**; $t_6 = 3.07$, $p < 0.05$). In addition, at 24 hours after poly-(I:C) administration, treated female C57BL6/N mice exhibited decreased percent weight change relative to controls (**Fig. 1e**; $t_{14} = 5.17$, $p = 0.0001$). Therefore, the poly-(I:C) used in our experiments elicits a prominent immune response in both 129S6/SvEv and C57BL6/N female mice, allowing its use for subsequent MIA experiments.

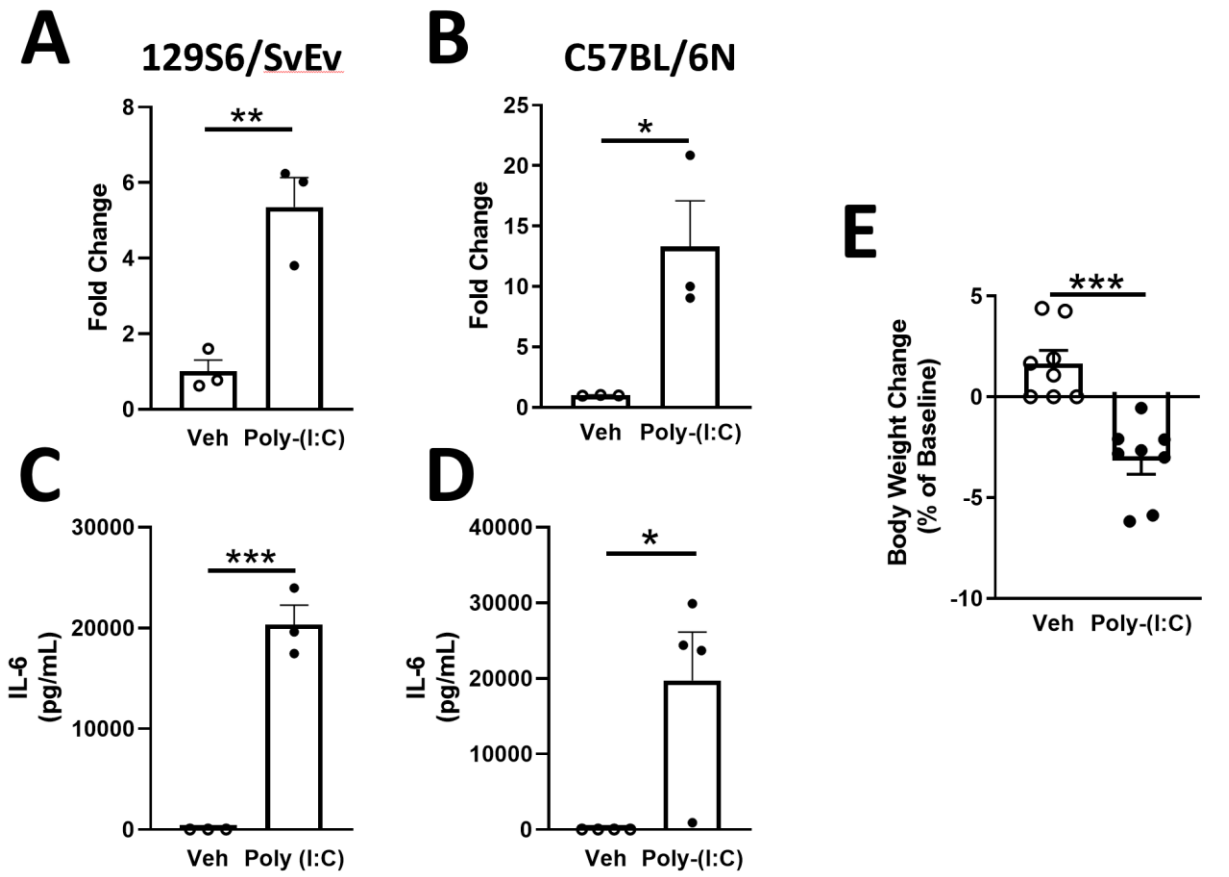

Fig. 1 | Poly-(I:C) elicits an immune response in injected mice. a-d. Adult female mice were injected i.p. with 20 mg/kg poly-(I:C) or vehicle 2.5 hours before sacrifice and IL-6 induction was assessed by either RT-qPCR in samples from mouse frontal cortex (**a,b**) or ELISA in mouse serum (**c,d**). **a,c.** In 129S6/SvEv mice, poly-(I:C) elicits an increase in *IL-6* mRNA (n = 3 mice/group; $t_4 = 5.21$, $p < 0.01$) as well as IL-6 protein (n = 3 mice/group; $t_4 = 10.65$, $p < 0.001$). **b,d.** In C57BL/6N mice, poly-(I:C) produces an increase in IL-6 mRNA (n = 3 mice/group; $t_4 = 3.25$, $p < 0.05$) as well as IL-6 protein (n = 4 mice/group; $t_6 = 3.07$, $p < 0.05$). **e.** WT C57BL/6N mice were injected i.p. with poly-(I:C) or vehicle and percent change in baseline weight was evaluated 24 hours later. Poly-(I:C) produces a decrease in percent body weight change at 24 hours relative to vehicle (n = 8 mice/group; $t_{14} = 5.17$, $p = 0.0001$). Statistical analysis was performed by two-tailed Student's *t*-test. *p < 0.05, **p < 0.01, ***p < 0.001.

RA.2. Mice used as mothers in our MIA experiments are positive for segmented filamentous bacteria

Segmented filamentous bacteria (*Candidatus* Savagella, SFB) within the maternal gut microbiome have been demonstrated to be necessary for MIA-induced phenotypes in offspring.[38] In those studies, mice from Taconic have been demonstrated to be SFB positive, while mice from Jackson Laboratories have

been demonstrated to be negative. To evaluate the gut microbiota of mice to be used as mothers in our studies, we extracted DNA from cecum contents from mice from our 129S6/SvEv colony, C57BL6/N mice from Charles River, C57BL6/J mice from Jackson Laboratories, and C57BL6/N from Taconic and performed qPCR for the 16S rRNA gene. Since the 16S rRNA gene is detectably variable by taxon, we used primers specific to the 16S rRNA gene of SFB.[38] To profile the total abundance of bacterial 16S rRNA in the cecum, we also used universal bacterial 16S rRNA gene primers, which detect the gene across the vast majority of bacterial taxa.[38] qPCR for the SFB 16S rRNA gene revealed that the gut microbiome from mice purchased from Charles River exhibit significantly greater enrichment of the gut microbiome for SFB compared to mice from the other three sources (**Fig. 2a**; $F[3,8] = 8.40$, $p < 0.01$; Bonferroni's post-hoc: $p < 0.05$ for CRL vs.129S6/SvEv, $p < 0.05$ for CRL vs JAX, $p < 0.05$ for TAC). Excluding mice from Charles River, both 129S6/SvEv mice from our colony as well as mice from Taconic exhibit significantly greater microbiome enrichment for SFB compared to mice from Jackson (**Fig. 2b**; $F[2,6] = 30.95$, $p < 0.001$; Bonferroni's post-hoc test: $p < 0.01$ for 129S6/SvEv vs. JAX, $p < 0.001$ for TAC vs. JAX, $p = 0.059$ for TAC vs. 129S6/SvEv), consistent with previous findings. Evaluating universal bacterial 16S rRNA, mice from Jackson exhibit significantly greater abundance of 16S rRNA gene copies in the cecum compared to mice from any of the other three sources (**Fig. 2c**; $F[3,8] = 11.09$, $p < 0.01$; Bonferroni's post-hoc test: $p < 0.01$ for JAX vs. 129S6/SvEv, $p < 0.05$ for JAX vs. CRL, $p < 0.01$ for JAX vs. TAC). Mice to be used as mothers in our MIA studies are therefore positive for SFB.

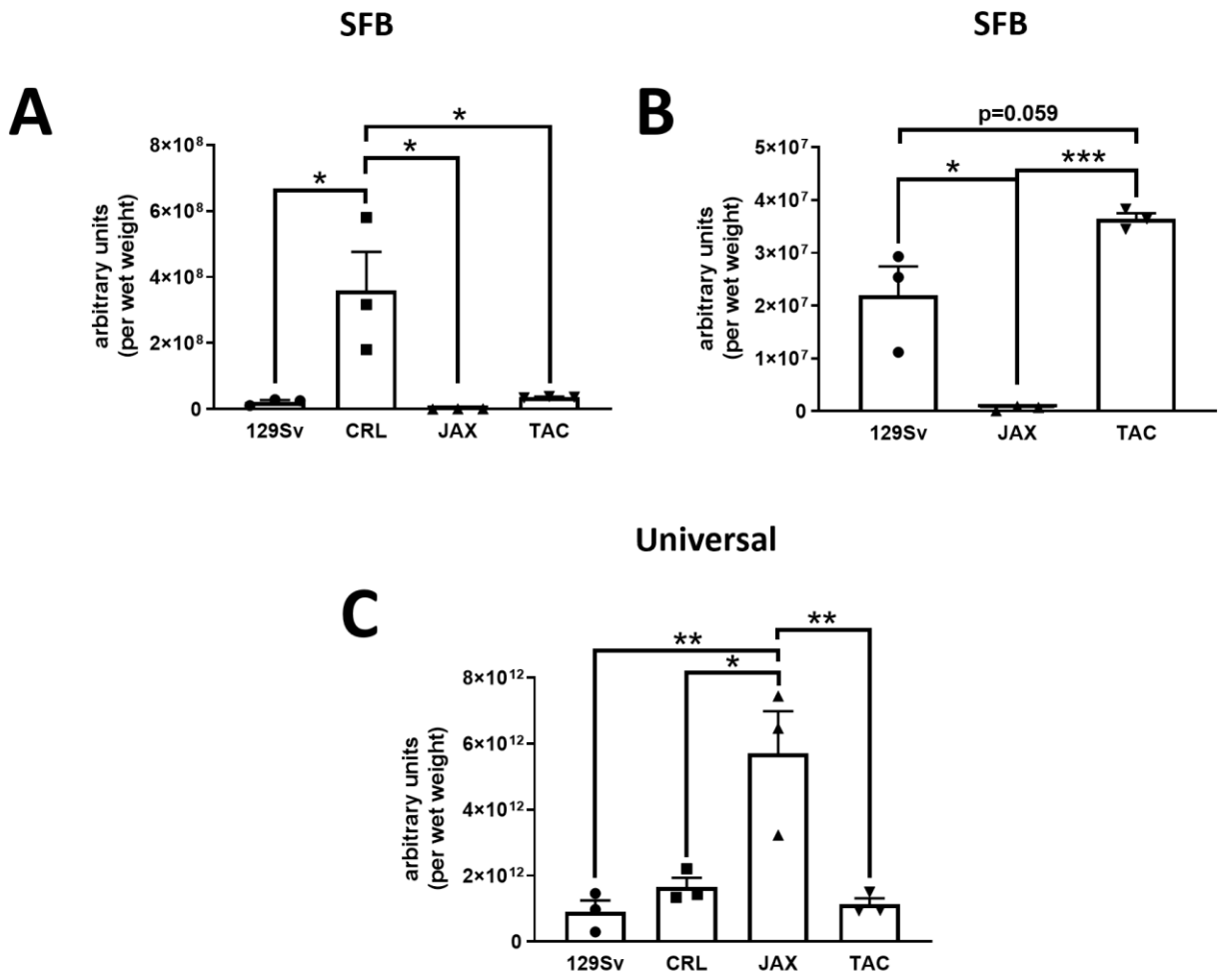

Fig. 2 | Female mice from Charles River (C57BL6/N), Taconic (C57BL6/N), and the in-house Maeso lab 129S6/SvEv colony, but not from Jackson Laboratories (C57BL6/J), have gut microbiota enriched for segmented filamentous bacteria. DNA was extracted from mouse cecum contents and qPCR was performed for the 16S ribosomal RNA gene using primers for either segmented filamentous bacteria (**a,b**) or universal bacterial primers that detect the gene across bacterial taxa (**c**). **a.** Mice from different sources exhibit differing levels of SFB DNA within cecum contents (n = 3 mice/group; $F[3,8] = 8.40$, $p < 0.01$). Mice from Charles River exhibit higher levels of SFB DNA compared to mice from any of the other three sources ($p < 0.05$ for CRL vs. 129S6/SvEv, $p < 0.05$ for CRL vs. JAX, $p < 0.05$ for CRL vs. TAC). **b.** The same data as in **a** are depicted, but the mice from Charles River are excluded. Similarly, mice from different sources exhibit differing levels of SFB DNA within cecum contents ($F[2,6] = 30.95$, $p < 0.001$). Mice from the Maeso lab 129S6/SvEv colony and from Taconic exhibit higher levels of SFB compared to mice from Jackson ($p < 0.01$ for 129S6/SvEv vs. JAX, $p < 0.001$ for TAC vs. JAX) and mice from Taconic exhibit a trend towards higher SFB DNA compared to the 129S6/SvEv colony ($p = 0.059$). **c.** Mice from different sources exhibit differing levels of total 16S rRNA gene DNA in cecum contents (n = 3 mice/group; $F[3,8] = 11.09$, $p < 0.01$). Mice from Jackson exhibit higher total 16S rRNA gene DNA compared to mice from the other three groups ($p < 0.01$ for JAX vs. 129S6/SvEv, $p < 0.05$ for JAX vs. CRL, $p < 0.01$ for JAX vs. TAC). Statistical analysis was performed by one-way ANOVA followed by Bonferroni's post-hoc test. *$p < 0.05$, **$p < 0.01$, ***$p < 0.001$.

RB. MIA induces *5-HT$_{2A}$R* dysregulation as well as alters 5-HT$_{2A}$R-related phenotypes in adult offspring

RB.1. Maternal poly-(I:C) induces MIA phenotypes in adult offspring

Following evaluation of our model components, we administered 20 mg/kg poly-(I:C) or vehicle control to pregnant C57BL6/N female mice on day E12.5 of pregnancy and evaluated MIA-associated phenotypes in adult offspring. MIA-induced dysregulation of the 5-HT$_{2A}$R in adult offspring frontal cortex has been shown by us and others, including at the receptor density level by radioligand binding and at the mRNA level by RT-qPCR.[21, 74] In order to both verify increased *5-HT$_{2A}$R* mRNA expression in mouse frontal cortex in our model as well as explore this dysregulation within the context of intact (as opposed to homogenized) tissue, we decided to take a fluorescence *in situ* hybridization (FISH) approach. Frontal cortex slices from brains of perfused adult MIA and control offspring were hybridized with a fluorescein labeled *5-HT$_{2A}$R* mRNA antisense probe. As validation of the specificity of the FISH signal, we observe decreasing signal with increasing dilution of the probe (**Fig. 3a**). Signal is absent with use of a sense strand *5-HT$_{2A}$R* mRNA probe (**Fig. 3b**). The location in frontal cortex used for quantification is depicted in **Fig. 3c**. FISH in MIA and control offspring frontal cortex demonstrates that cells from MIA offspring exhibit increased *5-HT$_{2A}$R* mRNA relative to cells from control offspring (**Fig. 3d,e**; $t_{120} = 2.12$, $p < 0.05$). Therefore *5-HT$_{2A}$R* mRNA is increased in MIA offspring frontal cortex.

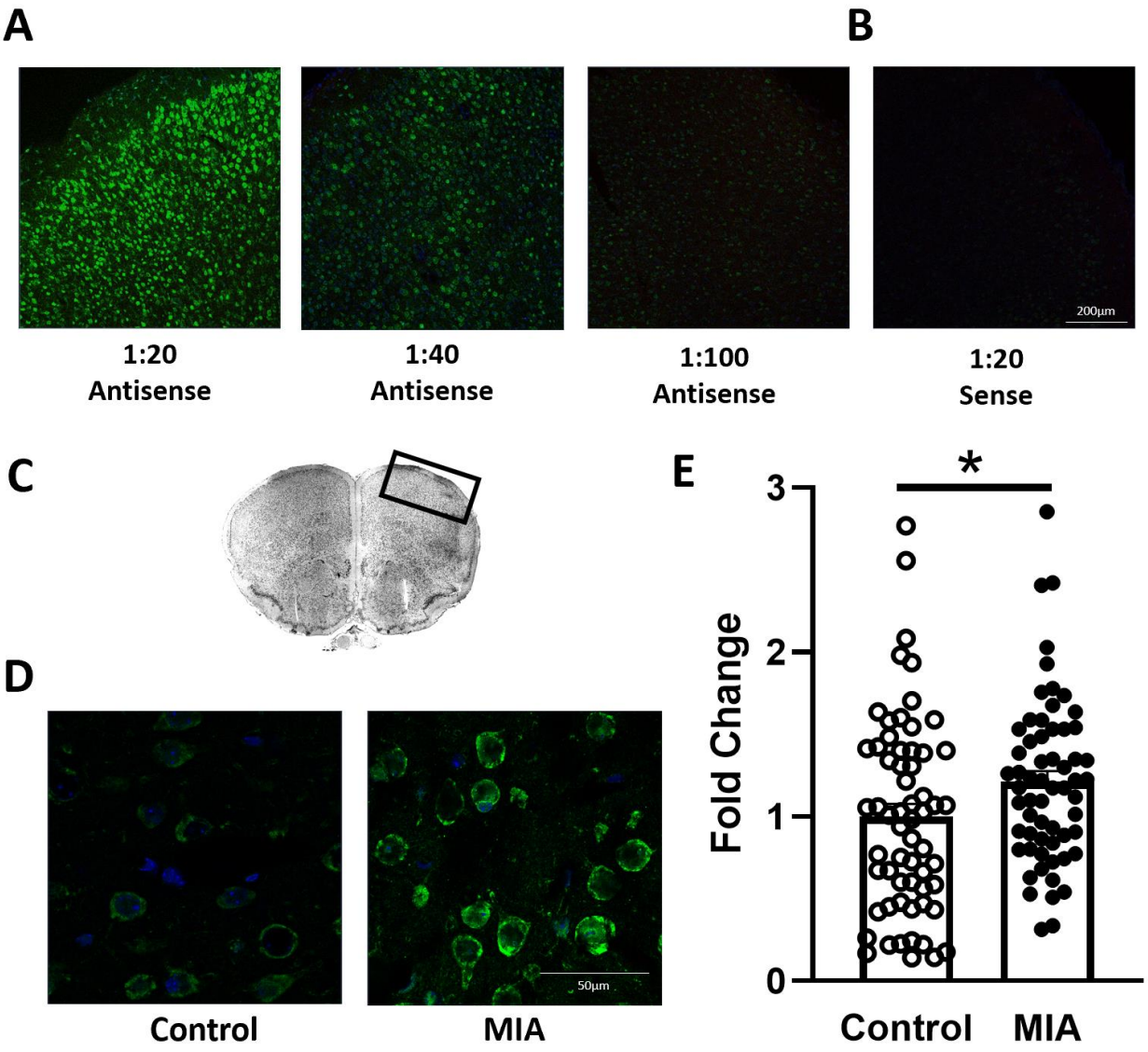

Fig. 3 | Maternal immune activation increases *5-HT$_{2A}$R* mRNA expression in frontal cortex of adult offspring. a,b. Control experiments demonstrate signal specificity. **a.** Signal in mouse frontal cortex decreases with increasing dilution factors of the antisense probe. **b**. Signal is absent when a sense probe is used. **c.** 20 µm sections from frontal cortex (1.4-1.9 mm relative to bregma; *see rectangle*) of adult mice born to poly-(I:C)-treated mothers or controls were hybridized with fluorescein-labeled antisense probes against *5-HT$_{2A}$R* mRNA. **d.** Representative images of probe-labeled cells in mouse frontal cortex (1:40 dilution) are shown. Mean fluorescence intensity within the boundaries of cells was used for quantification. **e.** MIA increases *5-HT$_{2A}$R* mRNA expression in mouse frontal cortex (n = 61 cells from 4 mice/group; 2-3 litters/group were used; $t_{120} = 2.12$, $p < 0.05$). Statistical analysis was performed by two-tailed Student's *t*-test. *$p < 0.05$.

Prepulse inhibition of startle (PPI) is a sensorimotor gating behavioral paradigm that has been shown to be altered in both schizophrenia as well as MIA animal models.[20, 44] The 5-HT_{2A}R has been implicated in PPI through pharmacology as well as human *5-HT_{2A}R* gene polymorphisms.[64, 77, 78] We conducted PPI assays according to a standard paradigm[101] (**Fig. 4a**) in both MIA and control C57BL6/N offspring mice. Similar to previous findings, we observed PPI deficits in MIA adult offspring relative to controls (**Fig. 4b**; Prepulse Intensity: $F[2,153] = 46.90$, $p < 0.0001$; Maternal Treatment: $F[1,153] = 12.52$, $p < 0.005$; Interaction: $F[2,153] = 0.044$, $p < 0.05$), both as a main effect as well as a trend towards a decrease in %PPI specifically at the 85 dB prepulse level (Bonferroni's post-hoc test: $p = 0.074$). In addition, adult MIA mice exhibit a decrease in startle magnitude during the initial 5 trials of our PPI paradigm (**Fig. 4c**; $t_{51} = 2.25$, $p < 0.05$). Our MIA offspring are therefore confirmed to have both molecular and behavioral alterations with relevance to 5-HT_{2A}R-related phenotypes.

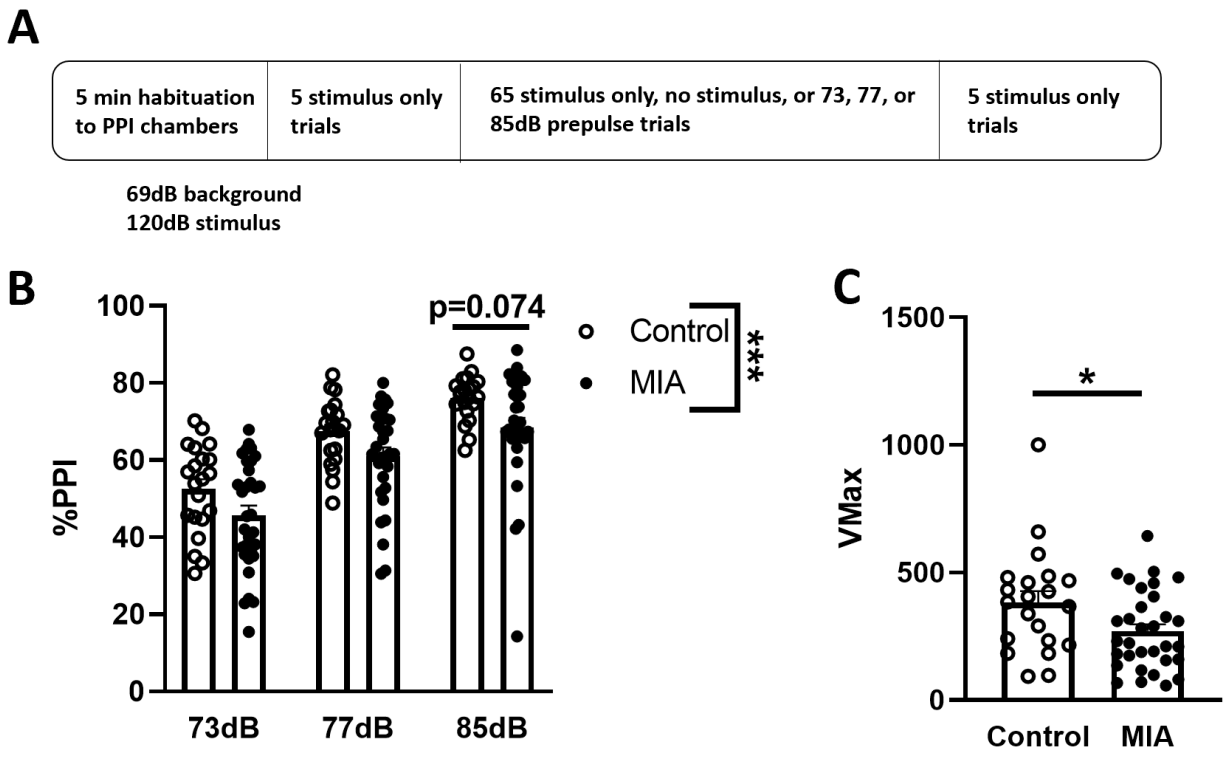

Fig. 4 | Maternal immune activation produces PPI deficits in adult offspring. a. Schematic of experimental paradigm for PPI. Adult mice born to poly-(I:C)-treated mothers or controls were placed in acoustic startle chambers and allowed to habituate to 69 dB of background noise for 5 minutes.

Following 5 stimulus only trials (120 dB), mice were subjected to 65 interspersed trials of startle stimulus alone, no stimulus, or prepulse followed by startle stimulus. Average values from these trials were used to calculate %PPI. **b.** MIA produces a main effect of decreased %PPI in adult offspring as well as a trend towards a decrease in %PPI at the 85 dB prepulse level (n = 21-32 mice/group; 3-4 litters/group were used; Prepulse Intensity: $F[2,153] = 46.90$, $p < 0.0001$; Maternal Treatment: $F[1,153] = 12.52$, $p < 0.005$; Interaction: $F[2,153] = 0.044$, $p > 0.05$; $p = 0.074$ at 85 dB prepulse level). **c.** MIA produces a decrease in startle magnitude in adult offspring (n = 21-32 mice/group; 3-4 litters/group were used; $t_{51} = 2.25$, $p < 0.05$). Statistical analysis was performed by two-way ANOVA followed by Bonferroni's post-hoc test (**b**) or two-tailed Student's *t*-test (**c**). *$p < 0.05$, ***$p < 0.001$.

RB.2. MIA decreases mushroom spine density in offspring frontal cortex in a 5-HT_{2A}R-dependent manner

Alterations in dendritic spine density in prefrontal cortex have been reported in samples from schizophrenia subjects relative to healthy controls.[49] 5-HT_{2A}R signaling has been reported to have relevance for dendritic spine density.[80, 83] To determine if MIA offspring exhibit alterations in dendritic spine density as well as if these alterations might be 5-HT_{2A}R dependent, we induced MIA in 129S6/SvEv 5-HT_{2A}R heterozygote female mice with 20 mg/kg poly-(I:C) or provided control treatment (**Fig. 5a**). We then sterotaxically injected the resulting WT and 5-HT_{2A}R KO adult offspring with an AAV8-*CaMKIIα*-eYFP viral vector to allow visualization of dendrites on cortical pyramidal neurons (**Fig. 5b**). For stubby spines, MIA induces a trend towards decreased spine density (**Fig. 6a, Table 1**; Maternal Treatment: $F[1,363] = 3.64$, $p = 0.057$; Genotype: $F[1,363] = 1.96$, $p > 0.05$; Interaction: $F[1,363] = 4.91e^{-005}$, $p > 0.05$). Neither MIA nor genotype affects density of thin spines (**Fig. 6b**; Maternal Treatment: $F[1,363] = 0.48$, $p > 0.05$; Genotype: $F[1,363] = 1.97$, $p > 0.05$; Interaction: $F[1,363] = 0.11$, $p > 0.05$). MIA produces a decrease in mushroom spine density (**Fig. 6c**; Maternal Treatment: $F[1,363] = 6.58$, $p < 0.05$) and a Maternal Treatment x Genotype Interaction ($F[1,363] = 8.46$, $p < 0.01$). There was also a trend towards decreased mushroom spine density in 5-HT_{2A}R KO mice (Genotype: $F[1,363] = 3.01$, $p = 0.084$) relative to WTs. MIA reduces mushroom spine density in WT (Bonferroni's post-hoc test: $p < 0.001$), but not 5-HT_{2A}R KO ($p >$

0.05) offspring. 5-HT_{2A}R KO offspring exhibit decreased mushroom spine density compared to WT controls, regardless of treatment ($p < 0.01$ for WT Control vs. 5-HT_{2A}R KO Control, $p < 0.05$ for WT Control vs. MIA 5-HT_{2A}R KO). For total spine density, there are trends towards a decrease in MIA offspring as well as 5-HT_{2A}R KO mice (**Fig. 6d**; Maternal Treatment: $F[1,363] = 3.72$, $p = 0.054$; Genotype: $F[1,363] = 3.58$, $p = 0.059$; Interaction: $F[1,363] = 0.55$, $p > 0.05$). Immunofluorescence confirms viral vector expression in layers 2/3 and 5 (**Fig. 6e**) and representative images of dendrites and spines are shown (**Fig. 6f**). Therefore, MIA induces a decrease in mature mushroom spines on cortical pyramidal neurons in mouse frontal cortex in a 5-HT_{2A}R-dependent manner.

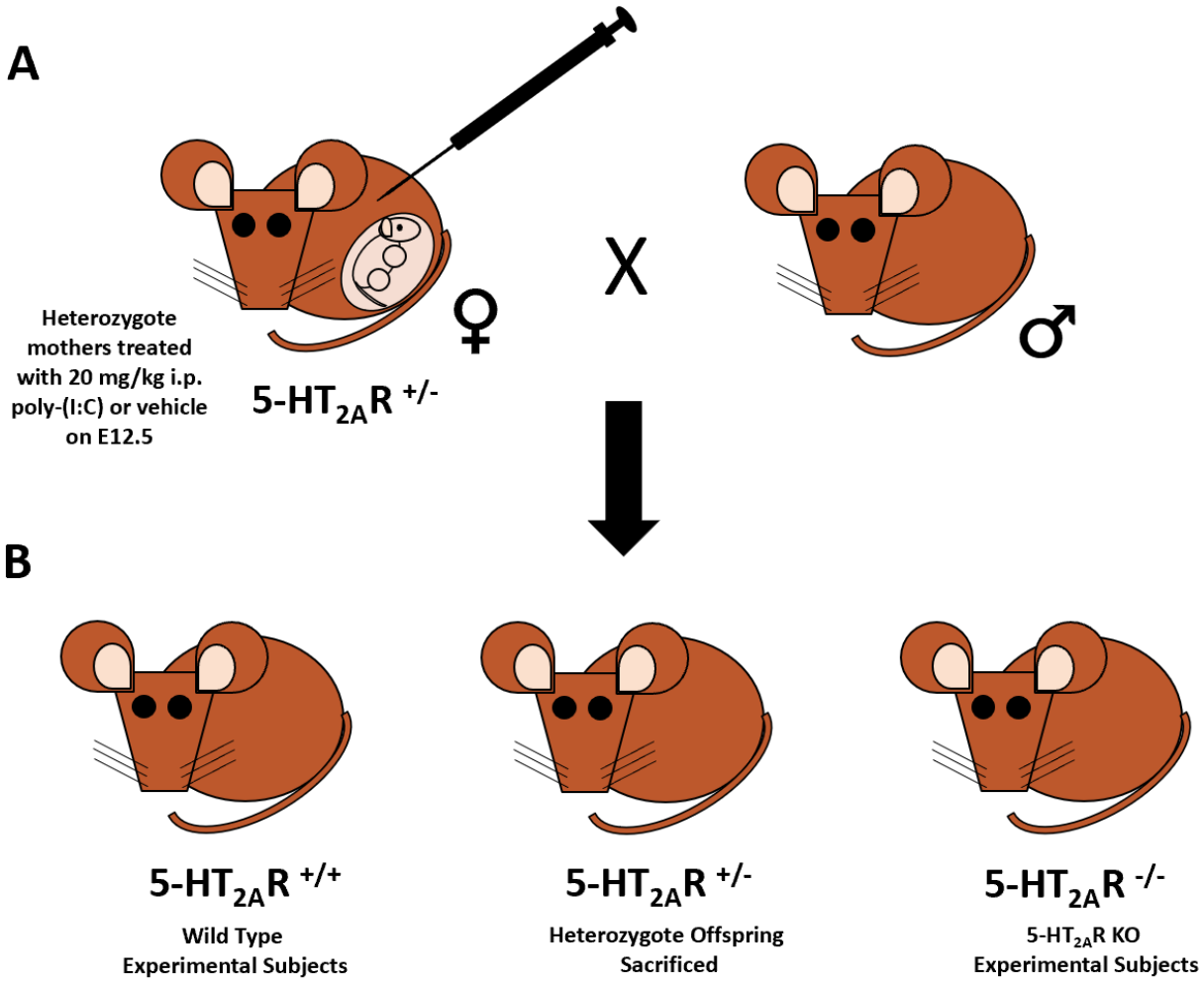

Fig. 5 | Maternal immune activation was induced in 5-HT$_{2A}$R heterozygote mothers to generate wild type and 5-HT$_{2A}$R KO offspring. The breeding scheme for generating MIA offspring for dendritic spine experiments is depicted. **a.** 5-HT$_{2A}$R heterozygote female mice were bred and used as mothers for these experiments. On E12.5 of pregnancy, the mice were injected with 20 mg/kg poly-(I:C) or vehicle. **b.** Adult WT and 5-HT$_{2A}$R KO offspring born to these mothers were used in dendritic spine experiments. Heterozygote offspring were sacrificed.

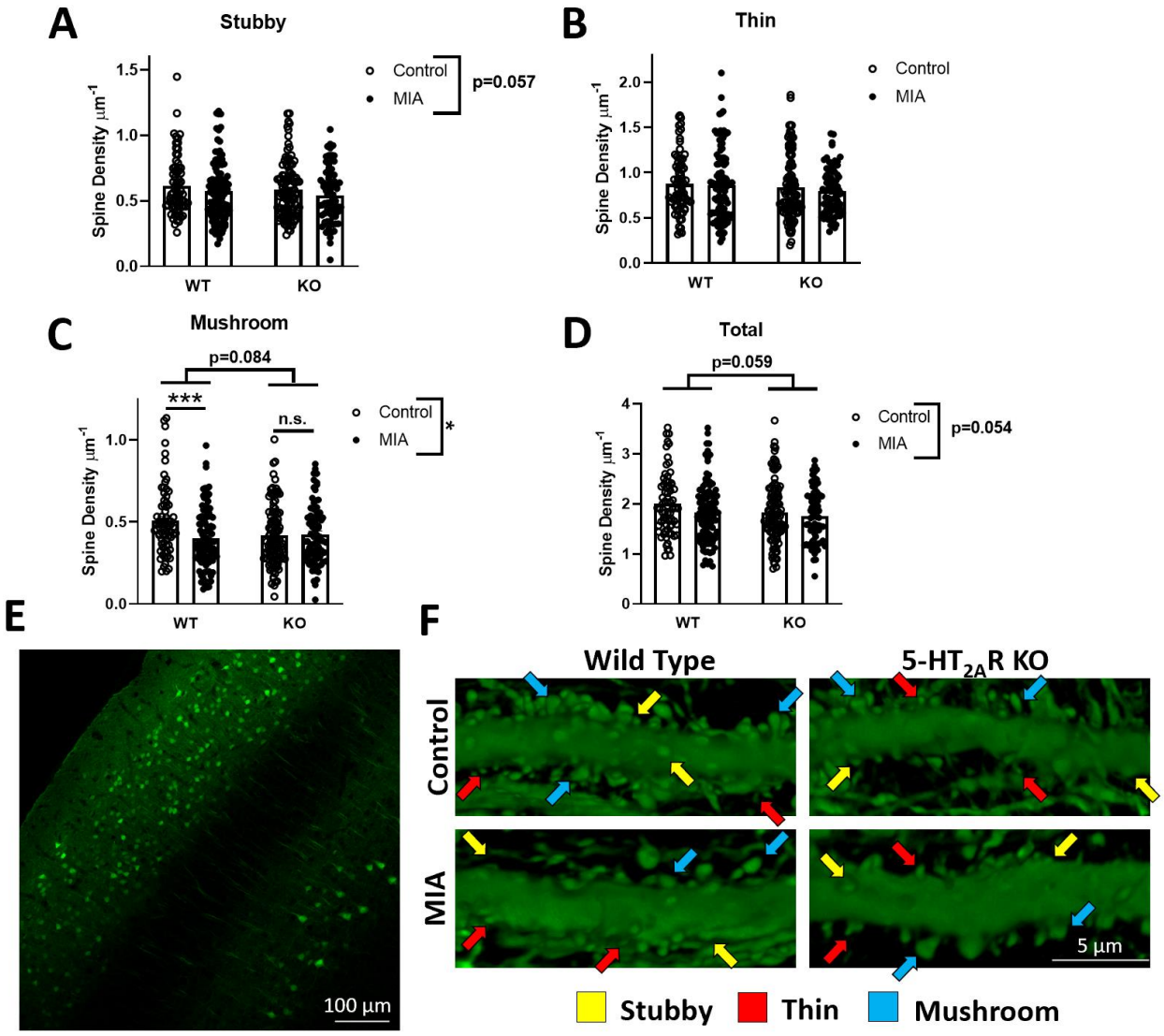

Fig. 6 | Maternal immune activation produces decreased mushroom spine density in frontal cortex of WT, but not 5-HT$_{2A}$R KO, adult offspring. An AAV8-*CaMKIIα*-eYFP viral vector was stereotaxically injected into mouse frontal cortex to allow visualization of dendrites (*see methods for coordinates*) (**e,f**). Dendritic spines were classified and quantified using NeuronStudio software (**a-d**). **a.** MIA produces a trend towards a main effect of decreased stubby spine density (n = 5-8 mice/group; 3-5 litters/group;

73-109 dendrites/group for all spine types; Maternal Treatment: F[1,363] = 3.64, p = 0.057; Genotype: F[1,363] = 1.96, p > 0.05; Interaction: F[1,363] = 4.91e^{-005}, p > 0.05). **b.** Neither MIA nor genotype affects thin spine density (Maternal Treatment: F[1,363] = 0.48, p > 0.05; Genotype: F[1,363] = 1.97, p > 0.05; Interaction: F[1,363] = 0.11, p > 0.05). **c.** MIA produces a main effect of decreased mushroom spine density (Maternal Treatment: F[1,363] = 6.58, p < 0.05) as well as a Maternal Treatment x Genotype Interaction (F[1,363] = 8.46, p < 0.01). In addition, there is a trend towards a main effect of Genotype (F[1,363] = 3.01, p = 0.084). Post-hoc tests reveal decreased mushroom spine density in MIA WT offspring relative to Control WT offspring (p < 0.001), but no difference between MIA and Control 5-HT$_{2A}$R KO offspring (p > 0.05). In addition, 5-HT$_{2A}$R KO offspring exhibit decreased mushroom spine density relative to Control WT offspring regardless of maternal treatment (p < 0.01 for WT Control vs. 5-HT$_{2A}$R KO Control, p < 0.05 for WT Control vs. 5-HT$_{2A}$R KO MIA). **d.** Both Maternal Treatment and Genotype produce trends towards a main effect on total spine density (Maternal Treatment: F[1,363] = 3.72, p = 0.054; Genotype: F[1,363] = 3.58, p = 0.059; Interaction: F[1,363] = 0.55, p > 0.05). **e.** eYFP from viral infection can be observed in layers 2/3 as well as layer 5. **f.** Representative images of dendritic segments are depicted. Statistical analysis was performed by two-way ANOVA followed by Bonferroni's post-hoc test. *p < 0.05, ***p < 0.001. To simplify the graphs, only group main effect comparisons and within genotype post-hoc comparisons are depicted in this figure. All comparison results are shown in Table 1.

Spine Type		Comparison	Significance
Stubby			
	Main Effects		
		Control vs. MIA	*p = 0.057*
		WT vs. 2A KO	*n.s.*
		Interaction	*n.s.*
Thin			
	Main Effects		
		Control vs. MIA	*n.s.*
		WT vs. 2A KO	*n.s.*
		Interaction	*n.s.*

Spine Type		Comparison	Significance
Mushroom			
	Main Effects		
		Control vs. MIA	*
		WT vs. 2A KO	*p = 0.084*
		Interaction	**
	Post-hoc Tests		
		WT Con vs. WT MIA	***
		WT Con vs. 2A KO Con	**
		WT Con vs. 2A KO MIA	*
		WT MIA vs. 2A KO Con	*n.s.*
		WT MIA vs. 2A KO MIA	*n.s.*
		2A KO Con vs. 2A KO MIA	*n.s.*
Total			
	Main Effects		
		Control vs. MIA	*p = 0.054*
		WT vs. 2A KO	*p = 0.059*
		Interaction	*n.s.*

Table 1 | Samples were generated and analyzed as in Fig. 6. All comparisons from a two-way ANOVA are reported in the table for each spine type. For spine types with significant main effects, the results of Bonferroni's post-hoc test are also reported. WT: wild type, 2A KO: 5-HT$_{2A}$R KO.

RC. MIA alters GR expression and *5-HT$_{2A}$R* promoter occupancy in mouse frontal cortex

RC.1. The GR binds the *5-HT$_{2A}$R* promoter in adult mouse frontal cortex

Following from these findings regarding alterations in *5-HT$_{2A}$R* expression and related phenotypes in MIA offspring, we sought to determine which mechanisms might underlie this dysregulation. Because 5-HT$_{2A}$R expression has been shown to be regulated by a wide variety of stressors and glucocorticoid signaling has been shown to regulate 5-HT$_{2A}$R expression in other experimental systems,[89, 91, 93, 95] we investigated alterations in GR signaling as a potential underlying mechanism for 5-HT$_{2A}$R alterations in MIA mice. A putative conserved *5-HT$_{2A}$R* promoter binding site has been proposed by Falkenberg and Rajeevan and demonstrated for the human *5-HT$_{2A}$R* promoter *in vitro*.[100] To determine whether the GR binds this predicted site in mouse frontal cortex, we first evaluated the site using the JASPAR transcription factor database. Using a consensus sequence for the GR (Matrix ID MA0113.1), JASPAR detects this predicted site as a GR binding site on the mouse *5-HT$_{2A}$R* promoter (**Fig. 7a**). We therefore performed chromatin immunoprecipitation (ChIP) to determine if the GR binds the *5-HT$_{2A}$R* promoter in mouse frontal cortex. Locations of our ChIP-qPCR primers along the *5-HT$_{2A}$R* gene are shown in **Fig. 7b**. ChIP-qPCR using an anti-GR antibody or species and isotype-matched IgG control reveals enrichment of the GR at the predicted binding site, but not at other locations, on the *5-HT$_{2A}$R* gene in mouse frontal cortex, confirming this GR binding site (**Fig. 7c**; Gene Site: $F[5,73] = 2.80$, $p < 0.05$; Antibody: $F[1,73] = 3.96$, $p = 0.0503$; Interaction: $F[5,73] = 2.80$, $p < 0.05$; Bonferroni's post-hoc test: $p < 0.001$ for GR vs. IgG at the predicted binding site, $p > 0.05$ for each other site).

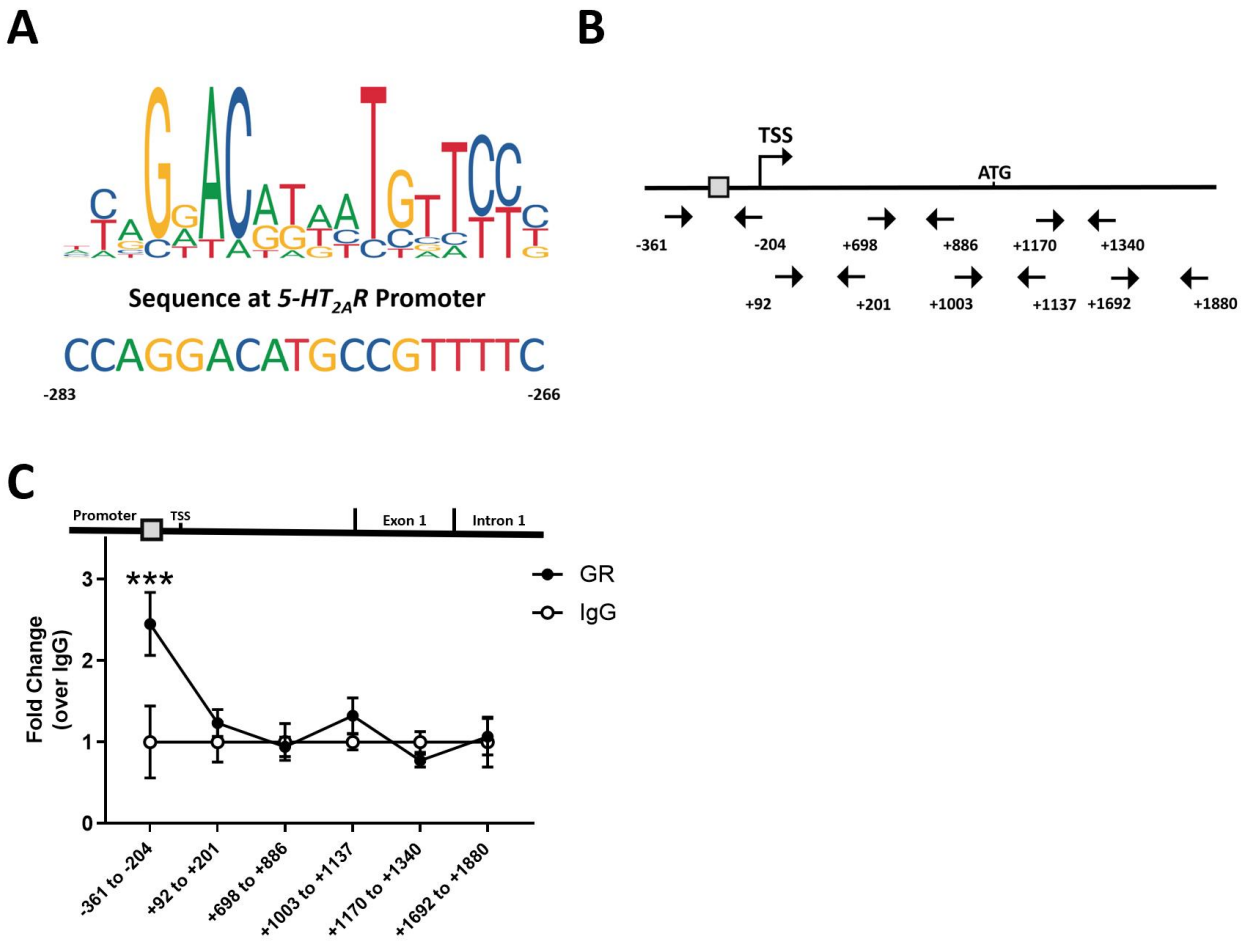

Fig. 7 | The glucocorticoid receptor binds a predicted site on the *5-HT$_{2A}$R* promoter in adult mouse frontal cortex. a. The JASPAR database consensus sequence for the GR (shown here as reverse complement of Matrix ID MA0113.1) is depicted alongside the *5-HT$_{2A}$R* promoter sequence predicted by Falkenberg and Rajeevan (2010). JASPAR detects this consensus binding site (score 12.98) on the mouse *5-HT$_{2A}$R* promoter. **b,c.** Chromatin immunoprecipitation was performed in frontal cortex samples from otherwise untreated adult mice using an anti-GR antibody or isotype and species matched IgG control. **b.** The predicted GR binding site, TSS, and ATG site for the mouse *5-HT$_{2A}$R* gene are depicted alongside the locations of the qPCR primers used for ChIP. **c.** There is a main effect of Gene Site, a trend towards an effect of Antibody, as well as a Gene Site x Antibody Interaction (n = 8 mice/group; Gene Site: $F[5,73] = 2.80$, $p < 0.05$; Antibody: $F[1,73] = 3.96$, $p = 0.0503$; Interaction: $F[5,73] = 2.80$, $p < 0.05$). Post-hoc tests reveal that the GR is enriched over IgG at the predicted binding site ($p < 0.001$), but not at other sites along the *5-HT$_{2A}$R* gene ($p > 0.05$). Statistical analysis was performed by two-way ANOVA followed by Bonferroni's post-hoc test. ***$p < 0.001$.

RC.2. MIA induces a decrease in both GR enrichment at the *5-HT$_{2A}$R* promoter and GR immunoreactivity in the nuclear compartment in mouse frontal cortex

Following this finding in untreated mice, we next sought to determine if MIA affects GR enrichment at the *5-HT$_{2A}$R* promoter in mouse frontal cortex. MIA was induced with 20 mg/kg i.p. poly-(I:C) in pregnant C57BL6/N female mice on E12.5 as before and ChIP was conducted in frontal cortex samples from adult MIA and control offspring. ChIP reveals that MIA produces a decrease in GR enrichment at the *5-HT$_{2A}$R* promoter binding site (**Fig. 8a**; $t_{10} = 3.57$, $p < 0.01$), but not a negative control site on the *5-HT$_{2A}$R* gene (**Fig. 8b**; $t_{10} = 0.23$, $p > 0.05$), relative to control offspring. Western blotting for the GR in the nuclear and cytoplasmic compartments of MIA and control mouse frontal cortex reveals that MIA induces a decrease in GR immunoreactivity in the nuclear (**Fig. 8c,e**; $t_{11} = 2.34$, $p < 0.05$), but not cytoplasmic (**Fig. 8d,f**; $t_{11} = 0.57$, $p > 0.05$), compartment. Decreased GR immunoreactivity coinciding with decreased GR enrichment at the *5-HT$_{2A}$R* promoter as well as increased *5-HT$_{2A}$R* mRNA suggests a negative regulatory relationship between GR signaling at the *5-HT$_{2A}$R* promoter and *5-HT$_{2A}$R* expression in mouse frontal cortex.

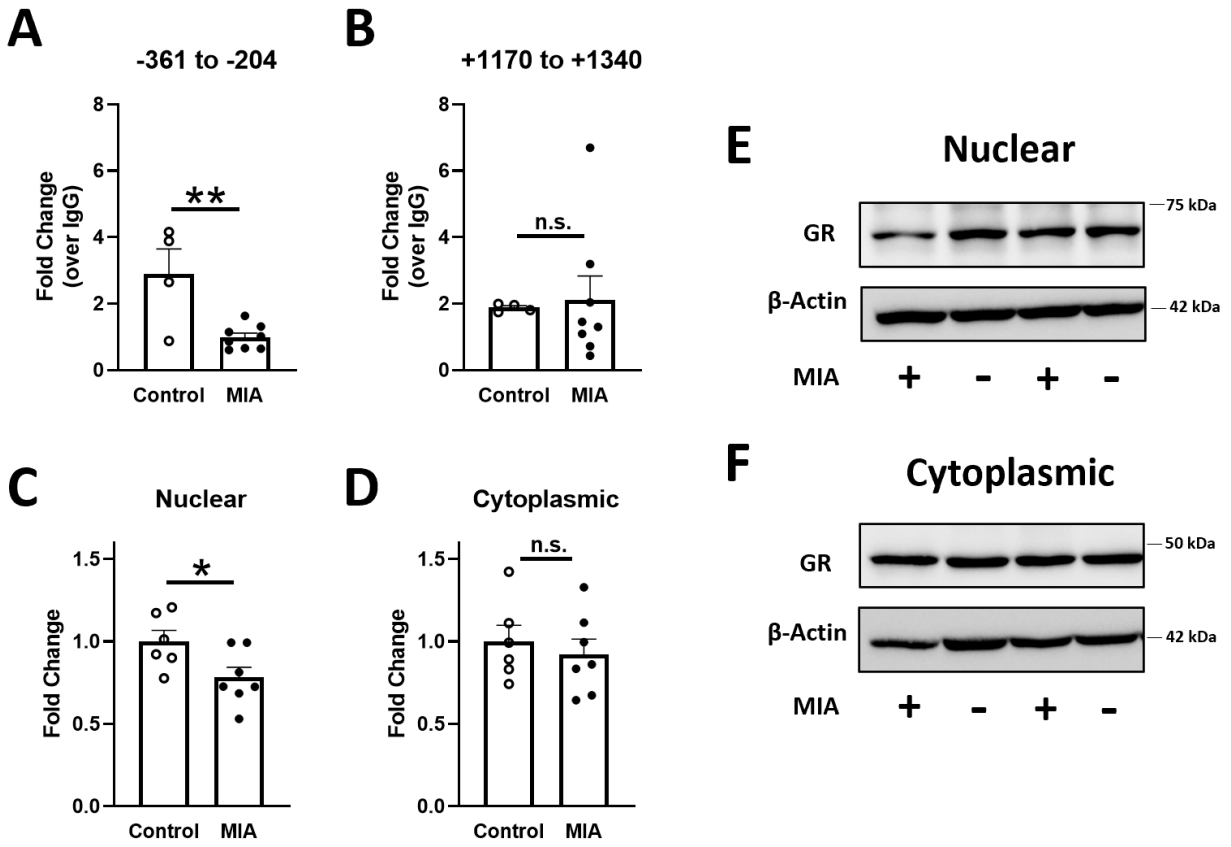

Fig. 8 | Maternal immune activation induces both decreased enrichment of the GR at the *5-HT$_{2A}$R* promoter binding site as well as decreased GR protein expression in the nuclear, but not cytoplasmic, compartment of mouse frontal cortex. a,b. ChIP using an anti-GR antibody or isotype-matched control was performed in frontal cortex samples from adult mice born to poly-(I:C) or control-treated mothers and qPCR was performed using primers encompassing the predicted binding site (**a**) or another site on the *5-HT$_{2A}$R* gene (**b**) as a negative control. **a.** MIA induces decreased enrichment of the GR at the *5-HT$_{2A}$R* promoter binding site (n = 4-8 mice/group; 3-4 litters/group; $t_{10} = 3.57$, $p < 0.01$). **b.** Enrichment of the GR at a negative control site of the *5-HT$_{2A}$R* gene is not affected by MIA ($t_{10} = 0.23$, $p > 0.05$). **c-f**. Western blotting for the GR was performed in nuclear (**c,e**) and cytoplasmic (**d,f**) compartments of frontal cortex samples from adult mice born to poly-(I:C) or control-treated mothers. **c.** MIA produces a decrease in nuclear GR immunoreactivity in mouse frontal cortex (n = 6-7 mice/group; 3-4 litters/group; $t_{11} = 2.34$, $p < 0.05$). **d.** Cytoplasmic GR immunoreactivity in mouse frontal cortex remains unchanged ($t_{11} = 0.57$, $p > 0.05$). **e,f.** Representative WB images for the nuclear and cytoplasmic compartments are shown. Molecular weight in kilodaltons (kDa) is reported to the right of the images. Statistical analysis was performed by two-tailed Student's *t*-test. *$p < 0.05$, **$p < 0.01$, n.s., not significant.

RC.3. Postmortem samples from schizophrenia subjects exhibit increased cytoplasmic GR immunoreactivity in prefrontal cortex relative to controls

Alterations in GR signaling pathways have been reported in postmortem prefrontal cortex samples from schizophrenia subjects relative to controls[88] and increased 5-HT_{2A}R receptor density has been found in prefrontal cortex samples from antipsychotic-free schizophrenia subjects.[53] Given our findings in mouse frontal cortex, we performed a similar fractionation protocol to separate nuclear and cytoplasmic compartments in postmortem prefrontal cortex samples from human schizophrenia subjects and age-matched controls. Western blotting in those compartments reveals that samples from schizophrenia subjects exhibit increased GR immunoreactivity in the cytoplasmic compartment relative to controls (**Fig. 9a,c**; $t_{31} = 0.46$, $p > 0.05$) while GR immunoreactivity in the nuclear compartment remains unchanged (**Fig. 9b,d**; $t_{28} = 2.25$, $p < 0.05$). This establishes GR dysregulation in prefrontal cortex in schizophrenia, reflecting alterations observed in MIA frontal cortex in mice.

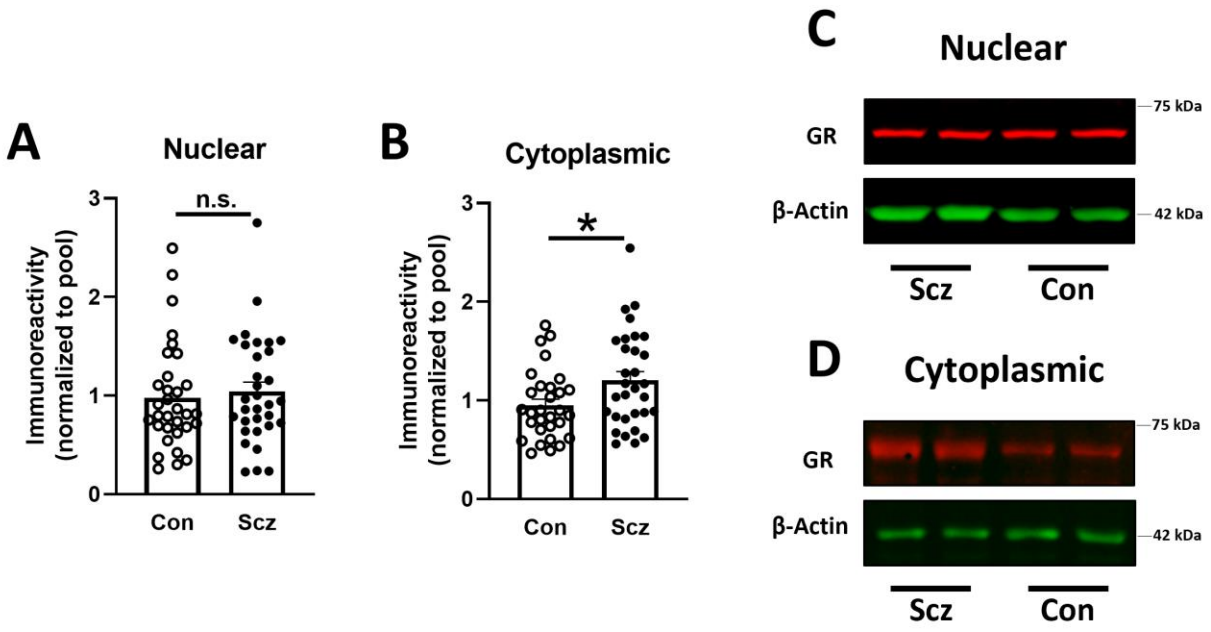

Fig. 9 | Postmortem samples from schizophrenia subjects exhibit increased GR immunoreactivity relative to matched controls in the cytoplasmic, but not nuclear, prefrontal cortex compartment. Western blotting was performed in the nuclear (**a,c**) and cytoplasmic (**b,d**) compartments of postmortem prefrontal cortex samples from schizophrenia subjects and age-matched paired controls. **a.**

There is no difference in nuclear GR immunoreactivity in prefrontal cortex samples from schizophrenia subjects and healthy controls ($t_{31} = 0.46$, $p > 0.05$). **b.** Prefrontal cortex samples from schizophrenia subjects exhibit increased cytoplasmic GR immunoreactivity compared to healthy controls ($t_{28} = 2.25$, $p < 0.05$). **c,d.** Representative WB images for the nuclear (**c**) and cytoplasmic (**d**) compartments are shown. Statistical analysis was performed by paired two-tailed Student's *t*-test. *$p < 0.05$, n.s., not significant.

RD. Short term, high dose corticosterone produces increased *5-HT$_{2A}$R* mRNA and decreased enrichment of the GR at the *5-HT$_{2A}$R* promoter in mouse frontal cortex

RD.1. A time course of corticosterone administration reveals *FKBP5* mRNA induction in mouse frontal cortex

MIA models have been shown to act as a pleiotropic insults, producing alterations in a variety of signaling pathways.[5] Following our data in mouse frontal cortex suggesting that MIA produces both increased *5-HT$_{2A}$R* mRNA and decreased enrichment of the GR on the *5-HT$_{2A}$R* promoter, we decided to investigate the effect of directly manipulating the glucocorticoid system on *5-HT$_{2A}$R* expression and related phenotypes. Berendsen et al reported that a regimen of 50 mg/kg s.c. corticosterone twice a day for four days produces increased head shakes in response to the 5-HT$_{2A}$R agonist DOI in rats.[94] To evaluate and optimize this experimental system in mice, we administered 50 mg/kg s.c. corticosterone or vehicle twice a day for 8 days to WT 129S6/SvEv mice before sacrifice. Mice received corticosterone for 0 (the Vehicle condition), 1, 2, 4, 6, or 8 of the days. An additional group that received no injections was also included. Following this treatment regimen, RT-qPCR was performed in mouse frontal cortex for mRNA for the *GR* as well as its positive and negative regulators, *FKBP4* and *FKBP5*, respectively. This time course produces a trend towards an effect on *GR* (**Fig. 10a**; Treatment: $F[6,21] = 2.17$, $p = 0.087$), but not *FKBP4* mRNA (**Fig. 10b**; Treatment: $F[6,21] = 1.38$, $p > 0.05$). *FKBP5* mRNA was altered during the time course. Post-hoc testing comparing each group to Vehicle reveals that *FKBP5* mRNA is increased with 1 day of corticosterone administration and remains increased over Vehicle with up to 8 days of

administration (**Fig. 10c**; Treatment: F[6,21] = 6.26, p < 0.001; Dunnett's multiple comparisons test: p < 0.01 for 1 Day Cort. vs. Vehicle; p < 0.05 for 2 Day Cort vs. Vehicle, 4 Day Cort vs. Vehicle, 6 Day Cort vs. Vehicle, and 8 Day Cort vs. Vehicle). This *FKBP5* mRNA induction suggests that this time course results in induction of, and negative feedback within, the GR pathway in mouse frontal cortex. We therefore elected to use 4 days as the treatment duration for our studies.

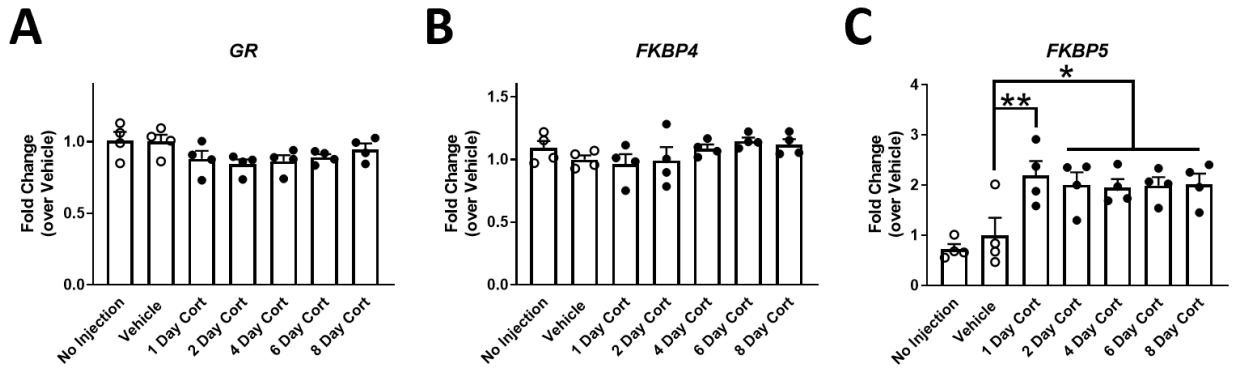

Fig. 10 | A time course of corticosterone administration reveals that short term, high dose corticosterone increases *FKBP5*, but not *GR* or *FKBP4* mRNA expression in mouse frontal cortex. Mice were treated with either 50 mg/kg s.c. corticosterone or vehicle twice a day for eight days or received no treatment (the No Injection group) before being sacrificed 8.5-13 hours after the last injection. RT-qPCR for GR pathway targets was performed in frontal cortex samples from these mice. **a.** The time course of corticosterone administration produces a trend towards an effect on *GR* mRNA expression in mouse frontal cortex (Treatment: F[6,21] = 2.17, p = 0.087). **b.** The time course did not affect *FKBP4* mRNA expression in mouse frontal cortex (Treatment: F[6,21] = 1.38, p > 0.05). **c.** The time course affects *FKBP5* mRNA expression in mouse frontal cortex (Treatment: F[6,21] = 6.26, p < 0.001). All durations of corticosterone administration produce an increase in *FKBP5* mRNA compared to vehicle (p < 0.01 for 1 Day Cort vs. Vehicle; p < 0.05 for 2 Day Cort vs. Vehicle, 4 Day Cort vs. Vehicle, 6 Day Cort vs. Vehicle, and 8 Day Cort vs. Vehicle). Statistical analysis was performed by one-way ANOVA followed by Dunnett's multiple comparisons test, with all groups being compared to Vehicle. *p < 0.05, **p < 0.01.

RD.2. Short term, high dose corticosterone results in increased *5-HT$_{2A}$R* mRNA in mouse frontal cortex

Adult WT mice were treated twice a day for four days with 50 mg/kg s.c. corticosterone or vehicle and sacrificed roughly 8.5-13.5 hours later (**Fig. 11a**). RT-qPCR was then conducted in mouse frontal cortex for neurotransmitter receptors. Short term, high dose corticosterone produces increased *5-HT$_{2A}$R* mRNA in mouse frontal cortex relative to vehicle treatment (**Fig. 11b**; $t_{16} = 2.98$, $p < 0.01$), while leaving *5-HT$_{2C}$R* (**Fig. 11c**; $t_{16} = 0.065$, $p > 0.05$) and dopamine *D$_2$* mRNA (**Fig. 11d**; $t_{16} = 0.23$, $p > 0.05$) unaffected. To further clarify the pattern of GR activation and signaling occurring, RT-qPCR was also conducted for known GR downstream targets.[112] At least at this time point, short term, high dose corticosterone did not produce changes in expression of *DUSP1* (**Fig. 12a**; $t_{16} = 0.12$, $p > 0.05$), *GILZ* (**Fig. 12b**; $t_{16} = 0.59$, $p > 0.05$), or *PER1* (**Fig. 12c**; $t_{16} = 0.81$, $p > 0.05$) mRNA expression in mouse frontal cortex. This regimen therefore specifically increases *5-HT$_{2A}$R* mRNA, supporting a relationship between GR signaling and *5-HT$_{2A}$R* expression.

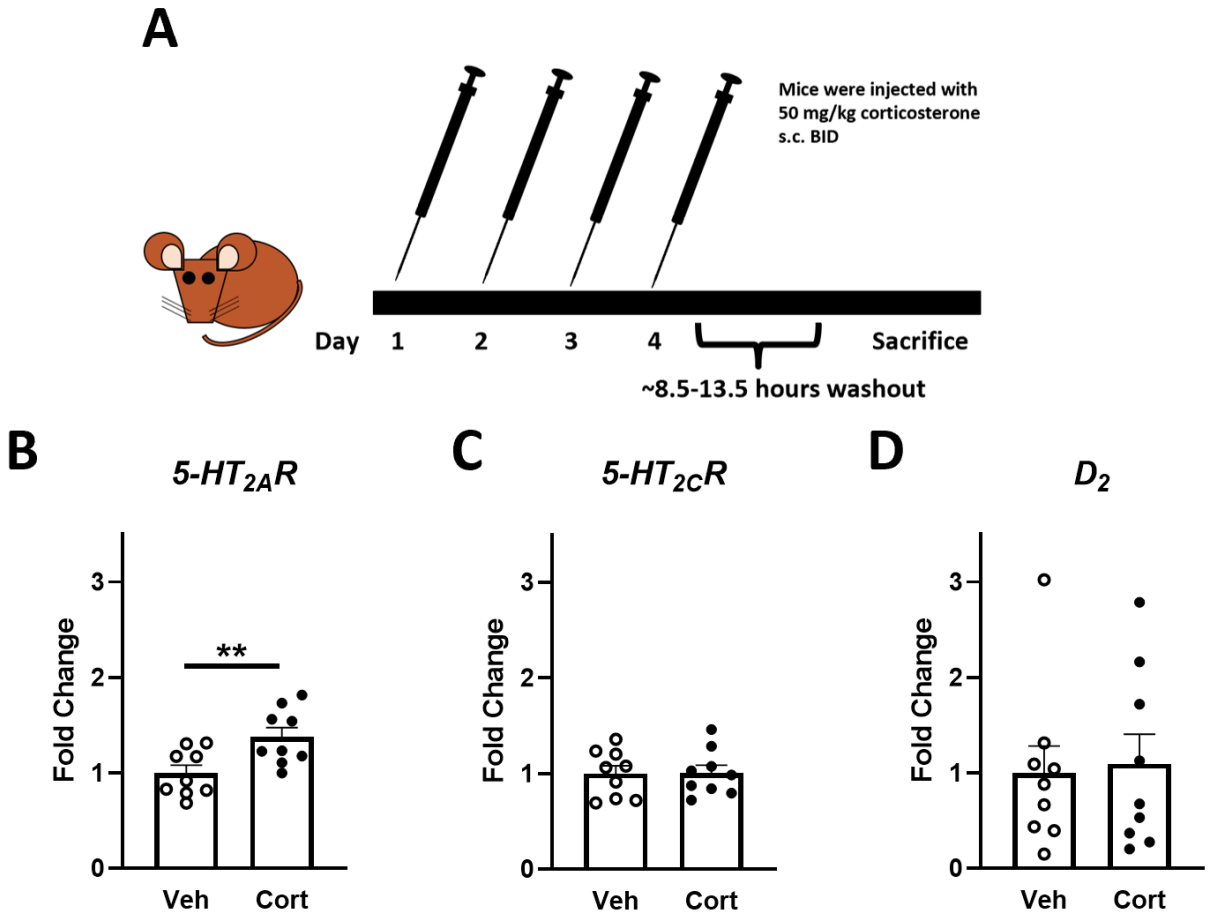

Fig. 11 | Short term, high dose corticosterone increases *5-HT$_{2A}$R*, but not *5-HT$_{2C}$R* or *D$_2$*, mRNA in mouse frontal cortex. a. The corticosterone administration paradigm is depicted. Mice were administered 50 mg/kg s.c. corticosterone or vehicle twice a day for four days and were sacrificed about 8.5-13.5 hours after the last injection. **b-d.** RT-qPCR for neurotransmitter receptors was performed in mouse frontal cortex samples following treatment. **b.** Short term, high dose corticosterone treatment produces an increase in *5-HT$_{2A}$R* mRNA in mouse frontal cortex (n = 9 mice/group; $t_{16} = 2.98$, $p < 0.01$). **c.** Short term, high dose corticosterone does not affect *5-HT$_{2C}$R* mRNA in mouse frontal cortex ($t_{16} = 0.065$, $p > 0.05$). **d.** Dopamine *D$_2$* mRNA is similarly unaffected ($t_{16} = 0.23$, $p > 0.05$). Statistical analysis was performed by two-tailed Student's *t*-test. **$p < 0.01$.

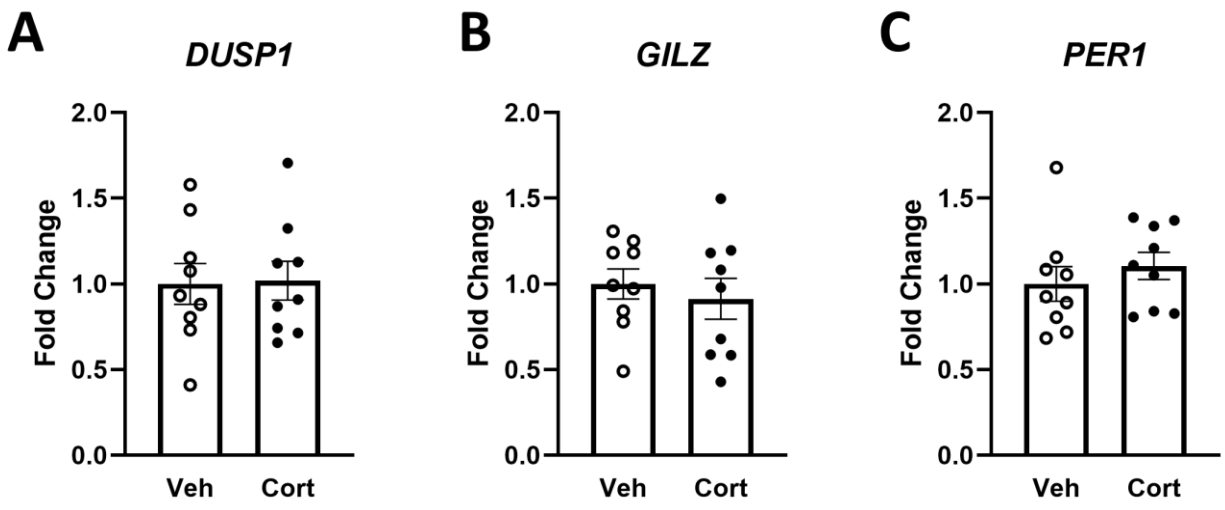

Fig. 12 | Short term, high dose corticosterone does not affect *DUSP1*, *GILZ*, or *PER1* mRNA expression in mouse frontal cortex. Mice were administered 50 mg/kg s.c. corticosterone or vehicle twice a day for four days and were sacrificed about 8.5-13.5 hours after the last injection (*same mice as in Fig. 11*). RT-qPCR for downstream GR targets was performed in mouse frontal cortex samples following treatment. **a.** Short term, high dose corticosterone treatment does not affect *DUSP1* mRNA expression in mouse frontal cortex (n = 9 mice/group; $t_{16} = 0.1154$, $p > 0.05$). **b.** *GILZ* mRNA expression is similarly unaffected ($t_{16} = 0.5865$, $p > 0.05$) in mouse frontal cortex. **c.** *PER1* mRNA is also unaffected ($t_{16} = 0.8149$, $p > 0.05$). Statistical analysis was performed by two-tailed Student's *t*-test.

RD.3. Short term, high dose corticosterone decreases GR enrichment at the *5-HT$_{2A}$R* promoter

To determine what might be occurring at the *5-HT$_{2A}$R* promoter following this manipulation, we performed ChIP-qPCR for the GR on the *5-HT$_{2A}$R* promoter following corticosterone treatment. Mice were administered corticosterone twice a day for four days as in **Fig. 11** and frontal cortex samples were collected about 8.5-13.5 hours later. ChIP was performed in these samples using an anti-GR antibody or species and isotype-matched IgG control. qPCR using primers flanking the GR binding site on the *5-HT$_{2A}$R* promoter demonstrates that short term, high dose corticosterone produces decreased enrichment of the GR at the *5-HT$_{2A}$R* promoter in mouse frontal cortex (**Fig. 13a**; $t_6 = 6.96$, $p < 0.001$). No change in GR enrichment was observed at a negative control site of the *5-HT$_{2A}$R* gene (**Fig. 13b**; $t_6 = 0.38$, $p > 0.05$). Short term, high dose corticosterone therefore produces increased *5-HT$_{2A}$R* mRNA alongside decreased

enrichment of the GR at the *5-HT$_{2A}$R* promoter, further suggesting a negative regulatory relationship between GR signaling and *5-HT$_{2A}$R* expression.

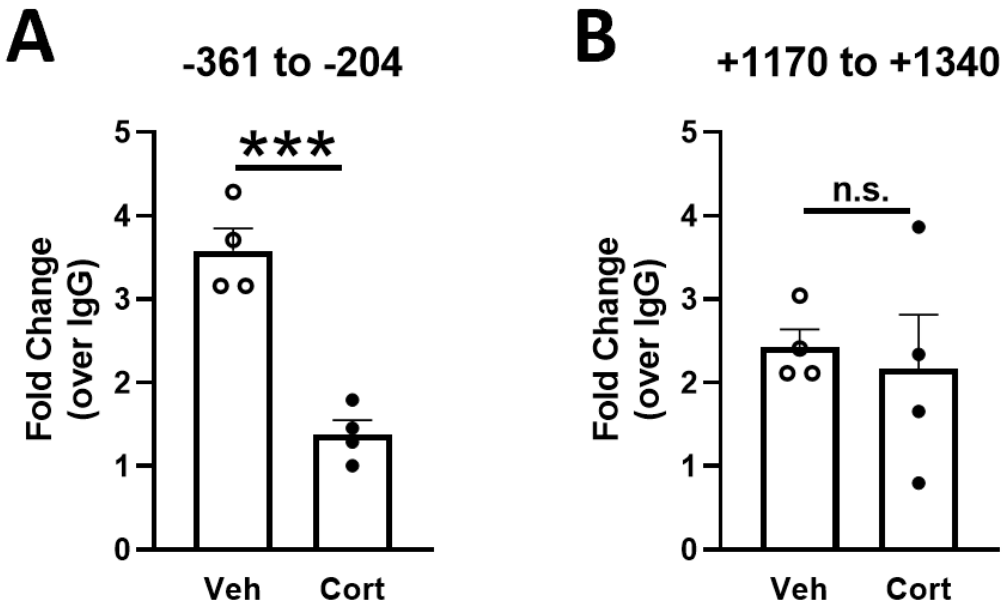

Fig. 13 | Short term, high dose corticosterone produces decreased enrichment of the GR at the *5-HT$_{2A}$R* promoter binding site. Mice were administered 50 mg/kg s.c. corticosterone or vehicle twice a day for four days and were sacrificed about 8.5-13.5 hours after the last injection. ChIP was performed in these samples using an anti-GR antibody or isotype-matched control. **a.** Short term, high dose corticosterone produces decreased enrichment of the GR at the *5-HT$_{2A}$R* promoter binding site in mouse frontal cortex (n = 4 mice/group; $t_6 = 6.96$, $p < 0.001$). **b.** Short term, high dose corticosterone does not affect GR enrichment at a negative control site of the *5-HT$_{2A}$R* gene ($t_6 = 0.38$, $p > 0.05$). Statistical analysis was performed by two-tailed Student's *t*-test. ***$p < 0.001$, n.s., not significant.

RD.4. Short term, high dose corticosterone induces PPI deficits regardless of 5-HT$_{2A}$R expression

In order to investigate the necessity of 5-HT$_{2A}$R expression for the behavioral effects of corticosterone administration in mice, we tested PPI in WT and 5-HT$_{2A}$R KO mice who had been treated with corticosterone or vehicle as before. Corticosterone decreases %PPI in WT mice (**Fig. 14a**; Prepulse Intensity: $F[2,84] = 67.28$, $p < 0.0001$; Treatment: $F[1,84] = 4.87$, $p < 0.05$; Interaction: $F[2,84] = 0.48$, $p > 0.05$) without affecting startle magnitude (**Fig. 14b**; $t_{28} = 1.28$, $p > 0.05$). A similar decrease in %PPI was

observed in 5-HT_{2A}R KO mice treated with corticosterone (**Fig. 14c**; Prepulse Intensity: $F[2,66] = 66.62$, $p < 0.0001$; Treatment: $F[1,66] = 4.20$, $p < 0.05$; Interaction: $F[2,66] = 0.24$, $p > 0.05$); startle magnitude was similarly unaffected (**Fig. 14d**; $t_{22} = 1.30$, $p > 0.05$). Performing a three-way ANOVA comparing both genotypes, main effects of Prepulse Intensity, Genotype, and Treatment were observed (**Table 2**). Therefore, corticosterone induces decreased %PPI in a manner not dependent on 5-HT_{2A}R expression. In addition, 5-HT_{2A}R KO mice exhibit increased %PPI when compared to WT mice. Comparing startle magnitudes across the two genotypes, trends are observed towards decreased startle magnitude in 5-HT_{2A}R KO mice (**Table 3**; $p = 0.091$) and in mice treated with corticosterone ($p = 0.090$). Thus, although corticosterone increases *5-HT_{2A}R* mRNA expression in WT mouse frontal cortex, this effect is not necessary for corticosterone-induced PPI deficits.

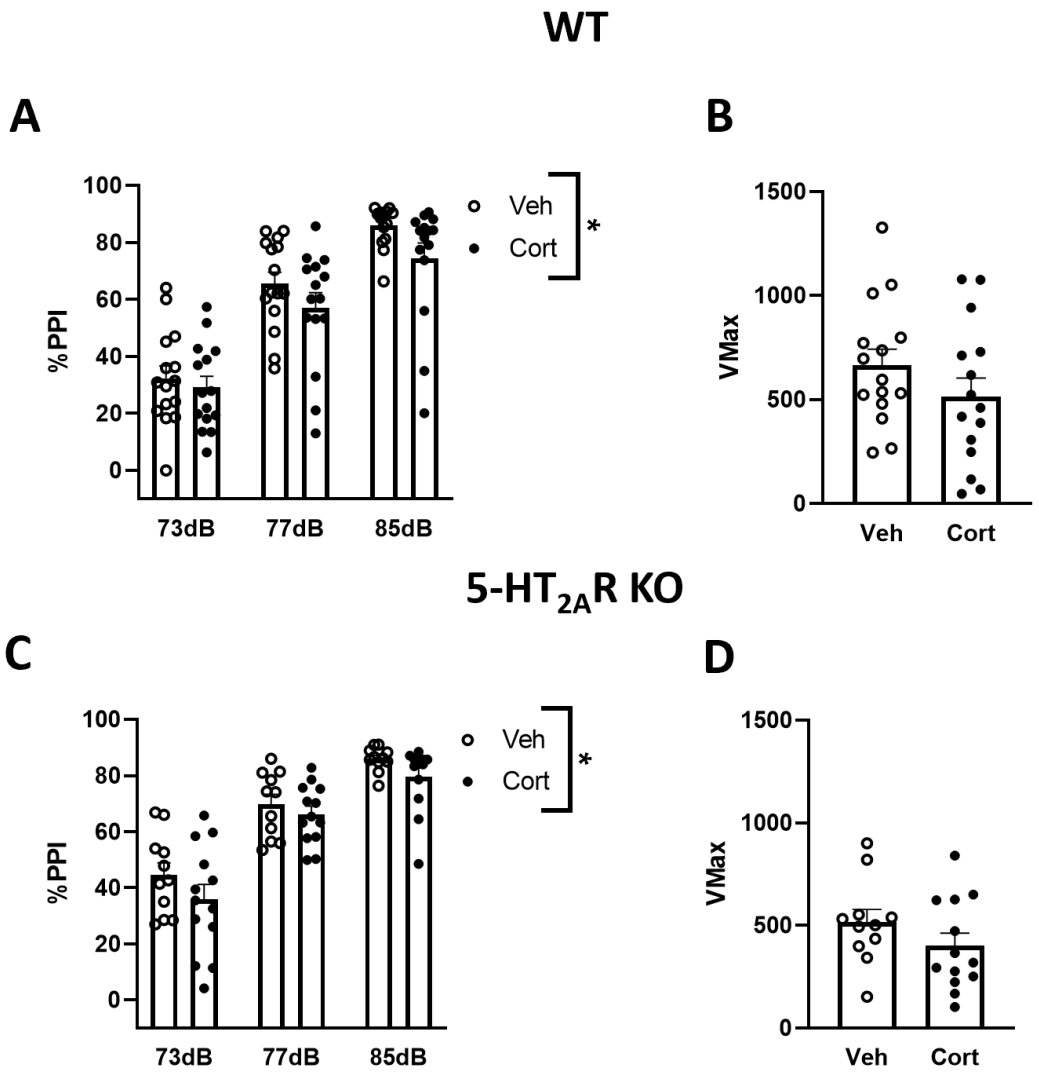

Fig. 14 | Short term, high dose corticosterone produces PPI deficits in both WT and 5-HT$_{2A}$R KO mice. The PPI experimental paradigm was performed as in Fig. 4. WT and 5-HT$_{2A}$R KO mice were treated with 50 mg/kg s.c. corticosterone or vehicle twice a day for four days and were tested about 8.5-13.5 hours after the last injection. Both %PPI (**a,c**) and VMax (**b,d**) are reported for both genotypes. **a.** Corticosterone treatment produces a main effect of decreased %PPI in WT mice (n = 15 mice/group; Prepulse Intensity: $F[2,84] = 67.28$, $p < 0.0001$; Treatment: $F[1,84] = 4.87$, $p < 0.05$; Interaction: $F[2,84] = 0.48$, $p > 0.05$). **b.** Startle magnitude was unaffected ($t_{28} = 1.28$, $p > 0.05$). **c.** Similarly, corticosterone treatment produces a main effect of decreased PPI in 5-HT$_{2A}$R KO mice (n = 11-13 mice/group; Prepulse Intensity: $F[2,66] = 66.62$, $p < 0.0001$; Treatment: $F[1,66] = 4.20$, $p < 0.05$; Interaction: $F[2,66] = 0.24$, $p > 0.05$). **d.** Startle magnitude was unaffected ($t_{22} = 1.30$, $p > 0.05$). Statistical analysis was performed by two-way ANOVA followed by Bonferroni's post-hoc test (**a,c**) or two-tailed Student's *t*-test (**b,d**). *$p < 0.05$.

Source of Variation	% of total variation	P value	P value summary	Significant?
Prepulse Intensity	58.68	<0.0001	***	Yes
Genotype	1.595	0.0098	**	Yes
Treatment	1.995	0.0040	**	Yes
Prepulse Intensity x Genotype	0.3288	0.50	n.s.	No
Prepulse Intensity x Treatment	0.08142	0.84	n.s.	No
Genotype x Treatment	0.02228	0.76	n.s.	No
Prepulse Intensity x Genotype x Treatment	0.2516	0.58	n.s.	No

Table 2 | Three-way ANOVA reveals improved PPI in 5-HT_{2A}R KO mice as well as PPI deficits in mice treated with corticosterone. This table analyzes the same WT and 5-HT_{2A}R KO mice treated with corticosterone or vehicle described in Fig. 14. Three-way ANOVA reveals a main effect of Prepulse Intensity ($F[2,150] = 125.7$, $p < 0.0001$). A main effect of Genotype reveals improved PPI in 5-HT_{2A}R KO mice ($F[1,150] = 6.84$, $p < 0.01$). A main effect of Treatment reveals PPI deficits in mice treated with corticosterone ($F[1,150] = 8.55$, $p < 0.01$). No significant interactions were observed (Prepulse Intensity x Genotype: $F[2,150] = 0.70$, $p > 0.05$; Prepulse Intensity x Treatment: $F[2,150] = 0.17$, $p > 0.05$; Genotype x Treatment: $F[1,150] = 0.095$, $p > 0.05$; Prepulse Intensity x Genotype x Treatment: $F[2,150] = 0.54$, $p > 0.05$). **$p < 0.01$, ***$p < 0.001$, n.s., not significant.

Comparison	Significance
Main Effects	
Veh. vs. Cort	*p = 0.090*
WT vs. 2A KO	*p = 0.091*
Interaction	*n.s.*

Table 3 | Two-way ANOVA reveals trends towards main effects of decreased startle magnitude in 5-HT_{2A}R KO and corticosterone-treated mice. This table analyzes the same startle magnitude values from WT and 5-HT_{2A}R KO mice treated with corticosterone or vehicle described in Fig. 14. Two-way ANOVA reveals a trend towards a main effect of decreased startle magnitude in 5-HT_{2A}R KO mice (Genotype: $F[1,50] = 2.98$, $p = 0.091$). There is also a trend towards a main effect of decreased startle magnitude in corticosterone-treated mice (Treatment: $F[1,50] = 2.99$, $p = 0.090$). No interaction was observed ($F[1,50] = 0.054$, $p = 0.82$). Data were analyzed by two-way ANOVA. n.s., not significant. WT: wild type, 2A KO: 5-HT_{2A}R KO.

RE. An AAV8-*CaMKIIα*-ΔGR-P2A-eYFP viral vector produces decreased *5-HT$_{2A}$R* mRNA in mouse frontal cortex accompanied by increased PPI in WT mice

RE.1. A ΔGR construct can be used to express a constitutively translocating GR, expression of which reduces *5-HT$_{2A}$R* expression in mouse frontal cortex

Systemically administered glucocorticoids exert a wide variety of effects throughout the body.[99] Following our MIA and corticosterone findings supporting an apparent negative regulatory relationship between GR signaling and *5-HT$_{2A}$R* expression, we searched for a third experimental system capable of manipulating GR signaling specifically in mouse frontal cortex. A GR truncation, ΔGR, was first identified due to its ability to activate a reporter gene even in the absence of hormone ligand. It was later found that ΔGR lacked the hormone binding domain[113] and was therefore able to constitutively translocate to the nucleus, where it has the potential to affect transcription.[114] We therefore generated a ΔGR construct from murine cDNA (see methods for additional details) and cloned it to generate a *CaMKIIα*-ΔGR-P2A-eYFP plasmid for packaging into an adeno-associated viral vector of serotype 8 (AAV8).[103] This plasmid (**Fig. 15a**) is expressed under the control of the *CaMKIIα* promoter, which restricts expression to pyramidal neurons in mouse cortex.[115] In addition, the inclusion of a P2A peptide sequence allows for expression of ΔGR and eYFP as independent proteins from the same transcript.[116] To validate this plasmid construct, we transfected Neuro-2a (N2a) mouse neuroblastoma cells, which endogenously express CaMKIIα. To compare subcellular localization of ΔGR with that of WT, we transfected N2a cells with a plasmid coding for a full-length human GR under the control of the *CMV* promoter. As a negative control, additional N2a cells were mock transfected. N2a cells from all three of these experimental groups were then processed for immunofluorescence (**Fig. 15b**), including incubation with an anti-GR primary antibody and Alexa 568-conjugated fluorescent secondary to allow for visualization of the GR. Nuclei were visualized with Hoechst staining. IF in these cells reveals absence of both eYFP (green channel) and GR signal (red channel) in mock transfected cells. As expected, eYFP signal is only observed

in cells transfected with the ΔGR construct. Alexa 568-GR signal is observed following transfection with either the ΔGR construct or the human GR construct, but the ΔGR construct produces a more nuclear fluorescence pattern than the full-length GR, suggesting appropriate ΔGR behavior. The difference in localization patterns for ΔGR and eYFP suggest appropriate function of the P2A peptide. To further demonstrate expression of the ΔGR plasmid, a WB was conducted in the nuclear fraction of cells transfected with the ΔGR plasmid or left untransfected as a negative control (**Fig. 15c**). Probing with an anti-GR antibody demonstrates GR overexpression relative to controls, further supporting appropriate ΔGR expression in the nuclear compartment.

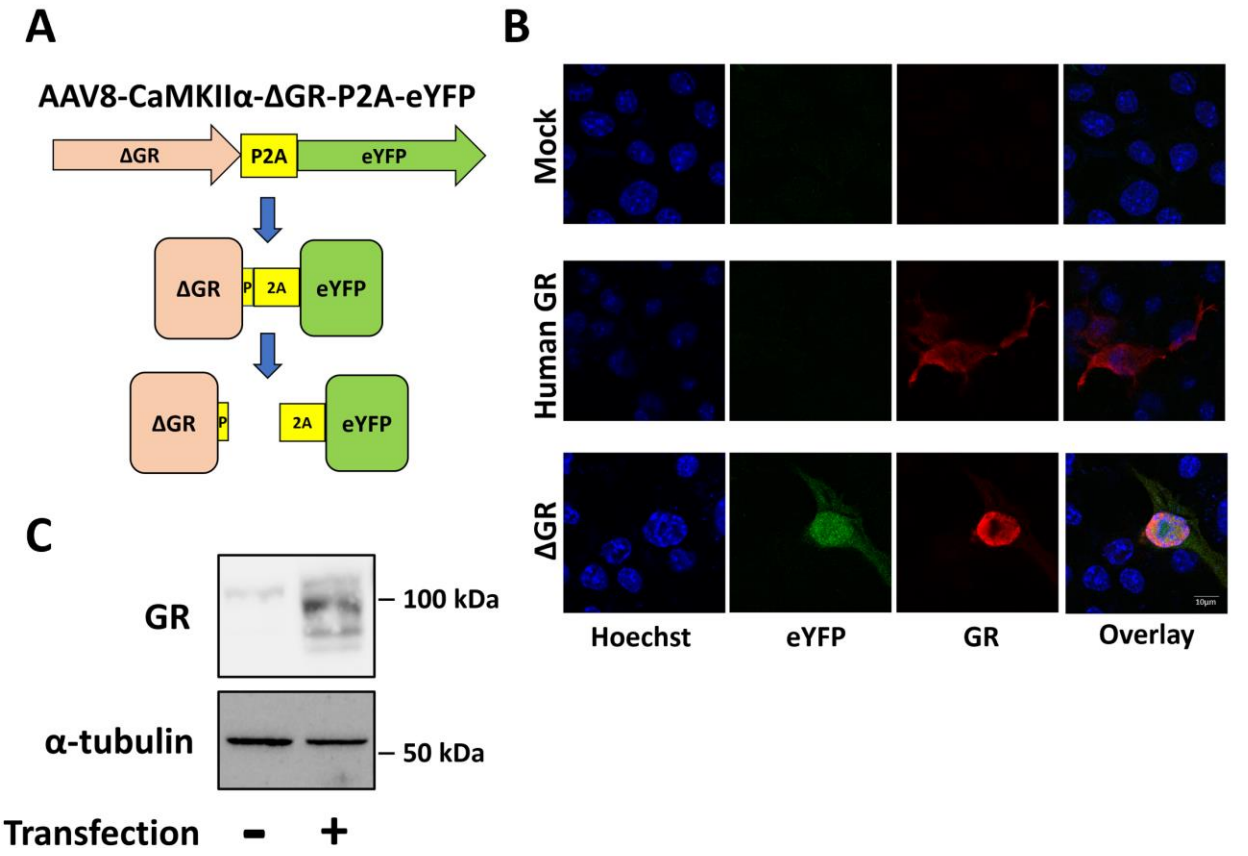

Fig. 15 | A *CaMKIIα*-ΔGR-P2A-eYFP construct independently expresses ΔGR and eYFP protein in Neuro-2a cells. a. The structure for a construct coding for ΔGR and eYFP under the control of the *CaMKIIα* promoter is depicted. A P2A peptide sequence is included to allow for expression of ΔGR and eYFP as independent proteins from a single transcript. **b.** N2a cells were either mock transfected, transfected with a plasmid coding for a full-length human GR under the control of the CMV promoter, or transfected with the plasmid coding for the ΔGR truncation and eYFP construct under the control of the *CaMKIIα*

promoter. The transfected cells were processes for immunofluorescence 48 hours later and an anti-GR primary antibody and Alexa 568-conjugated fluorescent secondary antibody were used to visualize GR protein. IF reveals that the ΔGR truncation exhibits a more nuclear localization pattern than the full-length human GR. The ΔGR construct expresses eYFP independently from ΔGR as expected, indicating appropriate function of the P2A peptide. **c.** N2a cells were transfected with a plasmid containing the ΔGR construct or mock transfected and western blotting was performed using an anti-GR antibody in samples from the nuclear compartment collected 48 hours after transfection. An anti-α-tubulin antibody was used as a loading control. Molecular weight in kDa is reported to the right of the images. Transfection with the ΔGR construct produces increased GR immunoreactivity in the nuclear compartment of N2a cells.

RE.2. An AAV8-*CaMKIIα*-ΔGR-P2A-eYFP viral vector decreases *5-HT$_{2A}$R* mRNA in mouse frontal cortex

After validating the ΔGR construct in cells, we had the plasmid packaged into an AAV8 viral vector, which was then stereotaxically injected into mouse frontal cortex (**Fig. 16a**; see methods for coordinates). Three weeks after surgical injection, mice were perfused and sections were processed for IF, including incubation with an anti-GR primary antibody and Alexa 568-conjugated fluorescent secondary (**Fig. 16b**). Similar to N2a cells, distinct localization patterns of eYFP and Alexa 568-GR signal can be observed, demonstrating expression and appropriate P2A function of the ΔGR vector in mouse frontal cortex. To further validate the vector, we performed RT-qPCR for the *GR* and associated genes in frontal cortex samples from mice that had been injected with AAV8-ΔGR or an AAV8-eYFP empty vector control. As expected, AAV8-ΔGR produces increased expression of *GR* mRNA in mouse frontal cortex (**Fig. 16c**; $t_6 = 3.93$, $p < 0.01$). While *FKBP4* mRNA remains unaffected (**Fig. 16d**; $t_6 = 0.098$, $p > 0.05$), *FKBP5* mRNA is also induced, suggesting negative feedback along the GR signaling pathway (**Fig. 16e**; $t_6 = 3.51$, $p < 0.05$). AAV8-ΔGR is therefore appropriately expressed and functions within mouse frontal cortex.

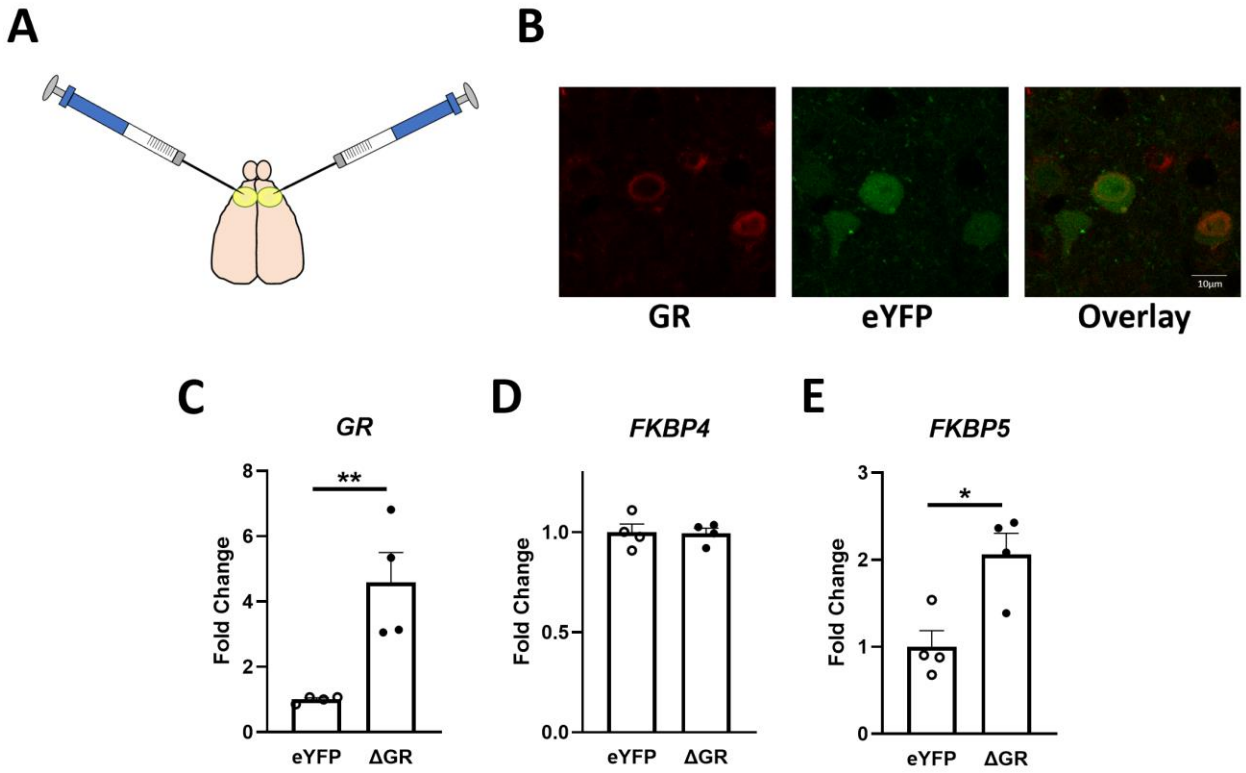

Fig. 16 | An AAV8-*CaMKIIα*-ΔGR-P2A-eYFP viral vector independently expresses ΔGR and eYFP in mouse frontal cortex. a. The construct described in Fig. 15 was packaged into an AAV8 serotype viral vector and stereotaxically injected bilaterally into mouse frontal cortex. The Hamilton syringe needles depict the injection sites (*see methods for coordinates*). Mice were sacrificed for analysis 3 weeks after vector injection. **b.** A representative IF image reveals that the construct is expressed in mouse frontal cortex and that ΔGR and eYFP are expressed independently due to the P2A peptide. An anti-GR primary antibody and Alexa 568-conjugated fluorescent secondary were used for GR visualization. **c-e.** RT-qPCR was conducted in mouse frontal cortex samples from mice that had been injected with the AAV8-ΔGR vector or a negative control AAV8-eYFP vector. **c.** The AAV8-ΔGR vector produces increased *GR* mRNA expression in mouse frontal cortex as expected (n = 4 mice/group; $t_6 = 3.93$, $p < 0.01$). **d.** ΔGR expression does not affect *FKBP4* mRNA expression in mouse frontal cortex ($t_6 = 0.098$, $p > 0.05$). **e.** ΔGR expression produces increased *FKBP5* mRNA expression in mouse frontal cortex ($t_6 = 3.51$, $p < 0.05$). Statistical analysis was performed by two-tailed Student's *t*-test. *$p < 0.05$, **$p < 0.01$.

To further explore the effect of ΔGR expression on GR signaling in mouse frontal cortex, we performed RT-qPCR for GR downstream target genes. At least at this time point, AAV8-ΔGR does not affect mRNA expression for the GR targets *DUSP1* (**Fig. 17a**; $t_6 = 1.14$, $p > 0.05$), *GILZ* (**Fig. 17b**; $t_6 = 1.01$, $p > 0.05$), or *PER1* (**Fig. 17c**; $t_6 = 0.17$, $p > 0.05$) in mouse frontal cortex. We next evaluated the effect of the ΔGR

construct on neurotransmitter receptor expression in mouse frontal cortex by conducting RT-qPCR in the samples from mice that had been injected with either AAV8-ΔGR or AAV8-eYFP vectors. RT-qPCR for *5-HT$_{2A}$R* mRNA reveals decreased frontal cortex expression in mice injected with AAV8-ΔGR relative to controls (**Fig. 18a**; $t_6 = 2.93$, $p < 0.05$). In contrast, *5-HT$_{2C}$R* (**Fig. 18b**; $t_6 = 0.66$, $p > 0.05$) and dopamine *D$_2$* (**Fig. 18c**; $t_6 = 0.32$, $p > 0.05$) mRNA were not affected by ΔGR expression. Therefore, overexpression of the GR using a ΔGR construct reduces *5-HT$_{2A}$R* expression, further supporting a negative regulatory relationship between GR signaling and *5-HT$_{2A}$R* expression. Thus, three independent experimental approaches support this regulatory relationship.

Fig. 17 | The AAV8-ΔGR vector does not affect *DUSP1*, *GILZ*, or *PER1* mRNA expression in mouse frontal cortex. a. RT-qPCR was performed in frontal cortex samples collected 3 weeks after mice were injected with bilateral frontal cortex with the AAV8-ΔGR vector an AAV8-eYFP vector control (*the same mice as in Fig. 16*). **a.** ΔGR expression does not affect *DUSP1* mRNA expression in mouse frontal cortex (n = 4 mice/group; $t_6 = 1.136$, $p > 0.05$). **b.** Similarly, ΔGR expression does not affect *GILZ* mRNA expression in mouse frontal cortex ($t_6 = 1.008$, $p > 0.05$). **c.** *PER1* mRNA expression was also unaffected by ΔGR expression ($t_6 = 0.1718$, $p > 0.05$). Statistical analysis was performed by two-tailed Student's *t*-test.

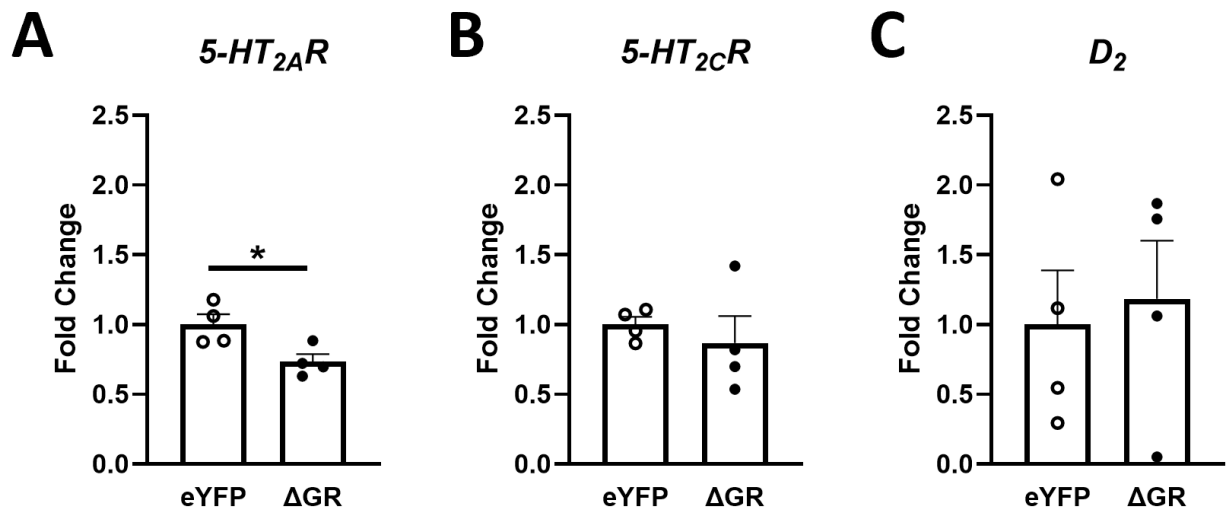

Fig. 18 | The AAV8-ΔGR vector decreases *5-HT$_{2A}$R*, but not *5-HT$_{2C}$R* or *D$_2$*, mRNA in mouse frontal cortex. RT-qPCR was performed in frontal cortex samples collected 3 weeks after mice were injected in bilateral frontal cortex with the AAV8-ΔGR vector or an AAV8-eYFP vector control (*the same mice as in Fig. 16*). **a.** ΔGR expression decreases *5-HT$_{2A}$R* mRNA expression in mouse frontal cortex (n = 4 mice/group; $t_6 = 2.93$, $p < 0.05$). **b**. ΔGR expression does not affect *5-HT$_{2C}$R* mRNA expression in mouse frontal cortex ($t_6 = 0.66$, $p > 0.05$). **c.** ΔGR expression does not affect dopamine *D2* mRNA expression in mouse frontal cortex ($t_6 = 0.32$, $p > 0.05$). Statistical analysis was performed by two-tailed Student's *t*-test. *$p < 0.05$.

RE.3. An AAV8-*CaMKIIα*-ΔGR-P2A-eYFP viral vector increases PPI in a 5-HT$_{2A}$R-dependent manner

Following from this finding that AAV8-ΔGR exerts an opposite effect than MIA on *5-HT$_{2A}$R* mRNA in mouse frontal cortex, we sought to determine the behavioral effects of ΔGR expression on PPI. To accomplish this, we injected adult WT and 5-HT$_{2A}$R KO mice with either an AAV8-ΔGR or an AAV8-eYFP control vector in frontal cortex and tested them for PPI three weeks later. In WT mice, ΔGR expression in frontal cortex produces increased %PPI relative to control (**Fig. 19a**; Prepulse Intensity: $F[2,84] = 159.6$, $p < 0.0001$; Vector: $F[1,84] = 8.30$, $p < 0.01$; Interaction: $F[2,84] = 0.43$, $p > 0.05$), as well as a trend towards increased %PPI specifically at the 77 dB prepulse intensity (Bonferroni's post-hoc test: $p = 0.092$). ΔGR expression had no effect on startle magnitude in WT mice (**Fig. 19b**; $t_{28} = 0.27$, $p > 0.05$). In 5-HT$_{2A}$R KO mice, ΔGR expression did not affect %PPI (**Fig. 19c**; Prepulse Intensity: $F[2,87] = 92.77$, $p <$

0.0001; Vector: F[1,87] = 1.32, p > 0.05; Interaction: F[2,87] = 0.36, p > 0.05) or startle magnitude (**Fig. 19d**; t_{29} = 1.22, p > 0.05). Performing a three-way ANOVA comparing both genotypes, main effects of Genotype, Prepulse Intensity, and Vector are observed (**Table 4**). Thus, 5-HT_{2A}R KO mice exhibit increased %PPI relative to WT mice. ΔGR increases %PPI as well, an effect that seems to be driven by WT mice given that there is no difference between 5-HT_{2A}R KO mice treated with AAV8-ΔGR and AAV8-eYFP vectors. In addition, WT mice exhibit increased startle magnitude relative to 5-HT_{2A}R KO mice (**Table 5**), with increased startle magnitude in WT mice treated with AAV8-ΔGR relative to 5-HT_{2A}R KO mice treated with AAV8-ΔGR. WT mice treated with AAV8-eYFP exhibit increased startle magnitude compared to 5-HT_{2A}R KO mice treated with AAV8-ΔGR (Bonferroni's post-hoc test: p < 0.05). Therefore ΔGR expression produces both decreased *5-HT_{2A}R* mRNA in mouse frontal cortex as well as increases %PPI in an 5-HT_{2A}R-dependent manner, in an apparently opposite pattern to the effects caused by MIA.

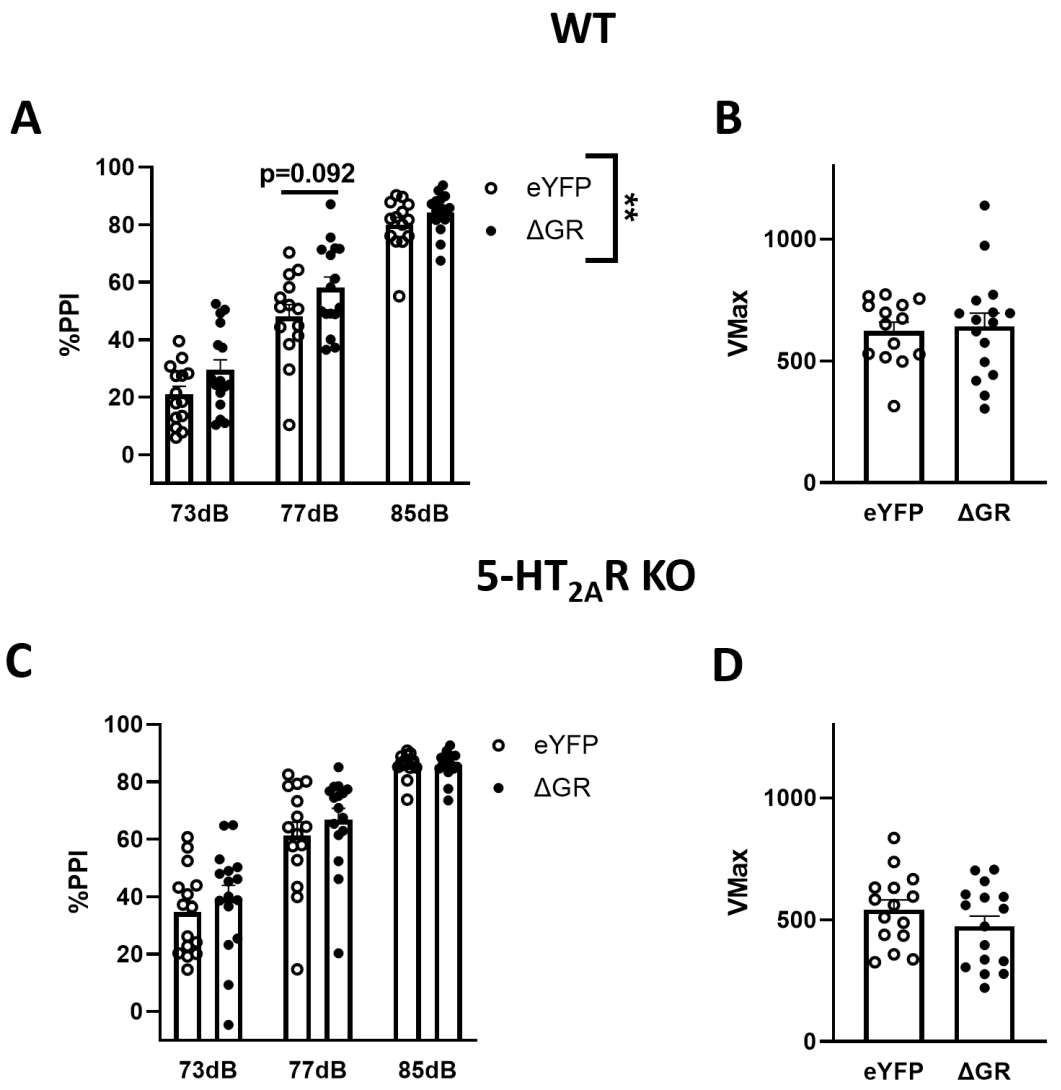

Fig. 19 | AAV8-ΔGR expression in frontal cortex improves PPI in mice in a 5-HT$_{2A}$R-dependent manner. The PPI experimental paradigm was performed as in Fig. 4. WT and 5-HT$_{2A}$R KO mice were injected with AAV8-eYFP or AAV8-ΔGR vectors 3 weeks before the experiment. Both %PPI (**a,c**) and VMax (**b,d**) are reported for both genotypes. **a.** ΔGR expression in frontal cortex produces a main effect of increased %PPI in WT mice as well as a trend towards improved PPI at the 77 dB prepulse level (n = 14-16 mice/group; Prepulse Intensity: $F[2,84] = 159.6$, $p < 0.0001$; Vector: $F[1,84] = 8.30$, $p < 0.01$; Interaction: $F[2,84] = 0.43$, $p > 0.05$; $p = 0.092$ at 77 dB prepulse level). **b.** ΔGR expression in frontal cortex does not affect startle magnitude in WT mice ($t_{28} = 0.27$, $p > 0.05$). **c.** ΔGR expression in frontal cortex does not affect %PPI in 5-HT$_{2A}$R KO mice (n = 15-16 mice/group; Prepulse Intensity: $F[2,87] = 92.77$, $p < 0.0001$; Vector: $F[1,87] = 1.32$, $p > 0.05$; Interaction: $F[2,87] = 0.36$, $p > 0.05$). **d.** ΔGR expression in frontal cortex does not affect startle magnitude in 5-HT$_{2A}$R KO mice ($t_{29} = 1.22$, $p > 0.05$). Statistical analysis was performed by two-way ANOVA followed by Bonferroni's post-hoc test (**a,c**) or two-tailed Student's *t*-test (**b,d**). **$p < 0.01$.

Source of Variation	% of total variation	P value	P value summary	Significant?
Prepulse Intensity	70.51	<0.0001	***	Yes
Genotype	2.906	<0.0001	***	Yes
Vector	1.116	0.0063	**	Yes
Prepulse Intensity x Genotype	0.4991	0.18	n.s.	No
Prepulse Intensity x Vector	0.2285	0.46	n.s.	No
Genotype x Vector	0.1607	0.30	n.s.	No
Prepulse Intensity x Genotype x Vector	0.0008252	0.997	n.s.	No

Table 4 | Three-way ANOVA reveals improved PPI in both 5-HT$_{2A}$R KO mice as well as mice injected with AAV8-ΔGR. This table analyzes the same WT and 5-HT$_{2A}$R KO mice injected with AAV8-ΔGR or AAV8-eYFP described in Fig. 19. Three-way ANOVA reveals a main effect of Prepulse Intensity ($F[2,171] = 241.5$, $p < 0.0001$). A main effect of Genotype reveals improved PPI in 5-HT$_{2A}$R KO mice ($F[1,171] = 19.90$, $p < 0.0001$). A main Vector effect reveals improved PPI following AAV8-ΔGR ($F[1,171] = 7.64$, $p < 0.01$), which seems to be driven by the Vector effect in WT mice. No significant effects of interactions were observed (Prepulse Intensity x Genotype: $F[2,171] = 1.71$, $p > 0.05$; Prepulse Intensity x Vector: $F[2,171] = 0.78$, $p > 0.05$; Genotype x Vector $F[1,171] = 1.10$, $p > 0.05$; Prepulse Intensity x Genotype x Vector: $F[2,171] = 0.0028$, $p > 0.05$). **p < 0.01, ***p < 0.001, n.s., not significant.

	Comparison	Significance
Main Effects		
	eYFP vs. ΔGR	*n.s.*
	WT vs. 2A KO	**
	Interaction	*n.s.*
Post-hoc Tests		
	eYFP WT vs. eYFP KO	*n.s.*
	eYFP WT vs. ΔGR WT	*n.s.*
	eYFP WT vs. ΔGR KO	*n.s.*
	eYFP KO vs. ΔGR WT	*n.s.*
	eYFP KO vs. ΔGR KO	*n.s.*
	ΔGR WT vs. ΔGR KO	*

Table 5 | Two-way ANOVA reveals a main effect of decreased startle magnitude in 5-HT$_{2A}$R KO mice. This table analyzes the same startle magnitude values from WT and 5-HT$_{2A}$R KO mice injected with AAV8-ΔGR or AAV8-eYFP described in Fig. 19. Two-way ANOVA reveals a main effect of decreased startle magnitude in 5-HT$_{2A}$R KO mice (Genotype: $F[1,57] = 8.07$, $p < 0.01$). No significant Vector ($F[1,57] = 0.34$, $p > 0.05$) or Interaction ($F[1,57] = 0.99$, $p > 0.05$) effects were observed. Post-hoc tests reveal a decrease in startle magnitude in AAV8-ΔGR injected 5-HT$_{2A}$R KO mice relative to AAV8-ΔGR-injected WT mice ($p < 0.05$). Data were analyzed by two-way ANOVA followed by Bonferroni's post-hoc. *p < 0.05, **p < 0.01, n.s., not significant. WT: wild type, 2A KO: 5-HT$_{2A}$R KO.

RE.4. ΔGR induces a negative correlation between average %PPI and startle magnitude in WT mice

Finally, we evaluated Pearson's correlation between average %PPI and VMax in mice from our ΔGR PPI experiment. WT mice injected with AAV-eYFP did not exhibit a correlation between Avg. %PPI and VMax (**Fig. 20a**; r = 0.056, p > 0.05). However, a negative correlation between Avg. %PPI and VMax was observed in WT mice injected with AAV-ΔGR (**Fig. 20b**; r = -0.66, p < 0.01). No significant correlation was observed in 5-HT_{2A}R KO mice injected with either AAV-eYFP (**Fig. 20c**; r = -0.26, p > 0.05) or AAV-ΔGR (**Fig. 20d**; r = -0.24, p > 0.05). Therefore, ΔGR expression induces a negative correlation between average %PPI and startle magnitude in WT, but not 5-HT_{2A}R KO mice, which coincides with improved PPI performance.

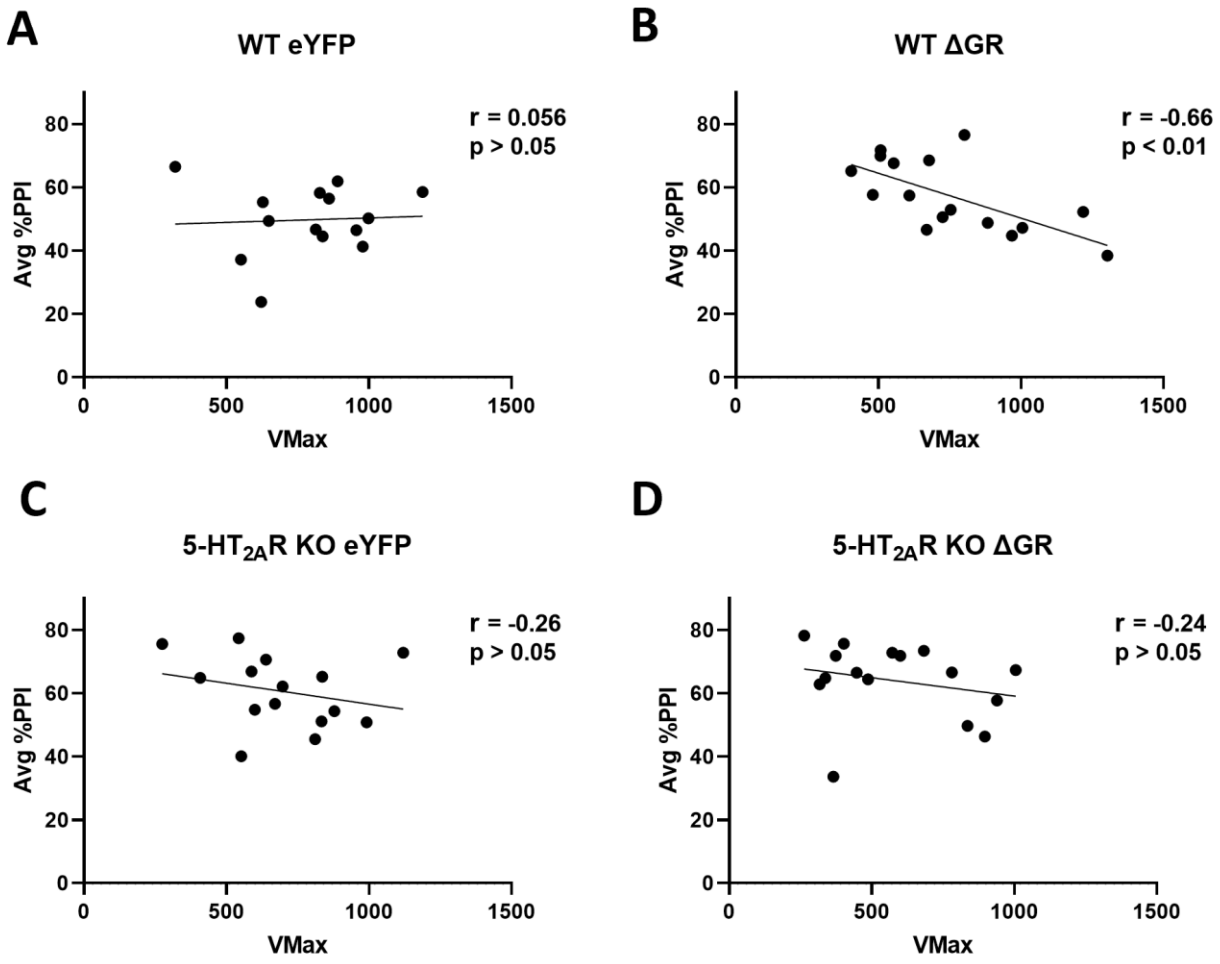

Fig. 20 | AAV8-ΔGR induces a negative correlation between average %PPI and startle magnitude in WT mice. This figure analyzes the startle magnitude and average of the three %PPI values in WT and 5-HT_{2A}R KO mice that had been injected with AAV8-eYFP or AAV8-ΔGR presented in Fig. 19. Pearson's correlation coefficient (r) was calculated between Avg. %PPI and VMax for mice from each treatment group. The fit from a simple linear regression is also included in each figure. **a.** No correlation between Avg. %PPI and VMax was observed in WT mice injected with AAV8-eYFP ($p > 0.05$). **b.** AAV8-ΔGR induces a negative correlation between Avg. %PPI and VMax in WT mice ($p < 0.01$). **c,d.** No correlation was observed for 5-HT_{2A}R KO mice injected with either AAV8-eYFP (**c**) or AAV8-ΔGR (**d**). The p-value for Pearson's r was calculated by a two-tailed test.

Discussion

D.1. Summary of Findings

These studies support, using three independent models, that GR signaling acts to suppress *5-HT$_{2A}$R* expression via direct regulation of the *5-HT$_{2A}$R* promoter. Within frontal cortex in a MIA mouse model, decreased GR immunoreactivity in the nuclear compartment and decreased enrichment of the GR at the *5-HT$_{2A}$R* promoter coincide with increased *5-HT$_{2A}$R* mRNA expression. In turn, MIA induces a 5-HT$_{2A}$R-dependent decrease in mushroom dendritic spine density on cortical pyramidal neurons. Thus, MIA-induced alterations in GR signaling appear to underlie 5-HT$_{2A}$R dysregulation and associated phenotypes within this model. Given that we also observe GR dysregulation in postmortem samples from schizophrenia subjects, there is evidence for translational implications of these phenotypes. This pattern of decreased GR signaling on the *5-HT$_{2A}$R* promoter and increased *5-HT$_{2A}$R* mRNA expression is further supported by our findings in corticosterone-treated mice, which reflect the changes observed in MIA offspring. Opposite to the pattern observed with MIA offspring and corticosterone-treated mice, ΔGR expression in mouse frontal cortex produces a decrease in *5-HT$_{2A}$R* mRNA expression and improves PPI in a 5-HT$_{2A}$R-dependent manner. These data, taken as a whole, suggest that MIA produces reduction in GR signaling in mouse frontal cortex, leading to increased *5-HT$_{2A}$R* expression and downstream alterations with relevance to both synaptic structure and behavior. This may provide insight into the mechanisms behind 5-HT$_{2A}$R dysregulation and schizophrenia symptoms. **Figure 21** depicts a flow chart that integrates our findings with those of other MIA studies.

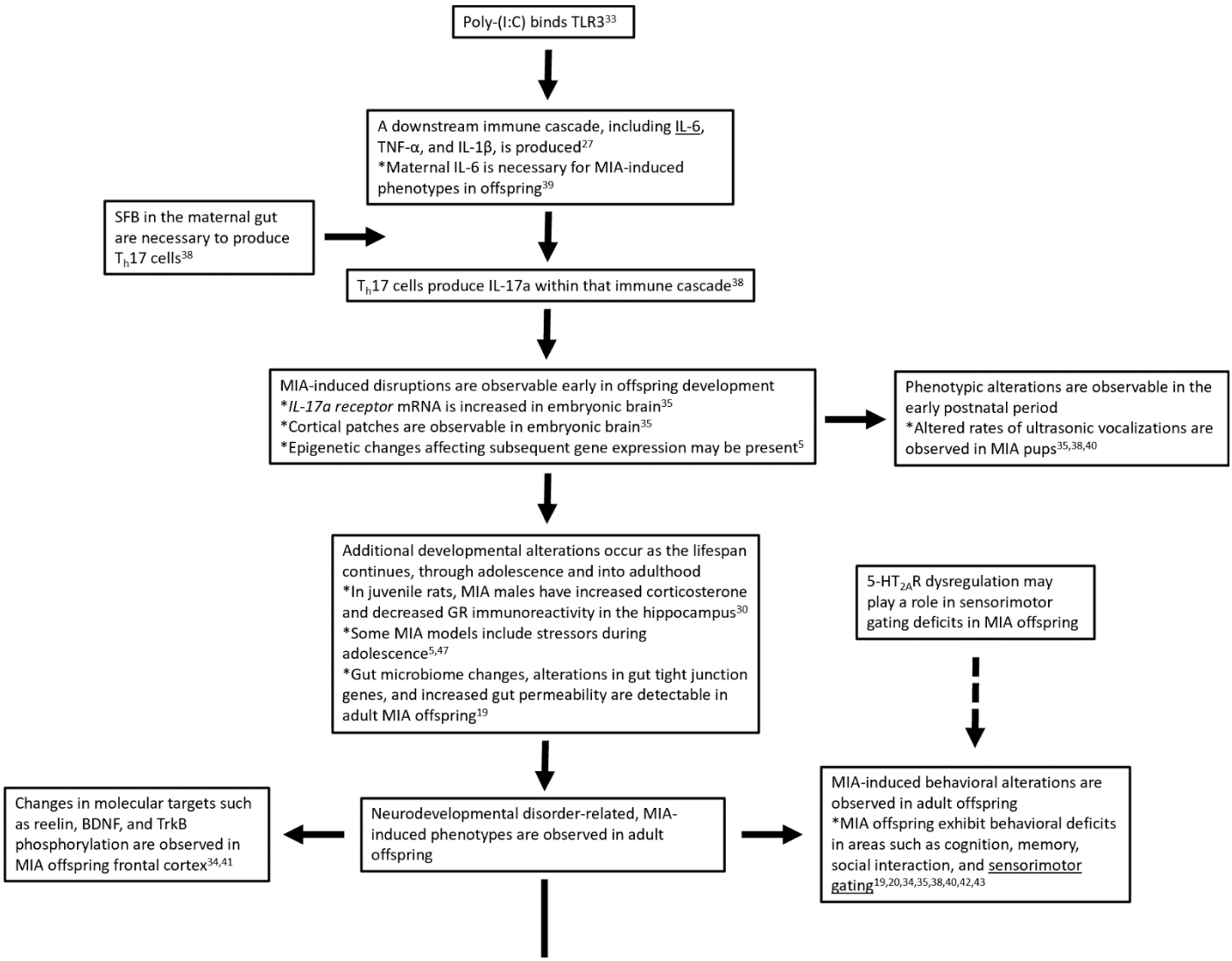
Poly-(I:C) binds TLR3[33]
A downstream immune cascade, including IL-6, TNF-α, and IL-1β, is produced[27]
*Maternal IL-6 is necessary for MIA-induced phenotypes in offspring[39]
SFB in the maternal gut are necessary to produce T_h17 cells[38]
T_h17 cells produce IL-17a within that immune cascade[38]
MIA-induced disruptions are observable early in offspring development
**IL-17a receptor* mRNA is increased in embryonic brain[35]
*Cortical patches are observable in embryonic brain[35]
*Epigenetic changes affecting subsequent gene expression may be present[5]
Phenotypic alterations are observable in the early postnatal period
*Altered rates of ultrasonic vocalizations are observed in MIA pups[35,38,40]
Additional developmental alterations occur as the lifespan continues, through adolescence and into adulthood
*In juvenile rats, MIA males have increased corticosterone and decreased GR immunoreactivity in the hippocampus[30]
*Some MIA models include stressors during adolescence[5,47]
*Gut microbiome changes, alterations in gut tight junction genes, and increased gut permeability are detectable in adult MIA offspring[19]
5-HT_{2A}R dysregulation may play a role in sensorimotor gating deficits in MIA offspring
Changes in molecular targets such as reelin, BDNF, and TrkB phosphorylation are observed in MIA offspring frontal cortex[34,41]
Neurodevelopmental disorder-related, MIA-induced phenotypes are observed in adult offspring
MIA-induced behavioral alterations are observed in adult offspring
*MIA offspring exhibit behavioral deficits in areas such as cognition, memory, social interaction, and sensorimotor gating[19,20,34,35,38,40,42,43]

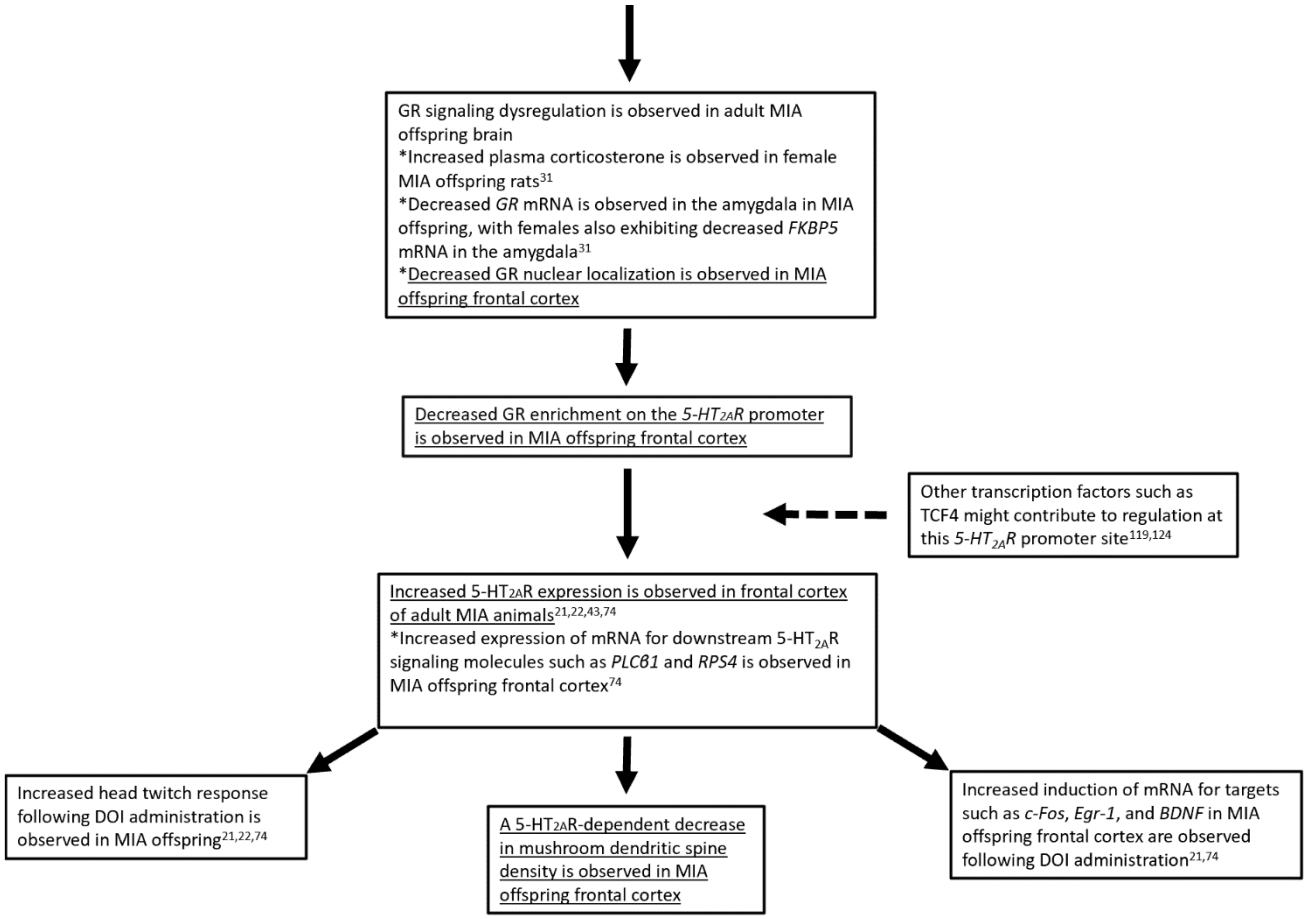

Fig. 21 | The process of maternal immune activation, from poly-(I:C) administration to adult phenotypes, is summarized in this flow chart. Solid arrows represent relationships between confirmed phenotypes, both from these studies and from the literature. Dashed arrows are potential relationships that would need to be evaluated in further studies. Our novel findings from these studies related to MIA offspring are underlined. Findings in these studies that replicate previous findings are both underlined and cited.

Prior to these studies, although 5-HT_{2A}R dysregulation in frontal cortex of MIA models had been demonstrated by our lab and others, the underlying cause of this dysregulation had remained unknown. Here, we provide strong evidence that altered GR signaling may participate in this process. To our knowledge, despite the independent data supporting 5-HT_{2A}R dysregulation in MIA[21, 22, 32, 74] and 5-HT_{2A}R regulation by the GR,[93-95] these are the first studies to investigate the relationship between these two

phenomena. Our results are therefore significant both in light of the association between 5-HT_{2A}R and schizophrenia-related phenotypes[53, 64, 73, 83] as well as the potential translational implications of a novel approach to prefrontal cortex 5-HT_{2A}R regulation in schizophrenia. Manipulations to correct GR dysregulation in schizophrenia may, therefore, be useful strategies to ameliorate 5-HT_{2A}R-implicated schizophrenia symptoms related to domains such as synaptic dysfunction and sensorimotor gating.

D.2. GR Signaling within our Models

Despite the converging evidence from our three independent models, our current data linking GR alterations and increased *5-HT_{2A}R* mRNA remain correlative. A variety of follow-up experiments could be used to directly establish the regulatory relationship between the GR and 5-HT_{2A}R. *In vitro*, a luciferase reporter assay using the GR and *5-HT_{2A}R* promoter could be used to determine the result of GR binding on *5-HT_{2A}R* promoter activity.[108] Direct evaluation of the effect of GR on the *5-HT_{2A}R* promoter could be accomplished in vivo through use of a clustered regulatory interspaced short palindromic repeat (CRISPR)/ nuclease dead Cas9 (dCas9) approach. dCas9, when fused to a transcription factor and expressed alongside a guide RNA (gRNA), can direct that transcription factor to a locus specified by the gRNA sequence.[117] Although our current AAV8-*CaMKIIα*-ΔGR vector approach is able to restrict GR overexpression to frontal cortex pyramidal neurons in mice,[84] the delivered GR remains able to interact with other glucocorticoid response elements (GREs) throughout the genome. The lack of effect of ΔGR on *5-HT_{2C}R* and *D_2* mRNA expression in our experiments suggests some degree of specificity to the effect on *5-HT_{2A}R* mRNA, but alternative signaling explanations cannot be excluded. A CRISPR/dCas9 approach involving a *5-HT_{2A}R* promoter gRNA and a GR-dCas9 fusion virally delivered to neuronal cells in mouse frontal cortex, however, would allow direct determination of the effect of GR occupancy on *5-HT_{2A}R* promoter activity.

The currently available data raise the question of why corticosterone and frontal cortex ΔGR expression exert opposite effects on both *5-HT$_{2A}$R* mRNA expression and PPI. Given that both approaches should promote GR signaling, one might expect them to produce similar phenotypes. One possible explanation for this discrepancy is the ability of negative feedback to constrain GR signaling.[99] Although both corticosterone and ΔGR result in increased *FKBP5* mRNA, suggesting the presence of negative feedback within both experimental systems, ΔGR results in a roughly fourfold, at least at the mRNA level, induction of *GR* expression. In addition, the ΔGR truncation is capable of constitutive nuclear translocation[113, 114] and is not expressed under the control of the endogenous *GR* locus, both of which could render it resistant to endogenous negative feedback mechanisms.[99] Our observation that corticosterone results in decreased enrichment of the GR at the *5-HT$_{2A}$R* promoter further supports the hypothesis that negative feedback may explain this discrepancy. Within this model, sustained ΔGR occupancy at the *5-HT$_{2A}$R* promoter would suppress *5-HT$_{2A}$R* expression while sustained glucocorticoid stimulation with corticosterone would lead to negative feedback, reducing GR occupancy of the *5-HT$_{2A}$R* promoter and stimulating *5-HT$_{2A}$R* expression. A follow-up study performing ChIP in frontal cortex of mice injected with AAV-ΔGR or an AAV-eYFP control would clarify the degree of GR occupancy at the *5-HT$_{2A}$R* promoter following ΔGR expression. In addition, while ΔGR-induced PPI improvements are 5-HT$_{2A}$R dependent, corticosterone-induced PPI deficits are not. While this might be explained by the systemic nature of corticosterone administration, in contrast to frontal cortex-specific ΔGR expression, further studies are needed to clarify what molecular alterations might underlie this difference.

While we observed decreased GR immunoreactivity in the nuclear compartment in MIA offspring frontal cortex, we observed increased GR immunoreactivity in the cytoplasmic compartment in postmortem schizophrenia prefrontal cortex. Increased 5-HT$_{2A}$R expression has been observed within both systems.[21, 53] Given that increased mRNA for the negative regulator *FKBP5* has been reported in postmortem schizophrenia prefrontal cortex, alongside dysregulation of mRNA for other GR interacting proteins,[88]

there is the possibility that dysregulation of other components of the GR signaling system may affect GR translocation in the context of schizophrenia frontal cortex. Increased FKBP5 expression could, for example, act to sequester the GR in the cytoplasm, resulting in increased cytoplasmic GR expression in the absence of increased GR signaling, though further studies would be needed to confirm this. Given the molecular weight of the dysregulated GR isoform (about 65 kDa), its most likely identity is the GR-A isoform. This isoform has been observed in humans, mice, and guinea pigs, but it has not been very well characterized.[118-120] Further studies are necessary to clarify the identity of the detected isoform as well as what its implications might be for both MIA models and schizophrenia.

D.3. The GR Binding Site on the *5-HT$_{2A}$R* Promoter

In a follow-up to the paper reporting the *5-HT$_{2A}$R* promoter GR binding site, Falkenberg et al predict that the GR acts to suppress *5-HT$_{2A}$R* promoter activity at the site.[121] Our experiments confirm GR binding to the site *in vivo* and support this negative regulatory relationship. As discussed in the previous paragraph, negative feedback could explain the apparently divergent effects of GR manipulations on 5-HT$_{2A}$R expression reported in the literature, such as similar phenotypes being observed following corticosterone administration and siRNA-mediated GR knockdown *in vivo*. Our studies therefore provide a crucial advancement to work on the relationship between the two receptors and provide a potential mechanism for the exquisite sensitivity of the 5-HT$_{2A}$R to stress.[89-92]

Transcription factors can act at a common locus to produce their genomic effects.[122] The follow-up paper by Falkenberg et al proposes that GR signaling at the *5-HT$_{2A}$R* binding site interactions with signaling from the E protein family transcription factor Th1-E47, part of which is a product of the *TCF3* gene. In contrast to the GR, they predict Th1-E47 would promote *5-HT$_{2A}$R* expression.[121, 123] While TCF3 and GR signaling have been shown to interact in the mouse liver,[124] TCF3 expression diminishes

dramatically in the mouse telencephalon after embryonic development.[125] We have observed that TCF3 immunoreactivity is detectable in mouse fetal tissue and adult mouse liver, but absent in adult mouse frontal cortex (*data not shown*). The closely related TCF4, however, is expressed in adult mouse cortex and has been identified as a key schizophrenia hub gene.[126] Investigation into TCF4 interaction with GR signaling may therefore be a valuable follow-up study.

D.4. MIA and 5-HT$_{2A}$R Dependence of Phenotypes

Given the numerous factors implicated in MIA processes,[37, 38] discussion of our specific experimental paradigms is warranted. In these studies, we used two strains of mice, 129S6/SvEv and C57BL/6N, for experiments. While IL-6 induction by poly-(I:C) was clear in both strains, the degree of induction observed between the strains was slightly different. In addition, mice from Charles River possess significantly more cecal SFB than mice from other vendors. Given the importance of both of these factors to MIA induction,[38, 39] we cannot exclude involvement of strain in our observed phenotypes. Follow-up studies to evaluate strain dependence of our observed phenotypes would therefore expand our knowledge. Additionally, given that poly-(I:C) signals primarily through a downstream signaling cascade starting with TLR3,[33] use of other agents such as influenza or LPS to confirm our phenotypes could be beneficial. MIA phenotypes have been demonstrated to rely on critical periods of induction.[40] Inducing MIA at earlier or later stages of murine pregnancy could determine the critical period for our observed phenotypes.

An important limitation of our studies is that they primarily use male mice. A sex difference has been observed in age of schizophrenia onset in humans[1] and autism spectrum disorder is diagnosed at increased rates in males as compared to females.[1] As discussed in the introduction, sex differences have been found in other MIA models, with domains such as the effect of DOI on c-Fos immunoreactivity in

MIA frontal cortex,[32] *FKBP5* dysregulation in MIA offspring amygdala,[31] and hippocampal GR immunoreactivity in juvenile MIA offspring being reported.[30] There is therefore the possibility that sex differences may play a role in the phenotypes observed in these studies. In addition, the GR binding site on the *5-HT$_{2A}$R* promoter was identified as a progesterone response element, providing a potential mechanism for sex-specific effects of hormones on 5-HT$_{2A}$R regulation.[100] Although there are examples of previous studies that used both sexes without addressing potential sex differences[20, 21] or used exclusively males,[35, 74] follow-up studies including sufficient numbers of female mice and properly addressing sex as a biological variable are necessary to determine to what degree our observed phenotypes are sex-dependent.

Our dendritic spine data show that the MIA-induced alterations in mushroom dendritic spine density are 5-HT$_{2A}$R dependent. Of note, 5-HT$_{2A}$R knockout mice exhibited lower mushroom spine density regardless of maternal treatment. Within a different experimental paradigm, we observed similar decreases in frontal cortex spine density in 5-HT$_{2A}$R knockout mice.[80] Given the implication of 5-HT$_{2A}$R ligands in synaptic plasticity,[81, 83, 84] decreased mature dendritic spine density in mice lacking endogenous signaling through the 5-HT$_{2A}$R receptor is not surprising. Additional studies are necessary, however, to clarify this mechanism. Given that MIA offspring have been shown to possess immune alterations relative to controls,[5] there is a possibility that altered immune responses may play a role in our dendritic spine findings. This possibility is made less likely by the absence of effect of MIA on spine density in 5-HT$_{2A}$R knockout mice. A 5-HT$_{2A}$R-dependent immune mechanism for altered dendritic spine density, however, cannot be excluded. As follow-up experiments, virally-mediated direct 5-HT$_{2A}$R overexpression in cortical pyramidal neurons to determine if 5-HT$_{2A}$R dysregulation is sufficient to affect its independent effect on dendritic spine density or alternative approaches to dendrite labeling could be used.[49, 127]

In line with these limitations to our explanations for our dendritic spine data, an important unresolved question within our MIA model is the cell type in which 5-HT$_{2A}$R dysregulation occurs in frontal cortex.

We hypothesize that the dysregulation occurs in pyramidal neurons, supported by their high degree of 5-HT_{2A}R expression in layer 5 of mouse cortex[60] and the sufficiency of ΔGR expression in pyramidal neurons to produce decreased *5-HT_{2A}R* mRNA expression detectable at the whole frontal cortex level. Given the absence of cell type-specific markers in our FISH studies and the fact that previous studies demonstrating increased 5-HT_{2A}R expression in frontal cortex have utilized approaches requiring homogenized tissue,[21, 22, 32, 74] this remains an open question. Combining our FISH approach with labeling for cell type specific markers is a follow-up approach that could definitively specify the cell type in which 5-HT_{2A}R is dysregulated within MIA.[62] Identification of this cell type (or types) would facilitate hypothesis generation into the mechanisms by which 5-HT_{2A}R dysregulation might contribute to MIA-induced phenotypes.

We independently demonstrate both PPI deficits in MIA models and 5-HT_{2A}R-dependent PPI improvement following ΔGR expression in frontal cortex pyramidal neurons. Follow-up experiments comparing MIA and control wild type and 5-HT_{2A}R knockout offspring could clarify to what degree 5-HT_{2A}R dysregulation is necessary for PPI deficits within the model. Our results suggest that decreased GR signaling at the *5-HT_{2A}R* promoter is ultimately responsible for 5-HT_{2A}R-dependent deficits in MIA models. To test this hypothesis, restoration of GR expression in frontal cortex of MIA offspring would be necessary. These experiments could be conducted using either our viral ΔGR approach or use of a dCas9-GR construct in MIA offspring frontal cortex. If either of these approaches is able to prevent 5-HT_{2A}R-dependent alterations in MIA offspring, this pathway would be confirmed.

In addition to the effects we observed on PPI, several of our experimental manipulations also produced effects on startle magnitude. MIA, corticosterone administration, and 5-HT_{2A}R knockout status all decrease startle magnitude and ΔGR induces a correlation between average %PPI and startle magnitude in a 5-HT_{2A}R-dependent manner. There is not a clearly established pattern of relationship between PPI and startle magnitude[128] and a variety of factors such as fear and habituation can influence startle

magnitude.[129] The significance of the observed effects on startle magnitude and the interpretation of 5-HT_{2A}R dependence in the effect of ΔGR on startle magnitude remain to be clarified by further studies.

For some of the phenotypes tested in these experiments, trends towards main or post-hoc effects were observed. **Table 6** contains power analysis to determine appropriate sample sizes for follow-up studies that are sufficiently powered to determine if the trends reflect genuine effects on the relevant phenotypes.

	Comparison with Trend	Reported p-value	Necessary sample size (per group)
Fig. 2b	*Post-hoc Test:* qPCR for SFB 16S rRNA in 129Sv and TAC mice	*p = 0.059*	7
Fig. 4b	*Post-hoc Test:* PPI at the 85 dB prepulse level in MIA and Control offspring	*p = 0.074*	46
Fig. 6a	*Main Effect:* Treatment effect for stubby spines in MIA and Control offspring	*p = 0.057*	197
Fig. 6c	*Main Effect:* Genotype effect for mushroom spines in MIA and Control offspring	*p = 0.084*	238
Fig. 6d	*Main Effect:* Genotype effect for total spines in MIA and Control offspring	*p = 0.059*	200
Fig. 6d	*Main Effect:* Treatment effect for total spines in MIA and Control offspring	*p = 0.054*	192
Table 3	*Main Effect:* Treatment effect for startle magnitude in Cort and Veh-treated mice	*p = 0.090*	34
Table 3	*Main Effect:* Genotype effect for startle magnitude in Cort and Veh-treated mice	*p = 0.091*	34
Fig. 18a	*Post-hoc Test:* PPI at the 77 dB prepulse level in ΔGR and eYFP-treated WT mice	*p = 0.092*	51

Table 6 | Power analysis reveals samples sizes to detect genuine effects on phenotypes that exhibited trends in the results. Power analysis was conducted using G*Power software. Both the experimental paradigms and p-values for the trends are included in the table. For post-hoc tests, α was based on 0.05 and adjusted based on the number of comparisons using the Bonferroni correction and β was set at 0.2 for a power of 0.8. Effect sizes were calculated using means and standard deviations from the relevant groups. For main effects, α was set at 0.05 and β was set at 0.2 for a power of 0.8. Effect sizes were calculated using η^2 calculated based on main effect and residual sums of squares from the relevant ANOVA. Calculated sample sizes are reported per group. 129Sv = 129S6/SvEv, TAC = Taconic, Cort = Corticosterone, Veh = Vehicle.

D.5. 5-HT_{2A}R-mGluR2 Heteromerization

Although not directly addressed in these studies, previous work from our lab has proposed that the 5-HT_{2A}R forms a heteromeric complex with metabotropic glutamate receptor 2 (mGluR2).[53] Crosstalk between the two receptors has been extensively demonstrated *in vitro*[69, 130] and mGluR2 expression has been found to be necessary for 5-HT_{2A}R agonist-induced head twitch response in mice.[131] In both MIA offspring frontal cortex and postmortem prefrontal cortex samples from antipsychotic-free human

schizophrenia subjects, increased 5-HT_{2A}R density is accompanied by decreased mGluR2 density.[21, 22, 53] In contrast to the 5-HT_{2A}R density from subjects testing positive for antipsychotics, which is not different from controls, mGluR2 density remains dysregulated in these samples.[53] This human finding is further validated in mice by chronic treatment with the atypical antipsychotic clozapine, which reduces 5-HT_{2A}R density in frontal cortex while also, downstream, reducing mGluR2 density.[108] MIA offspring and, potentially, schizophrenia subjects as well, are therefore characterized by an imbalance in heteromer component expression that is not corrected by antipsychotics. Our data propose a novel mechanism by which 5-HT_{2A}R expression is dysregulated and could therefore be manipulated within MIA offspring. In light of the fact that mGluR2 agonists have been proposed as a novel class of antipsychotics,[132] a GR targeting approach to restrain 5-HT_{2A}R expression might spare downstream mGluR2 expression, potentially allowing for use of mGluR2 agonists within schizophrenia treatment regimens.

D.6. Conclusion

Our data using three independent models suggest that alterations in GR signaling, including both decreased nuclear immunoreactivity and decreased GR enrichment at the *5-HT_{2A}R* promoter, underlie increased *5-HT_{2A}R* mRNA expression in MIA offspring mouse frontal cortex. This 5-HT_{2A}R dysregulation, in turn, is necessary for decreased mushroom spine density in MIA offspring frontal cortex, implicating this process in synaptic structure alterations in the model. Similar GR alterations are observed in frontal cortex of postmortem schizophrenia subjects. These studies therefore provide key insights into mechanisms producing *5-HT_{2A}R* dysregulation in the context of MIA, clarifying the GR to 5-HT_{2A}R signaling relationship and elucidating the mechanisms underlying synaptic and sensorimotor gating phenotypes within the model. These findings, in turn, could direct investigation into novel approaches to schizophrenia treatment.

References

1. American Psychiatric Association., American Psychiatric Association. DSM-5 Task Force. Diagnostic and statistical manual of mental disorders : DSM-5. 5th ed. Washington, D.C.: American Psychiatric Association; 2013. xliv, 947 p. p.

2. Fatemi SH, Folsom TD. Schizophrenia. In: Fatemi SH, Clayton PJ, editors. The medical basis of psychiatry Fourth edition. ed. New York: Springer; 2016. p. xix, 1064 pages.

3. Harvey PD, Koren D, Reichenberg A, Bowie CR. Negative symptoms and cognitive deficits: what is the nature of their relationship? Schizophr Bull. 2006;32(2):250-8.

4. Meltzer HY. Treatment-resistant schizophrenia--the role of clozapine. Curr Med Res Opin. 1997;14(1):1-20.

5. Estes ML, McAllister AK. Maternal immune activation: Implications for neuropsychiatric disorders. Science. 2016;353(6301):772-7.

6. Tsuang M. Schizophrenia: genes and environment. Biol Psychiatry. 2000;47(3):210-20.

7. Schizophrenia Working Group of the Psychiatric Genomics C. Biological insights from 108 schizophrenia-associated genetic loci. Nature. 2014;511(7510):421-7.

8. Du Q, de la Morena MT, van Oers NSC. The Genetics and Epigenetics of 22q11.2 Deletion Syndrome. Front Genet. 2019;10:1365.

9. Cardno AG, Gottesman, II. Twin studies of schizophrenia: from bow-and-arrow concordances to star wars Mx and functional genomics. Am J Med Genet. 2000;97(1):12-7.

10. Brown AS. The environment and susceptibility to schizophrenia. Prog Neurobiol. 2011;93(1):23-58.

11. Brown AS, Begg MD, Gravenstein S, Schaefer CA, Wyatt RJ, Bresnahan M, Babulas VP, Susser ES. Serologic evidence of prenatal influenza in the etiology of schizophrenia. Arch Gen Psychiatry. 2004;61(8):774-80.

12. Sorensen HJ, Mortensen EL, Reinisch JM, Mednick SA. Association between prenatal exposure to bacterial infection and risk of schizophrenia. Schizophr Bull. 2009;35(3):631-7.

13. Brown AS, Cohen P, Harkavy-Friedman J, Babulas V, Malaspina D, Gorman JM, Susser ES. A.E. Bennett Research Award. Prenatal rubella, premorbid abnormalities, and adult schizophrenia. Biol Psychiatry. 2001;49(6):473-86.

14. Brown AS, Schaefer CA, Quesenberry CP, Jr., Liu L, Babulas VP, Susser ES. Maternal exposure to toxoplasmosis and risk of schizophrenia in adult offspring. Am J Psychiatry. 2005;162(4):767-73.

15. Patterson PH. Maternal infection and immune involvement in autism. Trends Mol Med. 2011;17(7):389-94.

16. Atladottir HO, Thorsen P, Ostergaard L, Schendel DE, Lemcke S, Abdallah M, Parner ET. Maternal infection requiring hospitalization during pregnancy and autism spectrum disorders. J Autism Dev Disord. 2010;40(12):1423-30.

17. Gilmore JH, Jarskog LF. Exposure to infection and brain development: cytokines in the pathogenesis of schizophrenia. Schizophr Res. 1997;24(3):365-7.

18. Knuesel I, Chicha L, Britschgi M, Schobel SA, Bodmer M, Hellings JA, Toovey S, Prinssen EP. Maternal immune activation and abnormal brain development across CNS disorders. Nat Rev Neurol. 2014;10(11):643-60.

19. Hsiao EY, McBride SW, Hsien S, Sharon G, Hyde ER, McCue T, Codelli JA, Chow J, Reisman SE, Petrosino JF, Patterson PH, Mazmanian SK. Microbiota modulate behavioral and physiological abnormalities associated with neurodevelopmental disorders. Cell. 2013;155(7):1451-63.

20. Shi L, Fatemi SH, Sidwell RW, Patterson PH. Maternal influenza infection causes marked behavioral and pharmacological changes in the offspring. J Neurosci. 2003;23(1):297-302.

21. Moreno JL, Kurita M, Holloway T, Lopez J, Cadagan R, Martinez-Sobrido L, Garcia-Sastre A, Gonzalez-Maeso J. Maternal influenza viral infection causes schizophrenia-like alterations of 5-HT(2)A and mGlu(2) receptors in the adult offspring. J Neurosci. 2011;31(5):1863-72.

22. Holloway T, Moreno JL, Umali A, Rayannavar V, Hodes GE, Russo SJ, Gonzalez-Maeso J. Prenatal stress induces schizophrenia-like alterations of serotonin 2A and metabotropic glutamate 2 receptors in the adult offspring: role of maternal immune system. J Neurosci. 2013;33(3):1088-98.

23. Shi L, Smith SE, Malkova N, Tse D, Su Y, Patterson PH. Activation of the maternal immune system alters cerebellar development in the offspring. Brain Behav Immun. 2009;23(1):116-23.

24. Meyer U, Feldon J. To poly(I:C) or not to poly(I:C): advancing preclinical schizophrenia research through the use of prenatal immune activation models. Neuropharmacology. 2012;62(3):1308-21.

25. Harvey L, Boksa P. Prenatal and postnatal animal models of immune activation: relevance to a range of neurodevelopmental disorders. Dev Neurobiol. 2012;72(10):1335-48.

26. Chow KH, Yan Z, Wu WL. Induction of Maternal Immune Activation in Mice at Mid-gestation Stage with Viral Mimic Poly(I:C). J Vis Exp. 2016(109):e53643.

27. Cunningham C, Campion S, Teeling J, Felton L, Perry VH. The sickness behaviour and CNS inflammatory mediator profile induced by systemic challenge of mice with synthetic double-stranded RNA (poly I:C). Brain Behav Immun. 2007;21(4):490-502.

28. Whitfield C, Trent MS. Biosynthesis and export of bacterial lipopolysaccharides. Annu Rev Biochem. 2014;83:99-128.

29. Kentner AC, Khoury A, Lima Queiroz E, MacRae M. Environmental enrichment rescues the effects of early life inflammation on markers of synaptic transmission and plasticity. Brain Behav Immun. 2016;57:151-60.

30. Connors EJ, Shaik AN, Migliore MM, Kentner AC. Environmental enrichment mitigates the sex-specific effects of gestational inflammation on social engagement and the hypothalamic pituitary adrenal axis-feedback system. Brain Behav Immun. 2014;42:178-90.

31. Zhao X, Rondon-Ortiz AN, Lima EP, Puracchio M, Roderick RC, Kentner AC. Therapeutic efficacy of environmental enrichment on behavioral, endocrine, and synaptic alterations in an animal model of maternal immune activation. Brain Behav Immun Health. 2020;3.

32. Wischhof L, Irrsack E, Dietz F, Koch M. Maternal lipopolysaccharide treatment differentially affects 5-HT(2A) and mGlu2/3 receptor function in the adult male and female rat offspring. Neuropharmacology. 2015;97:275-88.

33. Alexopoulou L, Holt AC, Medzhitov R, Flavell RA. Recognition of double-stranded RNA and activation of NF-kappaB by Toll-like receptor 3. Nature. 2001;413(6857):732-8.

34. Han M, Zhang JC, Yao W, Yang C, Ishima T, Ren Q, Ma M, Dong C, Huang XF, Hashimoto K. Intake of 7,8-Dihydroxyflavone During Juvenile and Adolescent Stages Prevents Onset of Psychosis in Adult Offspring After Maternal Immune Activation. Sci Rep. 2016;6:36087.

35. Choi GB, Yim YS, Wong H, Kim S, Kim H, Kim SV, Hoeffer CA, Littman DR, Huh JR. The maternal interleukin-17a pathway in mice promotes autism-like phenotypes in offspring. Science. 2016;351(6276):933-9.

36. Harvey L, Boksa P. A stereological comparison of GAD67 and reelin expression in the hippocampal stratum oriens of offspring from two mouse models of maternal inflammation during pregnancy. Neuropharmacology. 2012;62(4):1767-76.

37. Estes ML, Farrelly K, Cameron S, Aboubechara JP, Haapanen L, Schauer JD, Horta A, Prendergast K, MacMahon JA, Shaffer CI, Le CT, Kincheloe GN, Tan DJ, van der List D, Bauman MD, Carter CS, Van de Water J, McAllister AK. Enhancing rigor and reproducibility in maternal immune activation models: practical considerations and predicting resilience and susceptibility using baseline immune responsiveness before pregnancy. bioRxiv. 2019:699983.

38. Kim S, Kim H, Yim YS, Ha S, Atarashi K, Tan TG, Longman RS, Honda K, Littman DR, Choi GB, Huh JR. Maternal gut bacteria promote neurodevelopmental abnormalities in mouse offspring. Nature. 2017;549(7673):528-32.

39. Smith SE, Li J, Garbett K, Mirnics K, Patterson PH. Maternal immune activation alters fetal brain development through interleukin-6. J Neurosci. 2007;27(40):10695-702.

40. Yim YS, Park A, Berrios J, Lafourcade M, Pascual LM, Soares N, Yeon Kim J, Kim S, Kim H, Waisman A, Littman DR, Wickersham IR, Harnett MT, Huh JR, Choi GB. Reversing behavioural abnormalities in mice exposed to maternal inflammation. Nature. 2017;549(7673):482-7.

41. Meyer U, Nyffeler M, Yee BK, Knuesel I, Feldon J. Adult brain and behavioral pathological markers of prenatal immune challenge during early/middle and late fetal development in mice. Brain Behav Immun. 2008;22(4):469-86.

42. Ibi D, Nakasai G, Koide N, Sawahata M, Kohno T, Takaba R, Nagai T, Hattori M, Nabeshima T, Yamada K, Hiramatsu M. Reelin Supplementation Into the Hippocampus Rescues Abnormal Behavior in a Mouse Model of Neurodevelopmental Disorders. Front Cell Neurosci. 2020;14:285.

43. Saunders JM, Moreno JL, Ibi D, Sikaroodi M, Kang DJ, Munoz-Moreno R, Dalmet SS, Garcia-Sastre A, Gillevet PM, Dozmorov MG, Bajaj JS, Gonzalez-Maeso J. Gut microbiota manipulation during the prepubertal period shapes behavioral abnormalities in a mouse neurodevelopmental disorder model. Sci Rep. 2020;10(1):4697.

44. Braff DL, Geyer MA, Swerdlow NR. Human studies of prepulse inhibition of startle: normal subjects, patient groups, and pharmacological studies. Psychopharmacology (Berl). 2001;156(2-3):234-58.

45. Braff DL, Geyer MA. Sensorimotor gating and schizophrenia. Human and animal model studies. Arch Gen Psychiatry. 1990;47(2):181-8.

46. Swerdlow NR, Geyer MA, Braff DL. Neural circuit regulation of prepulse inhibition of startle in the rat: current knowledge and future challenges. Psychopharmacology (Berl). 2001;156(2-3):194-215.

47. Giovanoli S, Engler H, Engler A, Richetto J, Feldon J, Riva MA, Schedlowski M, Meyer U. Preventive effects of minocycline in a neurodevelopmental two-hit model with relevance to schizophrenia. Transl Psychiatry. 2016;6:e772.

48. Coiro P, Padmashri R, Suresh A, Spartz E, Pendyala G, Chou S, Jung Y, Meays B, Roy S, Gautam N, Alnouti Y, Li M, Dunaevsky A. Impaired synaptic development in a maternal immune activation mouse model of neurodevelopmental disorders. Brain Behav Immun. 2015;50:249-58.

49. Glantz LA, Lewis DA. Decreased dendritic spine density on prefrontal cortical pyramidal neurons in schizophrenia. Arch Gen Psychiatry. 2000;57(1):65-73.

50. Baharnoori M, Brake WG, Srivastava LK. Prenatal immune challenge induces developmental changes in the morphology of pyramidal neurons of the prefrontal cortex and hippocampus in rats. Schizophr Res. 2009;107(1):99-109.

51. Ikezu S, Yeh H, Delpech JC, Woodbury ME, Van Enoo AA, Ruan Z, Sivakumaran S, You Y, Holland C, Guillamon-Vivancos T, Yoshii-Kitahara A, Botros MB, Madore C, Chao PH, Desani A, Manimaran S, Kalavai SV, Johnson WE, Butovsky O, Medalla M, Luebke JI, Ikezu T. Inhibition of colony stimulating factor 1 receptor corrects maternal inflammation-induced microglial and synaptic dysfunction and behavioral abnormalities. Mol Psychiatry. 2020.

52. Miyamoto S, Duncan GE, Marx CE, Lieberman JA. Treatments for schizophrenia: a critical review of pharmacology and mechanisms of action of antipsychotic drugs. Mol Psychiatry. 2005;10(1):79-104.

53. Gonzalez-Maeso J, Ang RL, Yuen T, Chan P, Weisstaub NV, Lopez-Gimenez JF, Zhou M, Okawa Y, Callado LF, Milligan G, Gingrich JA, Filizola M, Meana JJ, Sealfon SC. Identification of a serotonin/glutamate receptor complex implicated in psychosis. Nature. 2008;452(7183):93-7.

54. Kim K, Che T, Panova O, DiBerto JF, Lyu J, Krumm BE, Wacker D, Robertson MJ, Seven AB, Nichols DE, Shoichet BK, Skiniotis G, Roth BL. Structure of a Hallucinogen-Activated Gq-Coupled 5-HT2A Serotonin Receptor. Cell. 2020;182(6):1574-88 e19.

55. Thompson AJ, Lummis SC. 5-HT3 receptors. Curr Pharm Des. 2006;12(28):3615-30.

56. Roth BL, Willins DL, Kristiansen K, Kroeze WK. 5-Hydroxytryptamine2-family receptors (5-hydroxytryptamine2A, 5-hydroxytryptamine2B, 5-hydroxytryptamine2C): where structure meets function. Pharmacol Ther. 1998;79(3):231-57.

57. Weisstaub NV, Zhou M, Lira A, Lambe E, Gonzalez-Maeso J, Hornung JP, Sibille E, Underwood M, Itohara S, Dauer WT, Ansorge MS, Morelli E, Mann JJ, Toth M, Aghajanian G, Sealfon SC, Hen R, Gingrich JA. Cortical 5-HT2A receptor signaling modulates anxiety-like behaviors in mice. Science. 2006;313(5786):536-40.

58. Snir O, Hesselberg E, Amoudruz P, Klareskog L, Zarea-Ganji I, Catrina AI, Padyukov L, Malmstrom V, Seddighzadeh M. Genetic variation in the serotonin receptor gene affects immune responses in rheumatoid arthritis. Genes Immun. 2013;14(2):83-9.

59. Nichols CD. Serotonin 5-HT(2A) Receptor Function as a Contributing Factor to Both Neuropsychiatric and Cardiovascular Diseases. Cardiovasc Psychiatry Neurol. 2009;2009:475108.

60. Weber ET, Andrade R. Htr2a Gene and 5-HT(2A) Receptor Expression in the Cerebral Cortex Studied Using Genetically Modified Mice. Front Neurosci. 2010;4.

61. Glennon RA, Titeler M, McKenney JD. Evidence for 5-HT2 involvement in the mechanism of action of hallucinogenic agents. Life Sci. 1984;35(25):2505-11.

62. Gonzalez-Maeso J, Weisstaub NV, Zhou M, Chan P, Ivic L, Ang R, Lira A, Bradley-Moore M, Ge Y, Zhou Q, Sealfon SC, Gingrich JA. Hallucinogens recruit specific cortical 5-HT(2A) receptor-mediated signaling pathways to affect behavior. Neuron. 2007;53(3):439-52.

63. Nichols DE. Hallucinogens. Pharmacol Ther. 2004;101(2):131-81.

64. Halberstadt AL, Geyer MA. LSD but not lisuride disrupts prepulse inhibition in rats by activating the 5-HT(2A) receptor. Psychopharmacology (Berl). 2010;208(2):179-89.

65. Karaki S, Becamel C, Murat S, Mannoury la Cour C, Millan MJ, Prezeau L, Bockaert J, Marin P, Vandermoere F. Quantitative phosphoproteomics unravels biased phosphorylation of serotonin 2A receptor at Ser280 by hallucinogenic versus nonhallucinogenic agonists. Mol Cell Proteomics. 2014;13(5):1273-85.

66. Lopez-Gimenez JF, Gonzalez-Maeso J. Hallucinogens and Serotonin 5-HT2A Receptor-Mediated Signaling Pathways. Curr Top Behav Neurosci. 2018;36:45-73.

67. de la Fuente Revenga M, Shin JM, Vohra HZ, Hideshima KS, Schneck M, Poklis JL, Gonzalez-Maeso J. Fully automated head-twitch detection system for the study of 5-HT2A receptor pharmacology in vivo. Sci Rep. 2019;9(1):14247.

68. Schmid CL, Bohn LM. Serotonin, but not N-methyltryptamines, activates the serotonin 2A receptor via a ss-arrestin2/Src/Akt signaling complex in vivo. J Neurosci. 2010;30(40):13513-24.

69. Fribourg M, Moreno JL, Holloway T, Provasi D, Baki L, Mahajan R, Park G, Adney SK, Hatcher C, Eltit JM, Ruta JD, Albizu L, Li Z, Umali A, Shim J, Fabiato A, MacKerell AD, Jr., Brezina V, Sealfon SC, Filizola M, Gonzalez-Maeso J, Logothetis DE. Decoding the signaling of a GPCR heteromeric complex reveals a unifying mechanism of action of antipsychotic drugs. Cell. 2011;147(5):1011-23.

70. Vollenweider FX, Vollenweider-Scherpenhuyzen MF, Babler A, Vogel H, Hell D. Psilocybin induces schizophrenia-like psychosis in humans via a serotonin-2 agonist action. Neuroreport. 1998;9(17):3897-902.

71. Ebdrup BH, Rasmussen H, Arnt J, Glenthoj B. Serotonin 2A receptor antagonists for treatment of schizophrenia. Expert Opin Investig Drugs. 2011;20(9):1211-23.

72. Cummings J, Isaacson S, Mills R, Williams H, Chi-Burris K, Corbett A, Dhall R, Ballard C. Pimavanserin for patients with Parkinson's disease psychosis: a randomised, placebo-controlled phase 3 trial. Lancet. 2014;383(9916):533-40.

73. Diez-Alarcia R, Muguruza C, Rivero G, Garcia-Bea A, Gomez-Vallejo V, Callado LF, Llop J, Martin A, Meana JJ. Opposite alterations of 5-HT2A receptor brain density in subjects with schizophrenia: relevance of radiotracers pharmacological profile. Transl Psychiatry. 2021;11(1):302.

74. Malkova NV, Gallagher JJ, Yu CZ, Jacobs RE, Patterson PH. Manganese-enhanced magnetic resonance imaging reveals increased DOI-induced brain activity in a mouse model of schizophrenia. Proc Natl Acad Sci U S A. 2014;111(24):E2492-500.

75. Vollenweider FX, Csomor PA, Knappe B, Geyer MA, Quednow BB. The effects of the preferential 5-HT2A agonist psilocybin on prepulse inhibition of startle in healthy human volunteers depend on interstimulus interval. Neuropsychopharmacology. 2007;32(9):1876-87.

76. Wischhof L, Aho HE, Koch M. DOI-induced deficits in prepulse inhibition in Wistar rats are reversed by mGlu2/3 receptor stimulation. Pharmacol Biochem Behav. 2012;102(1):6-12.

77. Vohra HZ, Saunders JM, Jaster AM, de la Fuente Revenga M, Jimenez J, Fernandez-Teruel A, Wolstenholme JT, Beardsley PM, Gonzalez-Maeso J. Sex-specific effects of psychedelics on prepulse inhibition of startle in 129S6/SvEv mice. Psychopharmacology (Berl). 2021.

78. Quednow BB, Schmechtig A, Ettinger U, Petrovsky N, Collier DA, Vollenweider FX, Wagner M, Kumari V. Sensorimotor gating depends on polymorphisms of the serotonin-2A receptor and catechol-O-methyltransferase, but not on neuregulin-1 Arg38Gln genotype: a replication study. Biol Psychiatry. 2009;66(6):614-20.

79. Rochefort NL, Konnerth A. Dendritic spines: from structure to in vivo function. EMBO Rep. 2012;13(8):699-708.

80. de la Fuente Revenga M, Zhu B, Guevara CA, Naler LB, Saunders JM, Zhou Z, Toneatti R, Sierra S, Wolstenholme JT, Beardsley PM, Huntley GW, Lu C, González-Maeso J. Prolonged epigenetic and synaptic plasticity alterations following single exposure to a psychedelic in mice. bioRxiv. 2021:2021.02.24.432725.

81. Dong C, Ly C, Dunlap LE, Vargas MV, Sun J, Hwang IW, Azinfar A, Oh WC, Wetsel WC, Olson DE, Tian L. Psychedelic-inspired drug discovery using an engineered biosensor. Cell. 2021;184(10):2779-92 e18.

82. Carhart-Harris R, Giribaldi B, Watts R, Baker-Jones M, Murphy-Beiner A, Murphy R, Martell J, Blemings A, Erritzoe D, Nutt DJ. Trial of Psilocybin versus Escitalopram for Depression. N Engl J Med. 2021;384(15):1402-11.

83. Ly C, Greb AC, Cameron LP, Wong JM, Barragan EV, Wilson PC, Burbach KF, Soltanzadeh Zarandi S, Sood A, Paddy MR, Duim WC, Dennis MY, McAllister AK, Ori-McKenney KM, Gray JA, Olson DE. Psychedelics Promote Structural and Functional Neural Plasticity. Cell Rep. 2018;23(11):3170-82.

84. Ibi D, de la Fuente Revenga M, Kezunovic N, Muguruza C, Saunders JM, Gaitonde SA, Moreno JL, Ijaz MK, Santosh V, Kozlenkov A, Holloway T, Seto J, Garcia-Bea A, Kurita M, Mosley GE, Jiang Y, Christoffel DJ, Callado LF, Russo SJ, Dracheva S, Lopez-Gimenez JF, Ge Y, Escalante CR, Meana JJ, Akbarian S, Huntley GW, Gonzalez-Maeso J. Antipsychotic-induced Hdac2 transcription via NF-kappaB leads to synaptic and cognitive side effects. Nat Neurosci. 2017;20(9):1247-59.

85. Smith SM, Vale WW. The role of the hypothalamic-pituitary-adrenal axis in neuroendocrine responses to stress. Dialogues Clin Neurosci. 2006;8(4):383-95.

86. Sinclair D, Webster MJ, Wong J, Weickert CS. Dynamic molecular and anatomical changes in the glucocorticoid receptor in human cortical development. Mol Psychiatry. 2011;16(5):504-15.

87. Bradley AJ, Dinan TG. A systematic review of hypothalamic-pituitary-adrenal axis function in schizophrenia: implications for mortality. J Psychopharmacol. 2010;24(4 Suppl):91-118.

88. Sinclair D, Fillman SG, Webster MJ, Weickert CS. Dysregulation of glucocorticoid receptor co-factors FKBP5, BAG1 and PTGES3 in prefrontal cortex in psychotic illness. Sci Rep. 2013;3:3539.

89. Sood A, Pati S, Bhattacharya A, Chaudhari K, Vaidya VA. Early emergence of altered 5-HT2A receptor-evoked behavior, neural activation and gene expression following maternal separation. Int J Dev Neurosci. 2018;65:21-8.

90. Savignac HM, Couch Y, Stratford M, Bannerman DM, Tzortzis G, Anthony DC, Burnet PWJ. Prebiotic administration normalizes lipopolysaccharide (LPS)-induced anxiety and cortical 5-HT2A receptor and IL1-beta levels in male mice. Brain Behav Immun. 2016;52:120-31.

91. Maple AM, Zhao X, Elizalde DI, McBride AK, Gallitano AL. Htr2a Expression Responds Rapidly to Environmental Stimuli in an Egr3-Dependent Manner. ACS Chem Neurosci. 2015;6(7):1137-42.

92. Chiu HY, Chan MH, Lee MY, Chen ST, Zhan ZY, Chen HH. Long-lasting alterations in 5-HT2A receptor after a binge regimen of methamphetamine in mice. Int J Neuropsychopharmacol. 2014;17(10):1647-58.

93. Trajkovska V, Kirkegaard L, Krey G, Marcussen AB, Thomsen MS, Chourbaji S, Brandwein C, Ridder S, Halldin C, Gass P, Knudsen GM, Aznar S. Activation of glucocorticoid receptors increases 5-HT2A receptor levels. Exp Neurol. 2009;218(1):83-91.

94. Berendsen HH, Kester RC, Peeters BW, Broekkamp CL. Modulation of 5-HT receptor subtype-mediated behaviours by corticosterone. Eur J Pharmacol. 1996;308(2):103-11.

95. Islam A, Thompson KS, Akhtar S, Handley SL. Increased 5-HT2A receptor expression and function following central glucocorticoid receptor knockdown in vivo. Eur J Pharmacol. 2004;502(3):213-20.

96. Sever R, Glass CK. Signaling by nuclear receptors. Cold Spring Harb Perspect Biol. 2013;5(3):a016709.

97. Gong S, Miao YL, Jiao GZ, Sun MJ, Li H, Lin J, Luo MJ, Tan JH. Dynamics and correlation of serum cortisol and corticosterone under different physiological or stressful conditions in mice. PLoS One. 2015;10(2):e0117503.

98. Grad I, Picard D. The glucocorticoid responses are shaped by molecular chaperones. Mol Cell Endocrinol. 2007;275(1-2):2-12.

99. Oakley RH, Cidlowski JA. The biology of the glucocorticoid receptor: new signaling mechanisms in health and disease. J Allergy Clin Immunol. 2013;132(5):1033-44.

100. Falkenberg VR, Rajeevan MS. Identification of a potential molecular link between the glucocorticoid and serotonergic signaling systems. J Mol Neurosci. 2010;41(2):322-7.

101. Enga RM, Rice AC, Weller P, Subler MA, Lee D, Hall CP, Windle JJ, Beardsley PM, van den Oord EJ, McClay JL. Initial characterization of behavior and ketamine response in a mouse knockout of the post-synaptic effector gene Anks1b. Neurosci Lett. 2017;641:26-32.

102. Kiraly DD, Walker DM, Calipari ES, Labonte B, Issler O, Pena CJ, Ribeiro EA, Russo SJ, Nestler EJ. Alterations of the Host Microbiome Affect Behavioral Responses to Cocaine. Sci Rep. 2016;6:35455.

103. Aschauer DF, Kreuz S, Rumpel S. Analysis of transduction efficiency, tropism and axonal transport of AAV serotypes 1, 2, 5, 6, 8 and 9 in the mouse brain. PLoS One. 2013;8(9):e76310.

104. Rodriguez A, Ehlenberger DB, Dickstein DL, Hof PR, Wearne SL. Automated three-dimensional detection and shape classification of dendritic spines from fluorescence microscopy images. PLoS One. 2008;3(4):e1997.

105. American Psychiatric Association., American Psychiatric Association. Task Force on DSM-IV. Diagnostic and statistical manual of mental disorders : DSM-IV. 4th ed. Washington, DC: American Psychiatric Association; 1994. xxvii, 886 p. p.

106. American Psychiatric Association., American Psychiatric Association. Task Force on DSM-IV. Diagnostic and statistical manual of mental disorders : DSM-IV-TR. 4th ed. Washington, DC: American Psychiatric Association; 2000. xxxvii, 943 p. p.

107. Faul F, Erdfelder E, Lang AG, Buchner A. G*Power 3: a flexible statistical power analysis program for the social, behavioral, and biomedical sciences. Behav Res Methods. 2007;39(2):175-91.

108. Kurita M, Holloway T, Garcia-Bea A, Kozlenkov A, Friedman AK, Moreno JL, Heshmati M, Golden SA, Kennedy PJ, Takahashi N, Dietz DM, Mocci G, Gabilondo AM, Hanks J, Umali A, Callado LF, Gallitano AL, Neve RL, Shen L, Buxbaum JD, Han MH, Nestler EJ, Meana JJ, Russo SJ, Gonzalez-Maeso J. HDAC2 regulates atypical antipsychotic responses through the modulation of mGlu2 promoter activity. Nat Neurosci. 2012;15(9):1245-54.

109. Nguyen VT, Farman N, Maubec E, Nassar D, Desposito D, Waeckel L, Aractingi S, Jaisser F. Re-Epithelialization of Pathological Cutaneous Wounds Is Improved by Local Mineralocorticoid Receptor Antagonism. J Invest Dermatol. 2016;136(10):2080-9.

110. Lebsack TW, Fa V, Woods CC, Gruener R, Manziello AM, Pecaut MJ, Gridley DS, Stodieck LS, Ferguson VL, Deluca D. Microarray analysis of spaceflown murine thymus tissue reveals changes in gene expression regulating stress and glucocorticoid receptors. J Cell Biochem. 2010;110(2):372-81.

111. Zheng D, Sabbagh JJ, Blair LJ, Darling AL, Wen X, Dickey CA. MicroRNA-511 Binds to FKBP5 mRNA, Which Encodes a Chaperone Protein, and Regulates Neuronal Differentiation. J Biol Chem. 2016;291(34):17897-906.

112. Ng SS, Li A, Pavlakis GN, Ozato K, Kino T. Viral infection increases glucocorticoid-induced interleukin-10 production through ERK-mediated phosphorylation of the glucocorticoid receptor in dendritic cells: potential clinical implications. PLoS One. 2013;8(5):e63587.

113. Godowski PJ, Rusconi S, Miesfeld R, Yamamoto KR. Glucocorticoid receptor mutants that are constitutive activators of transcriptional enhancement. Nature. 1987;325(6102):365-8.

114. Revest JM, Di Blasi F, Kitchener P, Rouge-Pont F, Desmedt A, Turiault M, Tronche F, Piazza PV. The MAPK pathway and Egr-1 mediate stress-related behavioral effects of glucocorticoids. Nat Neurosci. 2005;8(5):664-72.

115. Dittgen T, Nimmerjahn A, Komai S, Licznerski P, Waters J, Margrie TW, Helmchen F, Denk W, Brecht M, Osten P. Lentivirus-based genetic manipulations of cortical neurons and their optical and electrophysiological monitoring in vivo. Proc Natl Acad Sci U S A. 2004;101(52):18206-11.

116. Szymczak-Workman AL, Vignali KM, Vignali DA. Design and construction of 2A peptide-linked multicistronic vectors. Cold Spring Harb Protoc. 2012;2012(2):199-204.

117. Hamilton PJ, Lim CJ, Nestler EJ, Heller EA. Neuroepigenetic Editing. Methods Mol Biol. 2018;1767:113-36.

118. Saif Z, Dyson RM, Palliser HK, Wright IM, Lu N, Clifton VL. Identification of Eight Different Isoforms of the Glucocorticoid Receptor in Guinea Pig Placenta: Relationship to Preterm Delivery, Sex and Betamethasone Exposure. PLoS One. 2016;11(2):e0148226.

119. Cuffe JSM, Saif Z, Perkins AV, Moritz KM, Clifton VL. Dexamethasone and sex regulate placental glucocorticoid receptor isoforms in mice. J Endocrinol. 2017;234(2):89-100.

120. Leventhal SM, Lim D, Green TL, Cantrell AE, Cho K, Greenhalgh DG. Uncovering a multitude of human glucocorticoid receptor variants: an expansive survey of a single gene. BMC Genet. 2019;20(1):16.

121. Falkenberg VR, Gurbaxani BM, Unger ER, Rajeevan MS. Functional genomics of serotonin receptor 2A (HTR2A): interaction of polymorphism, methylation, expression and disease association. Neuromolecular Med. 2011;13(1):66-76.

122. Diamond MI, Miner JN, Yoshinaga SK, Yamamoto KR. Transcription factor interactions: selectors of positive or negative regulation from a single DNA element. Science. 1990;249(4974):1266-72.

123. Belle I, Zhuang Y. E proteins in lymphocyte development and lymphoid diseases. Curr Top Dev Biol. 2014;110:153-87.

124. Hemmer MC, Wierer M, Schachtrup K, Downes M, Hubner N, Evans RM, Uhlenhaut NH. E47 modulates hepatic glucocorticoid action. Nat Commun. 2019;10(1):306.

125. Li H, Zhu Y, Morozov YM, Chen X, Page SC, Rannals MD, Maher BJ, Rakic P. Disruption of TCF4 regulatory networks leads to abnormal cortical development and mental disabilities. Mol Psychiatry. 2019;24(8):1235-46.

126. Doostparast Torshizi A, Armoskus C, Zhang H, Forrest MP, Zhang S, Souaiaia T, Evgrafov OV, Knowles JA, Duan J, Wang K. Deconvolution of transcriptional networks identifies TCF4 as a master regulator in schizophrenia. Sci Adv. 2019;5(9):eaau4139.

127. Feng G, Mellor RH, Bernstein M, Keller-Peck C, Nguyen QT, Wallace M, Nerbonne JM, Lichtman JW, Sanes JR. Imaging neuronal subsets in transgenic mice expressing multiple spectral variants of GFP. Neuron. 2000;28(1):41-51.

128. Curzon P, Zhang M, Radek RJ, Fox GB. The Behavioral Assessment of Sensorimotor Processes in the Mouse: Acoustic Startle, Sensory Gating, Locomotor Activity, Rotarod, and Beam Walking. In: nd, Buccafusco JJ, editors. Methods of Behavior Analysis in Neuroscience. Frontiers in Neuroscience. Boca Raton (FL)2009.

129. Valsamis B, Schmid S. Habituation and prepulse inhibition of acoustic startle in rodents. J Vis Exp. 2011(55):e3446.

130. Moreno JL, Miranda-Azpiazu P, Garcia-Bea A, Younkin J, Cui M, Kozlenkov A, Ben-Ezra A, Voloudakis G, Fakira AK, Baki L, Ge Y, Georgakopoulos A, Moron JA, Milligan G, Lopez-Gimenez JF, Robakis NK, Logothetis DE, Meana JJ, Gonzalez-Maeso J. Allosteric signaling through an mGlu2 and 5-HT2A heteromeric receptor complex and its potential contribution to schizophrenia. Sci Signal. 2016;9(410):ra5.

131. Moreno JL, Holloway T, Albizu L, Sealfon SC, Gonzalez-Maeso J. Metabotropic glutamate mGlu2 receptor is necessary for the pharmacological and behavioral effects induced by hallucinogenic 5-HT2A receptor agonists. Neurosci Lett. 2011;493(3):76-9.

132. Kinon BJ, Millen BA, Zhang L, McKinzie DL. Exploratory analysis for a targeted patient population responsive to the metabotropic glutamate 2/3 receptor agonist pomaglumetad methionil in schizophrenia. Biol Psychiatry. 2015;78(11):754-62.